EXPERIMENTAL AND ANALYTICAL INVESTIGATION OF REINFORCED CONCRETE BRIDGE PIER CAPS WITH AN EXTERNALLY BONDED STAINLESS STEEL SYSTEM

A Dissertation
Presented to
The Academic Faculty

by

Sung Hu Kim

In Partial Fulfillment
of the Requirements for the Degree
Doctor of Philosophy in the
School of Civil and Environmental Engineering

Georgia Institute of Technology
December 2014

EXPERIMENTAL AND ANALYTICAL INVESTIGATION OF REINFORCED CONCRETE BRIDGE PIER CAPS WITH AN EXTERNALLY BONDED STAINLESS STEEL SYSTEM

Approved by:

Dr. Abdul-Hamid Zureick, Advisor
School of Civil and Environmental Engineering
Georgia Institute of Technology

Dr. Bruce R. Ellingwood
School of Civil and Environmental Engineering
Georgia Institute of Technology

Dr. Rafi L. Muhanna
School of Civil and Environmental Engineering
Georgia Institute of Technology

Dr. Yang Wang
School of Civil and Environmental Engineering
Georgia Institute of Technology

Dr. George Kardomateas
School of Aerospace Engineering
Georgia Institute of Technology

Date Approved: October 21, 2014

ACKNOWLEDGEMENTS

I would like to express my deepest appreciation to my advisor, Dr. Abdul-Hamid Zureick, for mentoring me as his student. His invaluable contribution and insight into this research work made my dissertation possible. I would also like to extend my gratitude to Dr. Bruce Ellingwood for helpful guidance throughout this work. I also wish to thank my defense committee members, Dr. Rafi L. Muhanna, Dr. Yang Wang and Dr. George Kardomateas for their effort and valuable input.

I would also like to express sincere gratitude to my family and Eunice for believing in me. Without their motivation and support, I would not have been able to finish this work. I am truly grateful to Dr. Stanley Kim, who is a research fellow in Georgia Department of Transportation, and my friends who assisted me in conducting research: Falak Shah, Tim Wright, Jeremy Mitchell, Dr. Andrew Bechtel, Dr. Nicholas Reynolds, Dr. Jong-Su Jeon, and Chunhee Cho.

The research work presented in this dissertation was supported by the Georgia Department of Transportation and this support is gratefully acknowledged.

TABLE OF CONTENTS

LIST OF TABLES

LIST OF FIGURES

SUMMARY

This research is aimed at examining the behavior of reinforced concrete bridge pier caps strengthened with externally bonded reinforcement experimentally and analytically. In the experimental study, nine full-scale reinforced concrete bridge pier caps were built, externally strengthened with stainless steel reinforcement, and then tested to failure. Load, deflection, and strain measurements were collected and two potential failure mechanisms were identified. In the analytical work, mechanics-based equations were developed for calculating the shear strength of these types of structural elements when a diagonal shear crack is formed under loading. In addition, a strut-and-tie/truss model is proposed for determining the strength of reinforced concrete bridge caps with externally bonded reinforcement systems. Results from both experimental and analytical studies are compared and design recommendations are made for future adoption in bridge and building codes and specifications.

CHAPTER 1

INTRODUCTION

1.1 Motivation

In the State of Georgia, there are a large number of reinforced concrete bridge pier caps that was constructed prior to the 1970s. The shear reinforcement in these bridge pier caps does not meet the current shear design provisions of the AASHTO LRFD Bridge Design Specifications (2012).

According to the Bridge Inventory Management System (BIMS) of the Georgia Department of Transportation (GDOT), there are 7204 pier cap cantilever segments, similar to that shown in Fig. 1.1; the strengths of 4875 of those pier cap sections are controlled by the shear strength limit state of Article 5.8 of AASHTO (2012). Further examination of those 4875 pier cap sections has revealed that 1156 of these pier caps do not contain the minimum amount of transverse reinforcement stipulated in Article 5.8.2.5 of AASHTO (2012).

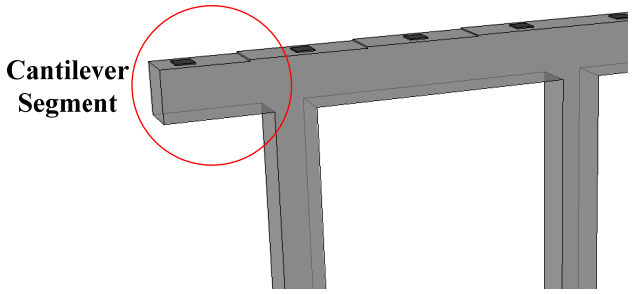

Figure 1.1- Cantilever segment of a bridge pier cap

To upgrade those reinforced concrete bridge pier caps to a level consistent with current AASHTO LRFD Bridge Design Specifications, a cost-effective and a reliable strengthening scheme must be developed.

1.2 Previous Work

While externally bonded fiber reinforced polymer (FRP) reinforcement systems for shear strengthening of reinforced concrete members have been extensively investigated (see e.g. *Zureick et al., 2010; Belarbi et al., 2011*), limited information (*Zhang et al., 2004; Islam et al., 2005; Bousselham et al., 2006; Cao et al., 2005*) is available for cases involving reinforced concrete bridge pier caps and deep beams with shear span-to-depth (a/d) ratios of less than 2.0. Zhang et al. (2004) tested to failure four groups of four deep reinforced concrete beams without web (transverse and longitudinal) steel reinforcement. Three beams from each group were shear strengthened prior to testing with a specific arrangement of externally bonded carbon fiber reinforced polymer (CFRP) composite materials and one beam was tested without the externally bonded reinforcement to establish the reference strength value of the particular group. The tests were conducted on beams with two different a/d ratios of 1.88 and 1.25. While the study showed that it was possible to increase the shear strength of reinforced concrete beams using externally bonded CFRP composite materials, independent analyses of the test results cannot be conducted with confidence due to the absence of any evidence establishing the experimental material properties of either the CFRP composites or the longitudinal flexural steel reinforcement. In Islam et al. (2005), six deep reinforced concrete beams having a shear span-to-depth ratio of 0.66 were tested. Five of the test beams were externally strengthened in shear with three different types of composite materials and one beam was tested for the purpose of establishing a reference strength value. Experimental results showed that the use of externally bonded shear reinforcement for strengthening deep reinforced concrete beams increases the shear strength from 24 to 43%. Similar to the study by Zhang et al. (2004), properties of the externally bonded polymer composite materials were not determined experimentally. Cao et al. (2005) tested 12 pre-cracked reinforced concrete beams, having span-to-depth ratios ranging from 1.35 to 2.7, externally strengthened with carbon fiber- and glass fiber-reinforced

polymer composite material strips wrapped completely around the beams. The authors did not conduct material property tests and reported, without documentation, carbon fiber properties in one case and glass-fiber reinforced polymer composite properties in two other cases. Bousselham et al. (2006) conducted experiments aimed at examining the behavior of deep reinforced concrete T-beams (a/d ratio = 1.5) externally strengthened with U-shaped carbon fiber-reinforced polymer composite materials. It was shown that FRP reinforcement increased the shear strength of reinforced concrete beams and that maximum strength was reached when FRP reinforcement delamination occurred at strain ranging from 1900 to 4520 micro strains. FRP material properties were reported to have a modulus of 35,244 ksi, a tensile strength of 450 ksi, and a tensile strain of 1.3%. These modulus and strength values are closer to the fiber properties than the polymer composite properties, and the test method used to determine these properties was not described, making it difficult to perform an independent analysis of their test results.

In addition to the above experimental studies, Park and Aboutaha (2009) analyzed the test results of 17 deep beams tested by Fanning and Kelley (1999) and Chaalal (1998) using a Strut and Tie Model. The strengths of externally strengthened reinforced concrete bridge pier caps with FRP system were calculated, and compared with analytical results conducted by Park and Aboutaha (2005). A finite element analysis was performed and compared with results from the experimental studies on externally strengthened reinforced concrete beams with FRP system carried out by Deniaud and Cheng (2001), Chaallal et al. (1998), and Fanning and Kelly (1999). The experimental studies included test specimens having a/d ratios greater than 2.5, which do not exhibit similar behavior to that of deep components. Thus, the finite element analysis carried out based on the experimental studies would not be applicable to reinforced concrete beams controlled by concrete tied arch behavior.

Based on the above reviews, it is evident that behavior of the reinforced concrete bridge pier caps strengthened with externally bonded reinforcement has not been studied

sufficiently to enable the development of design criteria for strengthening reinforced concrete pier caps with externally bonded stainless steel plates.

1.3 Objectives

The objectives of this research work are to:

1) Investigate the behavior of externally bonded stainless steel systems for strengthening reinforced concrete cantilever bridge pier caps through an experimental testing program; and
2) Develop an analytical method for estimating the strength of beams reinforced by externally bonded stainless steel plates.

1.4 Thesis Outline

This dissertation presents experimental and analytical studies of reinforced concrete bridge pier caps with externally bonded stainless steel reinforcement systems. Organization of this dissertation is listed as follows:

Chapter 2 presents current analytical models for computing the strength of reinforced concrete deep components. Sectional models, strut-and-tie models, and mechanics-based models are described in this chapter. To experimentally validate the analytical models, 156 experimental data are assembled and analyzed using the analytical models.

Chapter 3 presents an experimental investigation of reinforced concrete bridge pier caps with externally bonded stainless steel plates. The construction of full-scale bridge pier caps and the strengthening procedure of the externally bonded stainless steel plates are described. A description of the test set-up and results of the laboratory experiments are presented in this chapter.

Chapter 4 describes the development and application of analytical approaches for computing the strength of the reinforced concrete bridge pier caps with externally bonded

reinforcement system. Two analytical approaches are presented and experimentally validated using the bridge pier caps tested in this research work.

Chapter 5 presents a summary and conclusions drawn from the major findings of this research. Further research studies are also recommended in this chapter.

CHAPTER 2

ANALYTICAL MODELS FOR ESTIMATING THE SHEAR STRENGTH OF REINFORCED CONCRETE BRIDGE PIER CAPS

At present, the shear strength of reinforced concrete bridge elements is determined in accordance with AASHTO LRFD Bridge Design Specifications (2012). The AASHTO LRFD Bridge Design Specifications provides two different approaches: the sectional design model, and the strut-and-tie design model. Because of the advantage of the strut-and-tie model when applied to reinforced concrete deep members, other organizations such as the American Concrete Institute (ACI) and the Federation Internationale de la Precontrainte (FIP) have adopted variants of these strut-and-tie models. Brief reviews of these analytical models are presented in this chapter.

2.1 AASHTO Sectional Model

Article 5.8.3 of AASHTO LRFD Bridge Design Specifications (*AASHTO, 2012*) provides three sectional design models: the Simplified Procedure for Nonprestressed Sections, the General Procedure, and the Simplified Procedure for Prestressed and Nonprestressed Sections. For the beams controlled by inclined web cracks, on which this research work pays attention, the Simplified Procedure for Prestressed and Nonprestressed Sections yields analytical results that are practically identical to those obtained from the Simplified Procedure for Nonprestressed Sections. Thus, the Simplified Procedure for Prestressed and Nonprestressed is excluded in this chapter.

2.1.1 AASHTO Simplified Procedure for Nonprestressed Sections

This analytical approach is applicable to reinforced concrete members having an overall depth less than 16 in. and containing a minimum amount of transverse reinforcement satisfying the following equation (Article 5.8.2.5 of AASHTO, 2012):

$$A_v \geq 0.0316\sqrt{f_c'}\frac{b_v s}{f_y} \tag{2.1}$$

where,

A_v = area of a transverse reinforcement within distance s (in.^{2})

f_c' = specified compressive strength of concrete (ksi)

b_v = with of web adjusted for the presence of ducts (in.)

s = spacing of transverse reinforcement (in.)

f_y = yield strength of transverse reinforcement (ksi)

The nominal shear resistance of the members can be computed as follows:

$$V_n = V_c + V_s + V_p \tag{2.2}$$

$$V_c = 0.0316\beta\sqrt{f_c'}b_v d_v \tag{2.3}$$

$$V_s = \frac{A_v f_y d_v (\cot\theta + \cot\alpha)\sin\alpha}{s} \tag{2.4}$$

where,

β = tensile stress factor indicating ability of cracked concrete to transmit shear reinforcement component

θ = angle of inclination of diagonal compressive stresses

α = angle of inclination of transverse reinforcement to longitudinal axis

d_v = effective shear depth (in.)

For sections not subjected to axial tension and containing at least the minimum transverse reinforcement specified in Eq. 2.1, the values of β and θ can be taken as 2.0 and 45° respectively.

2.1.2 AASHTO General Procedure

This analytical procedure is based on the Modified Compression Field Theory (MCFT) developed by Vecchio and Collins (1986), and simplified by Bentz et al. (2006)

for practical applications. This procedure takes into consideration the strain effect of longitudinal tension reinforcement and the maximum size of the aggregates used in the concrete mix. In this approach, the parameter, β, shown in Eq. 2.3 is computed as follows:

$$\beta = \begin{cases} \dfrac{4.8}{(1+750\varepsilon_s)} & \text{for sections containing at least the minimum transverse reinforcement} \\ \dfrac{4.8}{(1+750\varepsilon_s)}\dfrac{51}{(39+s_{xe})} & \text{for sections not containing at least the minimum transverse reinforcement} \end{cases} \tag{2.5}$$

where,

$$s_{xe} = s_x \frac{1.38}{a_g + 0.63} \tag{2.6}$$

$$\varepsilon_s = \frac{\left(\dfrac{|M_u|}{d_v} + 0.5N_u + |V_u - V_p| - A_{ps} f_{po} \right)}{E_s A_s + E_p A_{ps}} \tag{2.7}$$

In the above equations,

ε_s = strain in nonprestressed longitudinal tension reinforcement

s_x = crack spacing parameter

a_g = maximum aggregate size (in.)

M_u = factored moment at the section (kip-in.)

N_u = applied factored axial force taken as positive if tensile (kip)

V_u = factored shear force at section (kip)

V_p = effective prestressing force (kip)

A_{ps} = area of prestressing steel (in.^{2})

f_{po} = a parameter taken as modulus of elasticity of prestressing tendons multiplied by the locked-in difference in strain between the prestressing tendons and the surrounding concrete (ksi)

E_s = modulus of elasticity of reinforcing bars (ksi)

E_p = modulus of elasticity of prestressing tendons (ksi)

A_s = area of nonprestressed tension reinforcement (in.^{2})

A_{ps} = area of prestressing steel (in.^{2})

The angle of inclination of diagonal compressive stress is defined as

$$\theta = 29 + 3500\varepsilon_s \tag{2.8}$$

2.2 AASHTO Strut-and-Tie Model

The AASHTO Strut-and-Tie Model specified in Article 5.6.3 of AASHTO (2012) may be applied to deep bridge components, subjected to loading such that the distance from the point of zero shear to the face of the support is less than twice the effective depth of the components. The AASHTO Strut-and Tie Model adopts a prismatic compressive strut, the strength of which is established as follows:

$$P_n = f_{cu} A_{cs} \tag{2.9}$$

$$P_n = f_y A_{st} + A_{ps}[f_{pe} + f_y] \tag{2.10}$$

$$f_{cu} = \frac{f_c'}{0.8 + 170\varepsilon_1} \leq 0.85 f_c' \tag{2.11}$$

$$\varepsilon_1 = \varepsilon_s + (\varepsilon_s + 0.002)\cot^2(\alpha_s) \tag{2.12}$$

where,

P_n = strength of unreinforced strut or tension tie (kip)

f_{cu} = limiting compressive stress in compressive strut (ksi)

A_{cs} = effective cross-sectional area of compressive strut (in.^{2})

A_{st} = total area of longitudinal mild steel reinforcement in the tie (in.^{2})

f_{pe} = stress in prestressing steel due to prestress after losses (ksi)

ε_l = principal tensile strain in cracked concrete due to factored loads

ε_s = tensile strain in the concrete in the direction of the tension tie

α_s = the smallest angle between the compressive strut and adjoining tension ties (degrees)

This model does not account for the contribution of either the transverse reinforcement or the crack control reinforcement specified in Article 5.6.3.6 of AASHTO (2012). To ensure ductile behavior of the deep reinforced concrete members, Article 3.6.3.6 of AASHTO LRFD Bridge Specifications requires that the crack control reinforcement have spacing not greater than one-fourth the effective depth of the member or 12 in. The crack control reinforcement in both vertical and horizontal directions must satisfy the following equations:

$$\frac{A_v}{b_w s_v} \geq 0.003 \quad \text{and} \quad \frac{A_h}{b_w s_h} \geq 0.003 \tag{2.13}$$

where,

A_v = total area of vertical crack control reinforcement within spacing s_v (in.^{2})

A_h = total area of horizontal crack control reinforcement within spacing s_h (in.^{2})

b_w = width of member's web (in.)

s_v = spacing of vertical crack control reinforcement (in.)

s_h = spacing of horizontal crack control reinforcement (in.)

2.3 ACI 318 Strut-and-Tie Model

In the ACI 318 strut-and-tie model (*ACI, 2008*), the compressive strut is assumed to have a bottle shape for which the strength is computed as a function of the amount of transverse reinforcement as follows:

$$F_{ns} = f_{ce} A_{cs} \tag{2.14}$$

$$f_{ce} = 0.85 \beta_s f_c' \tag{2.15}$$

where,

F_{ns} = nominal strength of a strut

f_{ce} = effective compressive strength of the concrete in a strut or a nodal zone (psi)

A_{cs} = cross-sectional area at one end of a strut in a strut-and-tie model, taken perpendicular to the axis of the strut (in.^{2})

β_s = factor accounting for the effect of cracking and confining reinforcement on the effective compressive strength of the concrete in a strut.

For the cases in which the compressive strength of concrete is less than 6 ksi, β_s is defined as follows:

$$\beta_S = \begin{cases} 0.75 & \text{if} \quad \sum \frac{A_{si}}{b_s s_i} \sin \alpha_i \geq 0.003 \\ 0.60\lambda & \text{if} \quad \sum \frac{A_{si}}{b_s s_i} \sin \alpha_i < 0.003 \end{cases} \tag{2.16}$$

where,

A_{si} = total area of surface reinforcement at spacing s_i (in.^{2})

b_s = width of a strut (in.)

s_i = spacing of transverse reinforcement in *i*-th layer (in.)

α_i = angle between the axis of a strut and the bars in the *i*-th layer of reinforcement crossing that strut

λ = modification factor reflecting the reduced mechanical properties of lightweight concrete

2.4 FIP Strut-and-Tie Model

The strut-and-tie model in FIP (1999) is constructed by considering two separate mechanisms: an inclined strut and a truss representing the vertical transverse reinforcement (Figure 2.1).

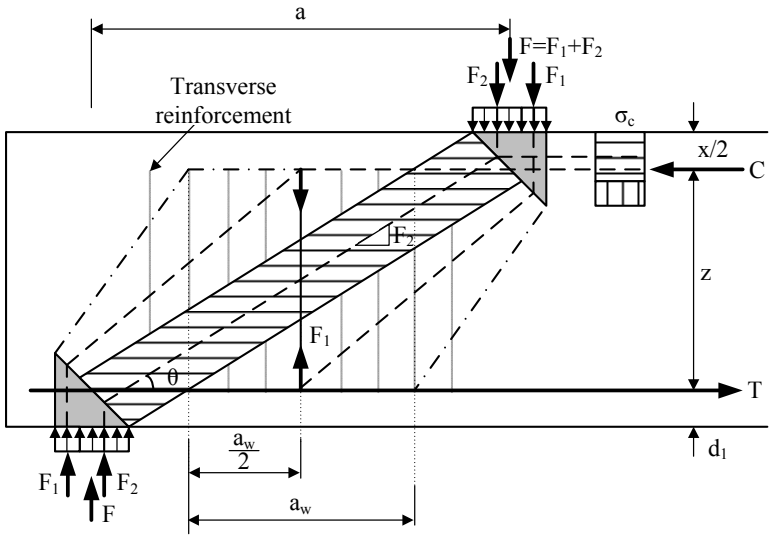

Figure 2.1- Strut-and-Tie Model for a deep component with a concentrated load (FIP, 1999)

FIP recommends that transverse reinforcement be distributed over the length a_w as shown in Fig. 2.1. FIP also recommends that the amount of transverse reinforcement be greater than 0.1% of the member. a_w can be computed using the following equation.

$$a_w = (0.85a - z/4) \tag{2.17}$$

where,

a = shear span

z = inner lever arm

The transverse reinforcement is determined as follows:

$$F_1 = \frac{2\frac{a}{z} - 1}{3} F \tag{2.18}$$

where,

F_1 = strength of transverse reinforcement

F = applied force of the deep component

a = shear span

z = inner lever arm

The resisting force of a strut and the effective strength of concrete are computed as follows:

$$F_{RCD} = A_c f_{cd,eff} \tag{2.19}$$

$$f_{cd,eff} = \nu_2 f_{1,cd} \tag{2.20}$$

where,

F_{RCD} = resisting force of a compression chord

A_c = area of a compression section or strut

$f_{cd,eff}$ = effective design value of concrete compressive strength

ν_2 = coefficient accounting for cracking on compressive strut

$f_{1,cd}$ = uniaxial design strength of concrete determined as shown in Section 2.1.2 of FIP (1999)

In the above equations,

$$\nu_2 = \begin{cases} 1.00 & \text{for uncracked struts with uniform strain distribution} \\ 0.80 & \text{for struts with cracks and bonded transverse reinforcement} \\ 0.60 & \text{for struts with normal crack widths} \\ 0.45 & \text{for struts with large crack widths} \end{cases} \tag{2.21}$$

2.5 Zararis' Analytical Approach

Zararis (2003) suggested a mechanics-based model for computing the shear strength of reinforced concrete beams having shear span to depth ratio between 1 and 2.5. Concrete tied arch behavior was considered after the diagonal crack is formed by a shear force. The ultimate shear force of the deep member is computed from:

$$V_u = \frac{bd}{a/d}\left[\frac{1-0.5c_s/d+0.5(\rho_h/\rho)(1-c_s/d)}{1+(\rho_h/\rho)(1-c_s/d)}\frac{c_s}{d}f_c'+0.5\rho_v f_{yv}\left(1-\frac{c_s}{d}\right)^2\left(\frac{a}{d}\right)^2\right] \quad (2.22)$$

where,

a = shear span

b = width of beam

c = depth of compression zone above flexural cracks

c_s = depth of compression zone above diagonal crack

d = effective depth to tension reinforcement

ρ = ratio of main tension reinforcement (A_s/bd)

ρ_v = ratio of vertical web reinforcement (A_{vh}/bd)

ρ_h = ratio of horizontal web reinforcement (A_v/bd)

A_s = area of tension reinforcement

A_{vh} = area of horizontal web reinforcement

A_v = area of vertical web reinforcement

f_{yv} = yield strength of vertical web reinforcement (MPa)

The depth of the compression zone at the onset of the diagonal crack formation is computed from the following equations:

$$c_s = \frac{1+0.27R(a/d)^2+0.27(\rho_h/\rho)}{1+R(a/d)^2}c \quad (2.23)$$

$$R = 1+(\rho_v/\rho)(a/d) \quad (2.24)$$

Depth of compression zone after the formation of flexural cracks is computed by the following quadratic equation.

$$\left(\frac{c}{d}\right)^2+600\frac{\rho}{f_c'}\left(\frac{c}{d}\right)-600\left(\frac{c}{d}\right)\frac{\rho}{f_c'}=0 \quad (2.25)$$

where,

f_c' = nominal compressive strength of concrete (MPa)

It should be noted that the strain distribution through the depth of the deep beam was assumed to be linear in the area of pure bending, and the strain of concrete at maximum strain was assumed to be 0.002.

2.6 Modification to the Zararis' Analytical Approach

The original form of Zararis Method was modified by Bechtel (2011) who considered yielding of the longitudinal tension reinforcement and revised the value of maximum compressive strain of concrete to be 0.003 in the area of pure bending. For the stress distribution of concrete, a parabolic stress distribution with the maximum stress of $0.85 f_c'$ was assumed. The depth of the compression zone at the formation of flexural cracks are then calculated from solving the following quadratic equation for the case when $\varepsilon_s \le \varepsilon_y$.

$$\left(\frac{c}{d}\right)^2 + 153{,}520\frac{\rho}{f_c'}\left(\frac{c}{d}\right) - 153{,}520\left(\frac{c}{d}\right)\frac{\rho}{f_c'} = 0 \tag{2.26}$$

For the case in which $\varepsilon_s > \varepsilon_y$, the depth of the compression zone above flexural cracks was computed as follows:

$$\frac{c}{d} = \frac{3A_s f_y}{2(0.85) f_c' b_v d} \tag{2.27}$$

The shear span to depth (a/d) ratio in Eqs. 2.22, 2.23 and 2.24 was replaced by an effective shear span to depth ratio $(a/d)_{effective}$ defined as

$$(a/d)_{effective} \approx \frac{a - \frac{l_{b\,comp}}{2} + \frac{l_b}{2}}{d\left(1 - \frac{3}{8}\left(\frac{c}{d}\right)\right)} \le a/d \tag{2.28}$$

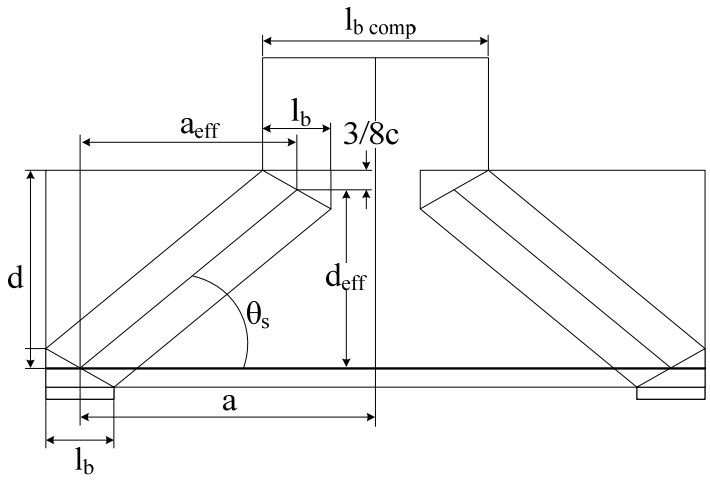

Figure 2.2-Geometry of effective shear span to depth ratio (*Bechtel, 2011*)

2.7 Validation of Analytical Models

The shear strength values computed from the seven analytical methods presented earlier in this chapter are compared with those obtained from 156 experimental tests (see Appendix B). These 156 experimental tests contain the following parameters which are required for the afore-mentioned analytical methods: 1) a/z ratio between 1 and 2 as specified in the FIP Strut-and-Tie Model, 2) compressive strength of concrete less than 6 ksi as specified by the ACI Strut-and-Tie Model, and 3) reported information about bearing areas and material properties by tests. The ratios of experimental strength to computed strength are shown graphically in Fig 2.3 and are summarized in Table 2.1.

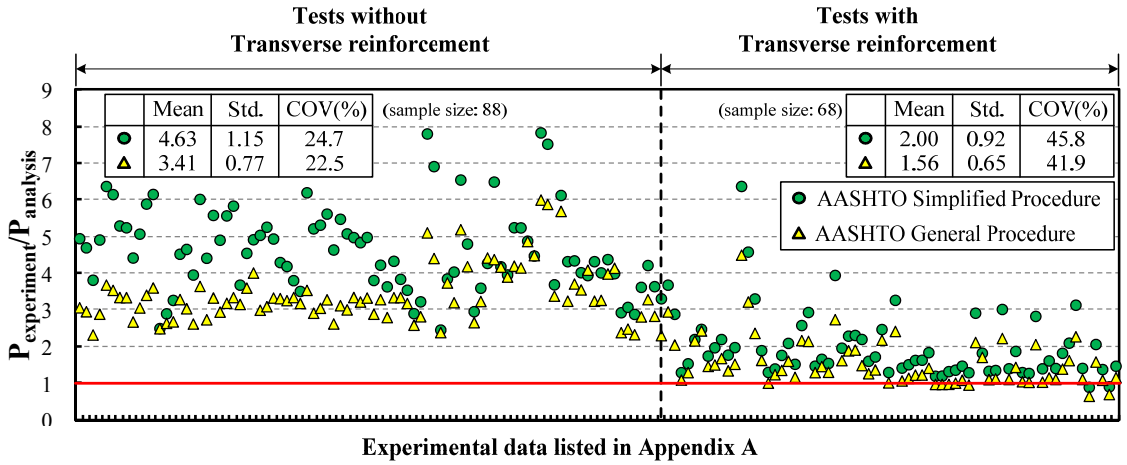

(a) AASHTO Sectional Models

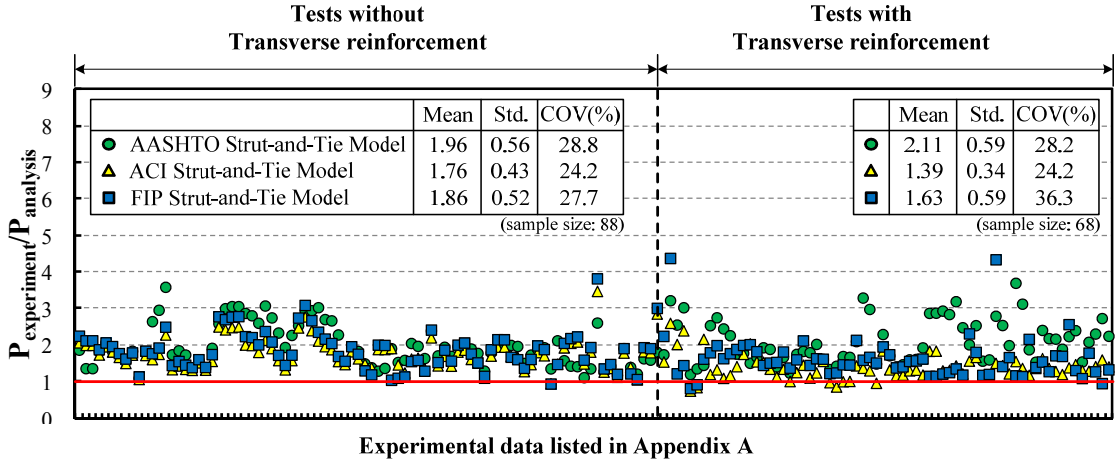

(b) Strut-and-Tie Models

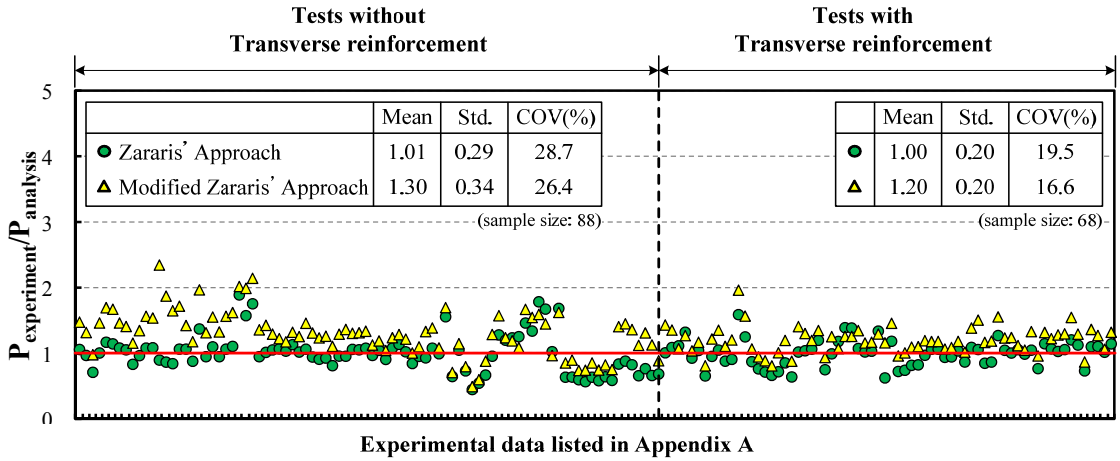

(c) Zararis' and Modified Zararis' Method

Figure 2.3- Comparison of analytical results with experimental results

Table 2.1- Comparison of analytical results to experimental results

	$P_{experiment}/P_{analysis}$		
	Mean	Std.	COV (%)
AASHTO Simplified Procedure	3.48	1.61	48.1
AASHTO General Procedure	2.60	1.17	44.9
AASHTO Strut-and-Tie Model	2.02	0.58	28.7
ACI Strut-and-Tie Model	1.60	0.43	26.8
FIP Strut-and-Tie Model	1.76	0.56	31.8
Zararis' Approach	1.00	0.25	25.1
Modified Zararis' Approach	1.26	0.29	23.3

Sample size : 156

Note: AASHTO Simplified Procedure was used for analysis despite the experimental data included the depth greater than 16 in.

It is evident from Fig. 2.3 and Table 2.1 that the experimental data can be well represented by an analytical approach derived from the Zararis' analytical model. Of interest is the fact that both the AASHTO Simplified Procedure and the General Procedure yielded greater values of $P_{experiment}/P_{analysis}$ than strut-and-tie models and mechanics-based approaches did. This is in line with the conclusion of Kani (1964), who demonstrated that for reinforced concrete members having a/d ratio less than 2.5, the strength is governed by the tied arch mechanism. In particular, the AASHTO Simplified Procedure yielded a mean $P_{experiment}/P_{analysis}$ ratio of 4.63 for the test specimens containing no transverse reinforcement. This is because the AASHTO Simplified Procedure does not consider size effect of the deep components.

The ratios of experimental results to analytical results using strut-and-tie models are shown in Fig. 2.3-(b). Strut-and-Tie Models yielded mean values of $P_{experiment}/P_{analysis}$ ranged from 1.60 to 2.02. In particular, for tests not containing the transverse reinforcement, sectional models yielded significantly greater values of $P_{experiment}/P_{analysis}$ than those resulting from the strut-and-tie models. These results are consistent with the findings of Collins and Mitchell (1991). The AASHTO Strut-and-Tie Model yielded mean $P_{experiment}/P_{analysis}$ ratio of 1.96 for the tests containing transverse reinforcement and 2.11 for the tests not containing transverse reinforcement. The small difference between these two ratios is due to the fact that AASHTO Strut-and-Tie Model does not account for the amount of transverse reinforcement contained in the cross section.

CHAPTER 3

EXPERIMENTAL WORK

This chapter describes the experimental work aimed at investigating the behavior of shear strength-deficient reinforced concrete bridge pier caps strengthened with externally bonded stainless steel reinforcement. The work is limited to cases in which the shear span-to-depth ratios is between 1.5 and 2, which are commonly found in reinforced concrete bridge pier caps constructed throughout the State of Georgia.

3.1 Pier Cap Specimens

Nine full-scale reinforced concrete pier cap specimens were designed and constructed for testing. Seven of the specimens were reinforced with externally bonded stainless steel reinforcement. The external reinforcement was made of UNS S32003 (ATI^{TM} 2003) duplex stainless steel plates having a width of 2.17 in. and a thickness of 0.055 in. Test specimens were classified into three groups, the details of which are presented below.

- **Group A**: The pier cap specimens in this group had a shear span-to-depth ratio of 1.5 and a longitudinal tension reinforcement ratio of 1.3% consisting of six #10 steel bars. These specimens were built without any transverse reinforcement in the shear span.
- **Group B**: These specimens were built to represent the bridge pier caps having the minimum amount of transverse reinforcement specified in AASHTO (2012). The specimens had a transverse reinforcement ratio of 0.11%, a shear span-to-depth ratio of 1.5, and a longitudinal reinforcement ratio of 1.3%.

- **Group C**: The specimens in this group were built to have a shear span-to-depth ratio of 2, a longitudinal tension reinforcement ratio of 0.85%, and a transverse reinforcement ratio of 0.11%.

Details and dimensions of all test specimens are given in Fig. 3.1 and Tables 3.1, 3.2 and 3.3. Details of each test specimen are presented in Appendix B.

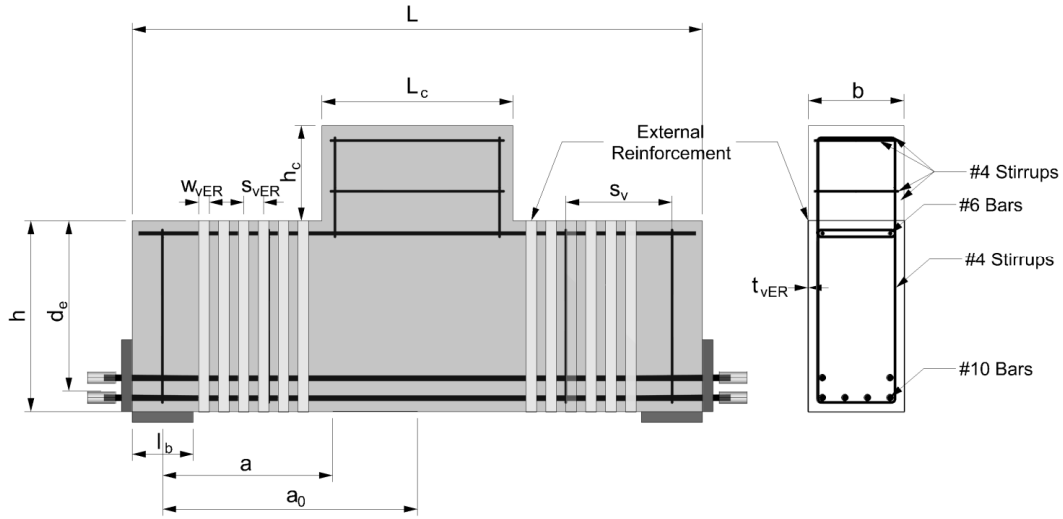

Figure 3.1- Details of Pier Cap Specimens

Table 3.1- Dimensions of specimens

Group	Specimen ID	L (in.)	a_0 (in.)	a (in.)	b (in.)	h (in.)	d_e (in.)	L_c (in.)	h_c (in.)	l_b (in.)
A	BL2*	107.5	48	30	18	36	32.12	36	18	11.5
	AR014	107.5	48	30	18	36	32.12	36	18	11.5
	AR035	107.5	48	30	18	36	32.12	36	18	11.5
B	BS00	107.5	48	30	18	36	32.12	36	18	11.5
	BSR008	107.5	48	30	18	36	32.12	36	18	11.5
	BSR014	107.5	48	30	18	36	32.12	36	18	11.5
C	CS00	127.5	68	50	18	36	33.36	36	18	11.5
	CSR018-1	127.5	68	50	18	36	33.36	36	18	11.5
	CSR018-2	127.5	68	50	18	36	33.36	36	18	11.5
	CSR035	127.5	68	50	18	36	33.36	36	18	11.5

* BL2 is the reference test specimen reported by Zureick et al. (2013)

L =length of specimen, a = shear span, b = width of specimen, h = height of specimen, d_e = effective depth of specimen, L_c =length of column, h_c =height of column, and l_b =length of bearing plate.

Table 3.2- Dimensions of internal and external reinforcements

Group	Specimen ID	s_v (in.)	w_{vER} (in.)	t_{vER} (in.)	s_{vER} (in.)
A	BL2*	-	-	-	-
	AR014	-	2.17	0.055	9.38
	AR035	-	2.17	0.055	3.75
B	BS00	20	-	-	-
	BSR008	20	2.17	0.055	17.13
	BSR014	20	2.17	0.055	9.38
C	CS00	20	-	-	-
	CSR018-1	20	2.17	0.055	7.50
	CSR018-2	20	2.17	0.055	7.50
	CSR035	20	2.17	0.055	3.75

* BL2 is the reference test specimens reported by Zureick et al. (2013)

s_v = spacing of internal transverse reinforcement, w_{vER} = width of stainless steel plate, t_{vER} = thickness of stainless steel plate, and s_{vER} = spacing of external reinforcement.

Table 3.3- Shear span-to-depth and reinforcement ratios

Group	Specimen ID	a_0/d_e	a/d_e	ρ (%)	ρ_v (%)	ρ_{vER} (%)
A	AR014	1.5	0.9	1.30	-	0.14
	AR035	1.5	0.9	1.30	-	0.35
B	BS00	1.5	0.9	1.30	0.11	-
	BSR008	1.5	0.9	1.30	0.11	0.08
	BSR014	1.5	0.9	1.30	0.11	0.14
C	CS00	2.0	1.5	0.85	0.11	-
	CSR018-1	2.0	1.5	0.85	0.11	0.18
	CSR018-2	2.0	1.5	0.85	0.11	0.18
	CSR035	2.0	1.5	0.85	0.11	0.35

a_0/d_e = reference shear span to effective depth ratio, a/d_e = shear span to effective depth ratio, ρ = longitudinal tension reinforcement ratio (A_s/bd_e), ρ_v = internal transverse reinforcement ratio (A_v/bs_v), and ρ_{vER} = external stainless steel reinforcement ratio (A_{vER}/bs_{vER}).

3.2 Fabrication of the Stainless Steel Reinforcement System

The external reinforcement system consists of UNS S32003 duplex stainless steel channels fabricated from coils having a width of 2.17 in. and thickness of 0.055 in. The dimensions of the channels are $h + 2t_a^{top/bottom} = 18.25 in.$, $b + 2t_a^{side} = 36.25 in.$, and $R = 0.5 in.$ Two stainless steel channels were externally bonded with adhesives having a thickness of approximately 1/8 in. ($t_a^{top/bottom}$ and t_a^{side}) on each surface of the pier cap specimens. To achieve a confinement effect due to the stainless steel reinforcement, flanges of the two channels were welded together using Gas Tungsten Arc Welding (GTAW). Figure 3.2 shows details of the externally bonded stainless steel reinforcement system.

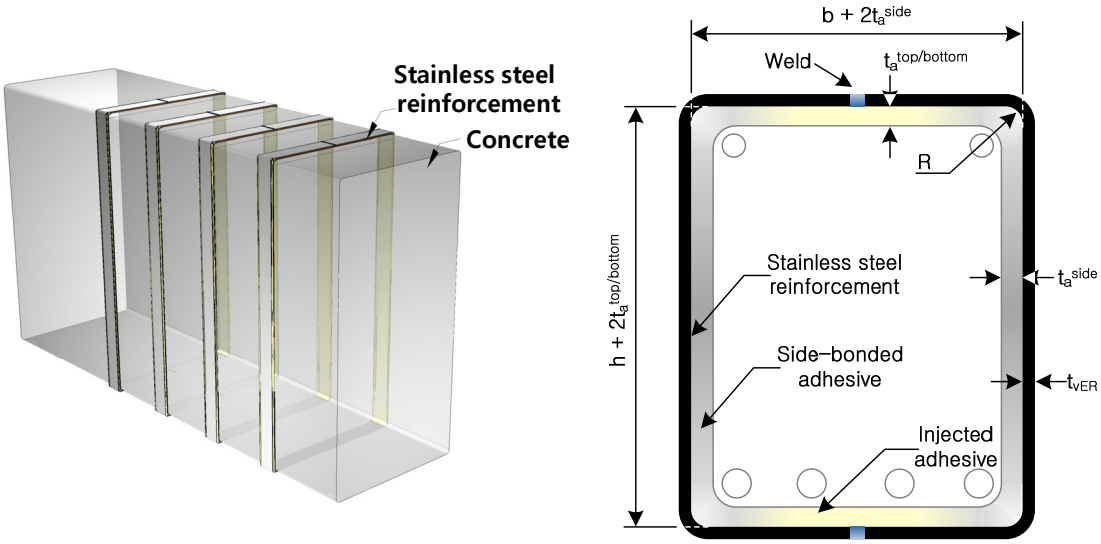

Figure 3.2- Externally bonded stainless steel reinforcement system

3.3 Strengthening Procedure

The externally bonded stainless steel reinforcement system was applied to the pier cap specimens. UNS S32002 duplex stainless steel coils having a width of 2.17 in. and a thickness of 0.055 in. were used for the externally bonded reinforcement system. The

procedure for bonding the stainless steel reinforcement was reported (*Zureick et al., 2014*) and is repeated here for clarity:

- Step 1 – Surface preparation: the concrete surface was grooved so that level 2 Concrete Surface Profiles (CSP2) recommended by the International Concrete Repair Institute (ICRI), was obtained (Figure 3.3).

(a) before (b) after

Figure 3.3- Surface preparation

- Step 2 – Side bonding of the stainless steel reinforcement: the fabricated channels were bonded on both sides of the specimen using Sikadur 30 adhesive. The thickness of the adhesive layer on each side of the specimens was approximately 1/16 in. Figure 3.4 shows the side bonding procedure in progress.

Figure 3.4- Side bonding

- Step 3 – Welding of stainless steel channel flanges: The top and bottom flanges of each of the two opposing stainless steel channels were welded using a GTAW process with a 1/8 in. thick ceramic backing plate, placed underneath the joint in the gaps between the channel flanges and the concrete surface. ER2209 stainless steel filler materials were used for the GTAW process.

Figure 3.5- Welding stainless steel bottom flanges

- Step 4 – Top and bottom epoxy injection: In the 1/8 in. gaps present between the flanges and the concrete surface, Sikadur Crack Fix adhesive was injected as shown in Fig. 3.6.

Figure 3.6- Adhesive Injection

3.4 Material Properties

Concrete: A maximum aggregate size of 1 in. was used for concrete. On the day of testing, the concrete properties of the beam and column were determined for each specimen by testing three concrete cylinders in accordance with ASTM C39/C39M and C469/C469M. These values are listed in Table 3.4.

Table 3.4- Material properties of concrete

Group	Specimen ID	Column	Beam	
		f_c' (psi)	f_c' (psi)	E_c (ksi)
A	AR014	-	3402	3849
	AR035	-	3599	-
B	BS00	6472	6164	4273
	BSR008	6738	6085	3880
	BSR014	6592	6024	3896
C	CS00	6427	6655	3794
	CSR018-1	6699	6258	3473
	CSR018-2	6471	6008	4034
	CSR035	6667	6419	4023

Steel reinforcement: In accordance with ASTM E8, yield strengths of No. 4, 6 and 10 A615/Grade 60 steel reinforcing bars were determined and listed in Table. 3.5. Stress vs. strain curves of the steel reinforcements are shown in Fig. 3.7.

Table 3.5- Material properties of steel reinforcements

Group	Yield strength of steel reinforcements f_y (ksi)		
	No.10	No.6	No.4
A	80.0	-	-
B	74.6	83.9	89.4
C	74.6	83.9	89.4

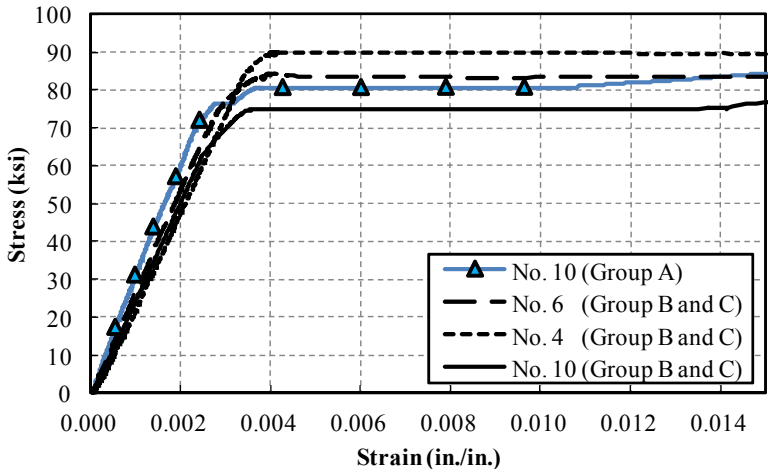

Figure 3.7- Stress vs. strain curves of steel reinforcement

Stainless Steel Reinforcement: To determine material properties of the stainless steel plates, tensile tests on five coupons of the parent material and five coupons welded at the center of the coupons were determined in accordance with ASTM E8. Test results from these coupons as reported by Zureick et al. (2014) are listed in Table 3.6. The stress-strain diagrams of tested coupons are shown in Fig. 3.8.

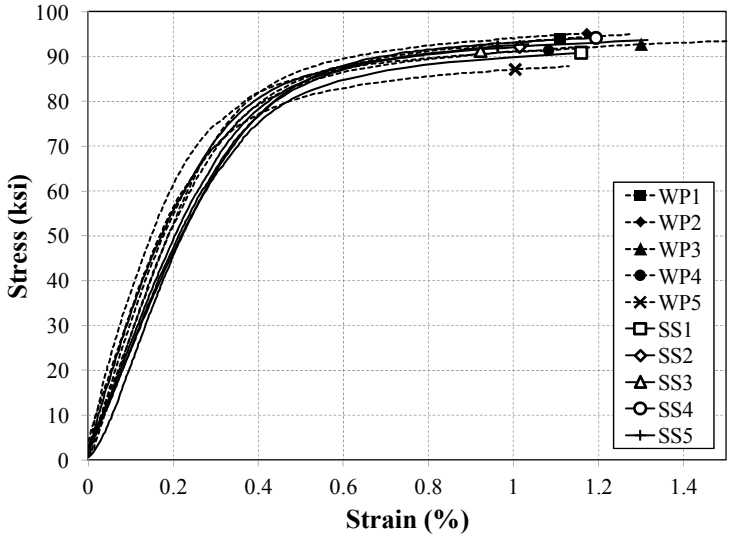

Figure 3.8- Stress vs. strain curve of stainless steel plates (*Zureick et al., 2014*)

Table 3.6- Dimensions and test results of stainless steel plates

Specimen ID	Width (in.)	Thickness (in.)	Yield Strength (ksi)		Tensile Strength (ksi)	Elongation in 2″ (%)
			0.2% offset method	0.005 strain		
WP1	0.503	0.0442	86.8	85.1	105.0	7.5
WP2	0.505	0.0495	87.6	86.9	109.6	10.5
WP3	0.505	0.0544	85.8	83.8	107.3	11.0
WP4	0.505	0.0529	85.0	85.5	104.1	10.0
WP5	0.504	0.0548	84.6	80.8	107.1	10.5
SS1	0.505	0.0548	84.8	82.0	112.3	26.5
SS2	0.497	0.0550	85.7	84.6	116.1	31.5
SS3	0.503	0.0560	86.9	85.4	113.8	28.0
SS4	0.504	0.0562	89.0	84.1	116.6	30.0
SS5	0.500	0.0556	87.4	83.8	115.8	31.0
Note: The 0.2% offset method was used in subsequent calculations						

3.5 Experimental Set-up and Measurements

Reinforced concrete pier cap specimens were tested under a simply supported boundary condition with a concentrated load applied at the center of the column (Fig. 3.9). The concentrated load was applied by a 1000 kip hydraulic ram, and the applied load was measured by a load cell mounted at the hydraulic ram. A string potentiometer was used to measure the deflection at the center span of the test specimens. Strains in the externally bonded stainless steel plates were measured by linear variables displacement transducers (LVDTs) mounted on the surfaces of the plates. In the compression zone of the test specimens, four horizontal LVDTs were mounted to obtain the strain distribution. To monitor strain variation in the longitudinal direction of the test specimens, both strain gauges mounted on the compression and tension reinforcements and a horizontal LVDT mounted at the location of the resultant tensile force were used. Figure 3.9 shows the test set-up and locations of LVDTs. The locations of strain gauges mounted on the steel reinforcing bars are shown in Fig. 3.10 and Table. 3.7.

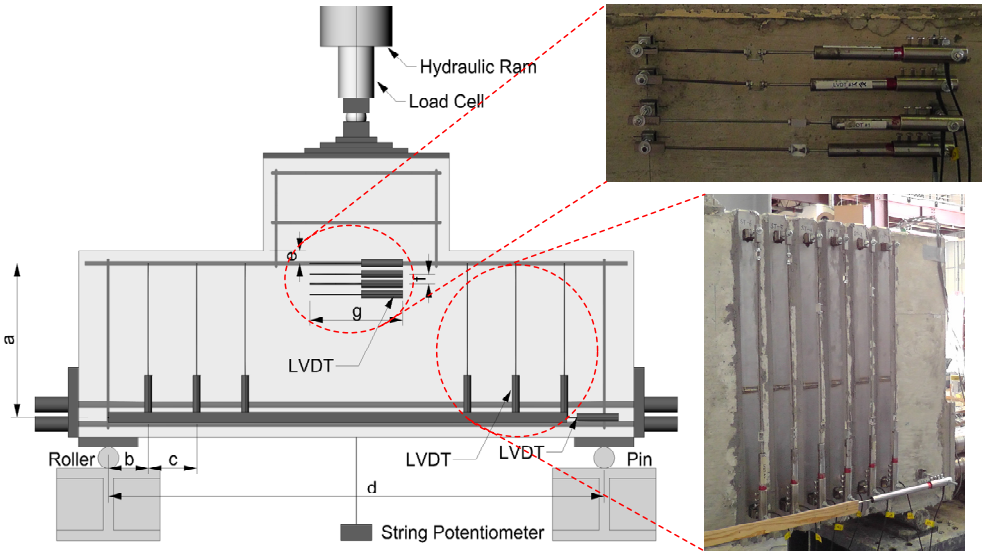

Figure 3.9- Measurements and Test Set-up

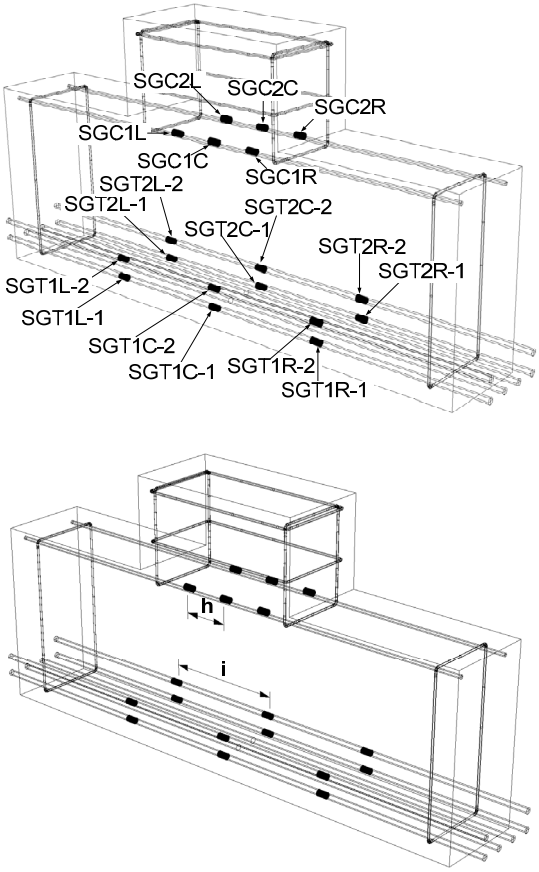

Figure 3.10- Locations of strain gauges

Table 3.7- Locations of measurement devices

Group	Specimen ID	a (in.)	b (in.)	c (in.)	d (in.)	e (in.)	f (in.)	g (in.)	h (in.)	i (in.)
A	AR014	29.75	7.76	9.38	96.0	2.38	2.0	16.0	8.0	30.25
	AR035	29.75	7.76	3.75	96.0	2.38	2.0	16.0	8.0	30.25
B	BS00	29.75	7.76	9.38	96.0	2.38	2.0	16.0	8.0	24.00
	BSR008	29.75	7.76	9.38	96.0	2.38	2.0	16.0	8.0	24.00
	BSR014	29.75	7.76	9.38	96.0	2.38	2.0	16.0	8.0	24.00
C	CS00	31.00	9.00	7.50	136.0	2.38	2.0	16.0	8.0	34.00
	CSR018-1	31.00	9.00	7.50	136.0	2.38	2.0	16.0	8.0	34.00
	CSR018-2	31.00	9.00	7.50	136.0	2.38	2.0	16.0	8.0	34.00
	CSR035	31.00	9.00	3.75	136.0	2.38	2.0	16.0	8.0	34.00

3.6 Test Results

All specimens were loaded monotonically to failure to investigate the behavior of the reinforced concrete pier caps with externally bonded stainless steel reinforcement systems. Observations and findings from all tests conducted are summarized below.

3.6.1 Failure Mode of Pier Cap Specimens

Failure of specimens AR014, BS00, BSR008, BSR014, and CS00 occurred after the formation of diagonal cracks. Failure of specimens CSR018-1, CSR018-2, and CSR035 occurred gradually after yielding of the longitudinal tension reinforcement. Table 3.8 summarizes loads at the formation of a diagonal crack, loads at failure, and failure modes. Crack patterns of the tested specimens are shown in Fig. 3.11.

Specimens AR014, BSR00, BSR008, and BSR014 developed diagonal cracks and continued to resist the applied load up to failure. For the specimens with externally bonded stainless steel system, AR014, BSR008, and BSR014, the diagonal crack occurred in the web and extended from the support to the column-pier cap re-entrant corner. This was followed by failure of the specimens. Figure 3.12 shows propagation of a diagonal crack for specimen BSR008.

Table 3.8- Diagonal cracking and collapse loads

Group	Specimen ID	Load at the formation of the diagonal crack (kips)	Load at failure (kips)	Failure mode
A	BL2*	631	631	Diagonal crack
	AR014	554	748	Diagonal crack and crushing at the compression zone
	AR035	871	**	Column crack and plate debonding
B	BS00	824	824	Diagonal crack
	BSR008	888	980	Diagonal crack and crushing at the compression zone
	BSR014	945	1050	Diagonal crack and crushing at the compression zone
C	CS00	508	508	Diagonal crack and crushing at the compression zone
	CSR018-1	514***	547	Yielding of tension reinforcements
	CSR018-2	481***	533	Yielding of tension reinforcements
	CSR035	520***	590	Yielding of tension reinforcements

* BL2 is the reference test specimen reported by Zureick et al. (2013)
** Diagonal cracks spread through the column
*** Load at yielding of the longitudinal tension reinforcement

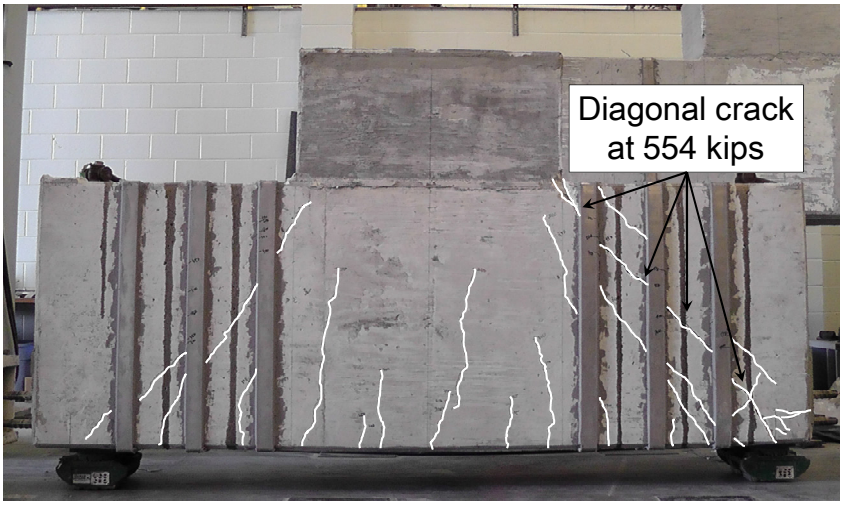

Figure 3.11-(a) Crack patterns of AR014 specimen

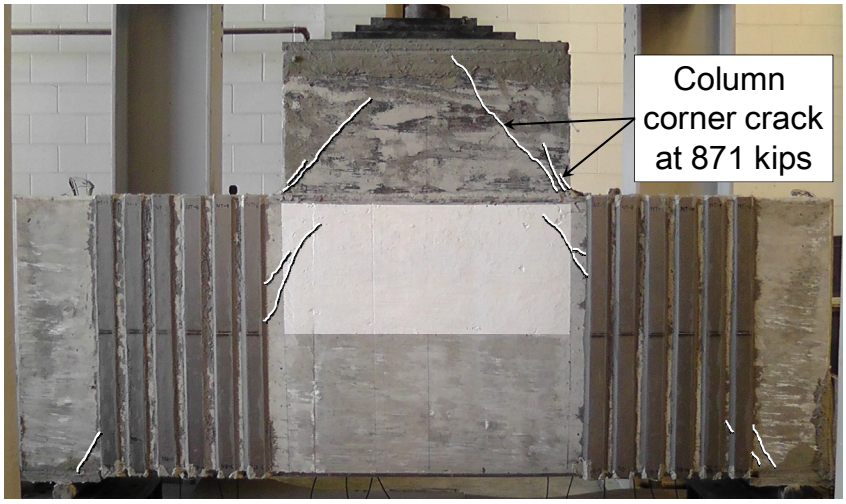

Figure 3.11-(b) Crack patterns of AR035 specimen

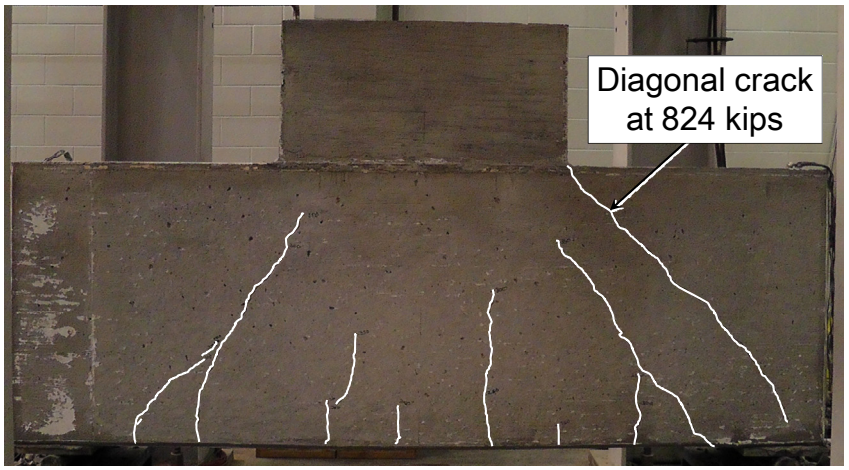

Figure 3.11-(c) Crack patterns of BS00 specimen

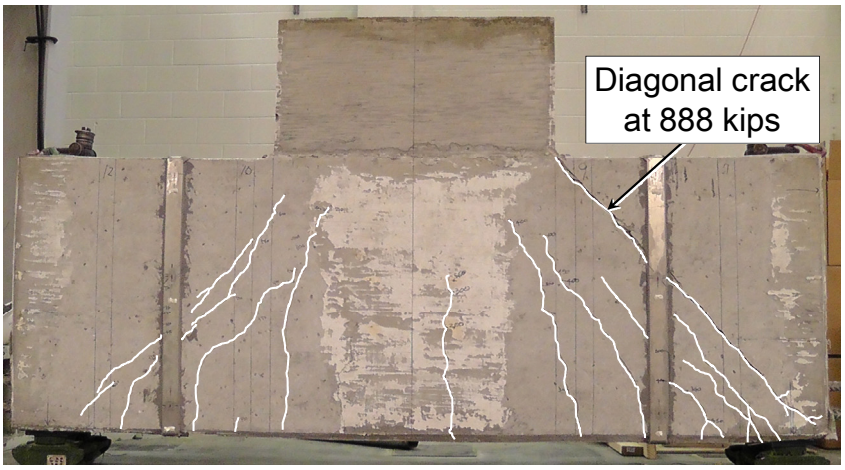

Figure 3.11-(d) Crack patterns of BSR008 specimen

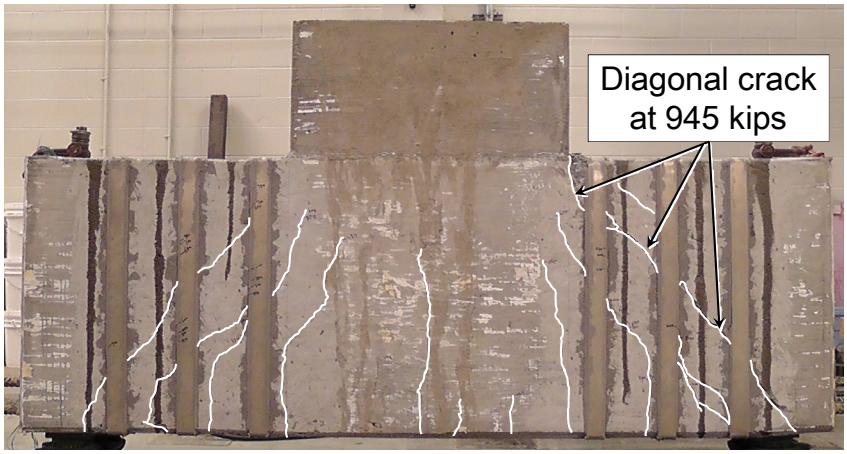

Figure 3.11-(e) Crack patterns of BS008 specimen

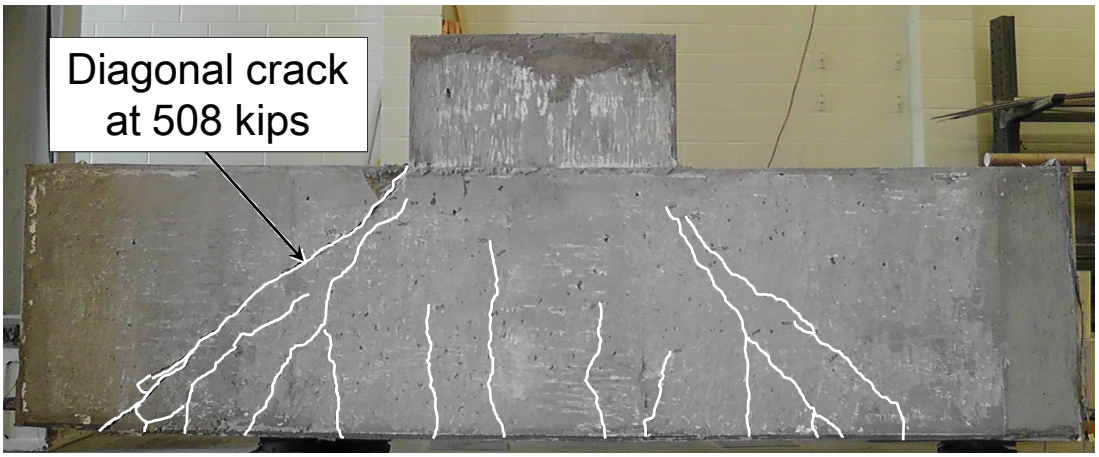

Figure 3.11-(f) Crack patterns of CS00 specimen

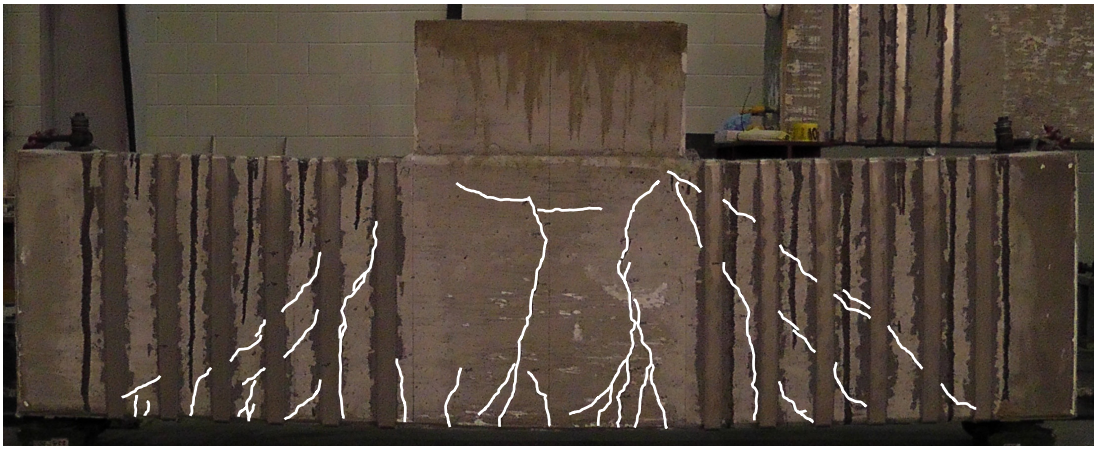

Figure 3.11-(g) Crack patterns of CSR018-1 specimen

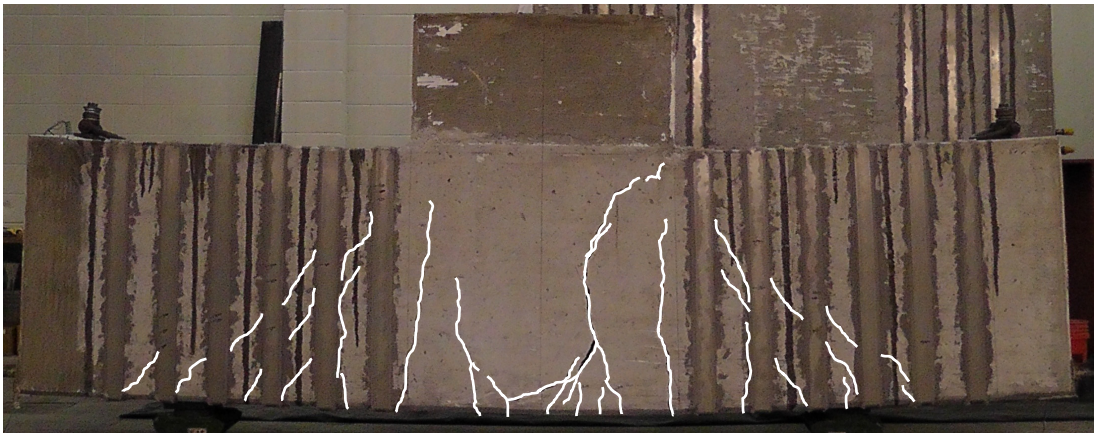

Figure 3.11-(h) Crack patterns of CSR018-2 specimen

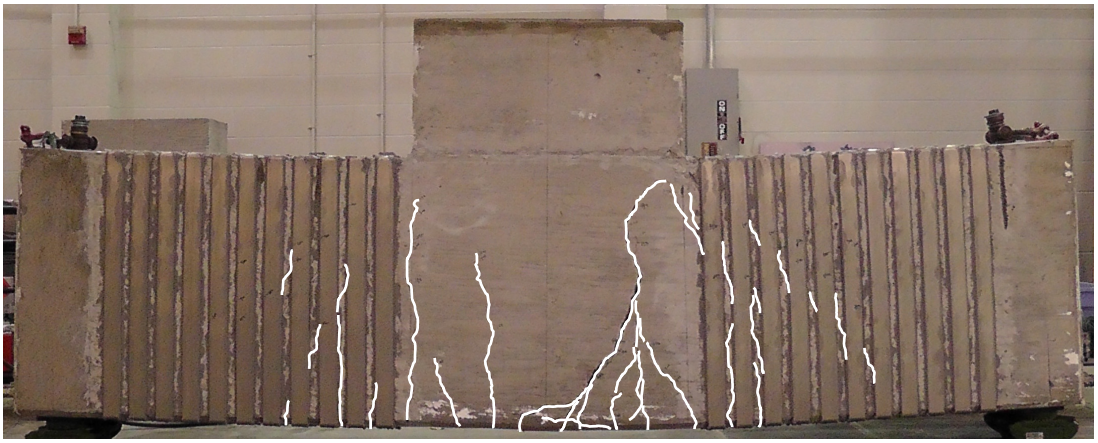

Figure 3.11-(i) Crack patterns of CSR018-2 specimen

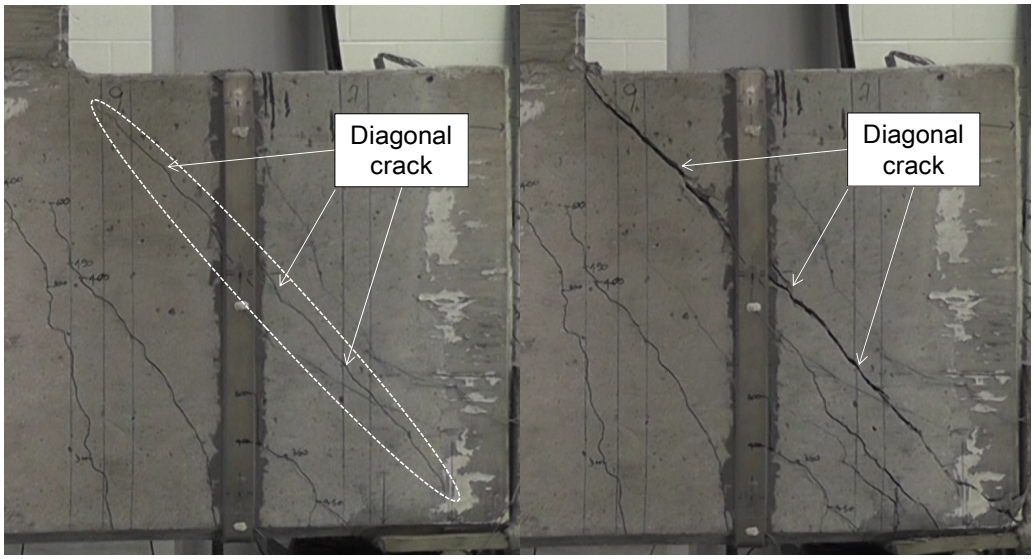

(a) Load at formation of diagonal crack (b) Load at failure

Figure 3.12- Progression of diagonal crack for BSR008 specimen

Specimen AR035, containing six externally bonded stainless steel plates on each shear span, showed plate debonding and column cracking. Figure 3.13 shows the column cracking at failure.

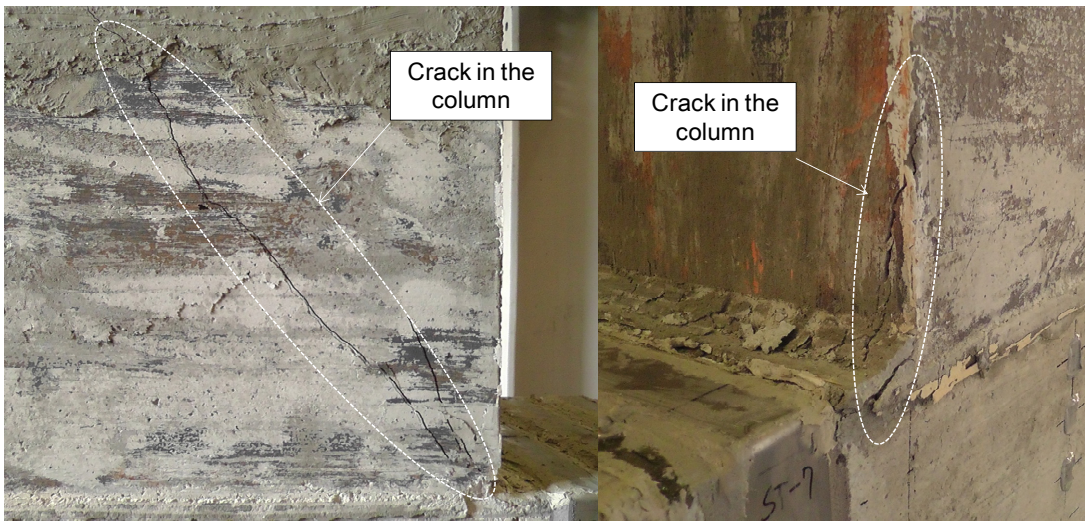

Figure 3.13- Column cracks for AR035 specimen

For the externally reinforced specimens in group C, CSR018-1, CSR018-2 and CSR035, a flexural failure mode was initiated by yielding of the longitudinal tension reinforcement at the mid-span. At approximately 200 kips, flexural cracks occurred at mid-span as shown in Fig. 3.14-(a). As the applied load increased up to 400 kips, the flexural cracks propagated along the entire span and diagonal cracks occurred within the shear span occurred (Fig. 3.14-(b)). At failure, the diagonal cracks did propagate through the shear span while flexural cracks that occurred at the mid-span spread though the entire depth of the specimens. Figure 3.14-(c) shows the flexural crack pattern when the failure occurred.

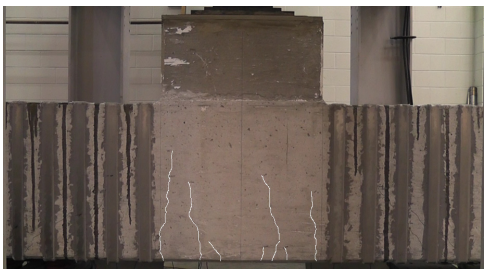

Figure 3.14-(a) Flexural cracks at the load of 200 kips (CSR018-2 specimen)

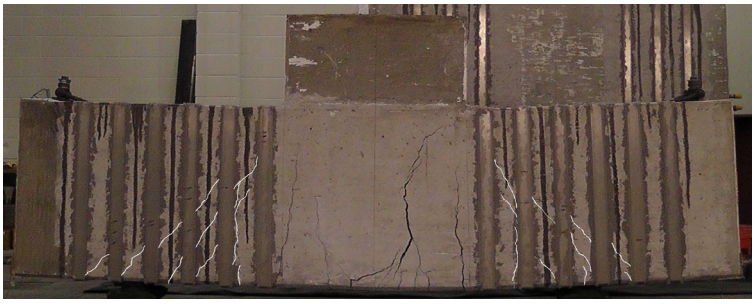

Figure 3.14-(b) Diagonal cracks at the load of 400 kips (CSR018-2 specimen)

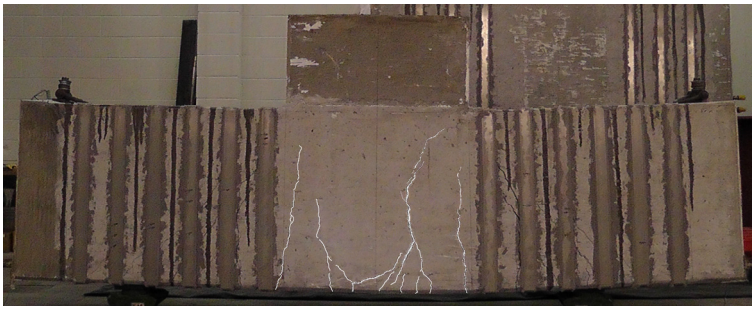

Figure 3.14-(c) Flexural cracks at failure (CSR018-2 specimen)

In specimens AR014, BSR008, BSR014, and CS00, the concrete crushed at failure. This was followed by the formation of diagonal cracks in the web. This observation agrees with the experimental works conducted by both Foster and Gilbert (1998) and Bechtel (2011). Figure 3.15 shows concrete crushing of specimens AR014, BS008, BSR014, and CS00.

(a) AR014 Specimen

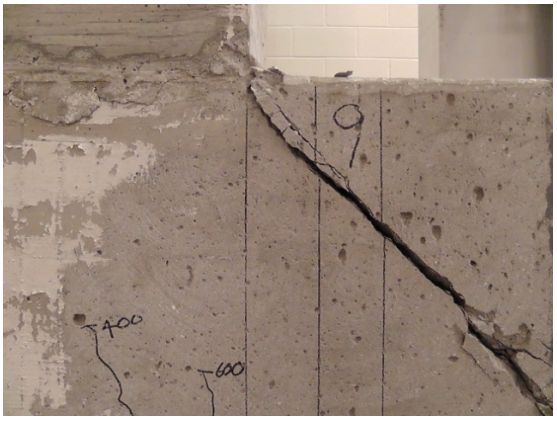


(b) BS008 Specimen


(c) BSR014 Specimen (d) CS00 Specimen

Figure 3.15- Concrete crushing at pier cap-column corner

In specimens, AR014, AR035, BSR008 and BSR014, progressive debonding of the stainless steel plates was observed. The debonding initiated at the location of diagonal cracks and propagated as the applied load increased. At failure, complete debonding of the plates was observed where splitting of concrete occurred (Fig. 3.16-(a) and 3.16-(b)).

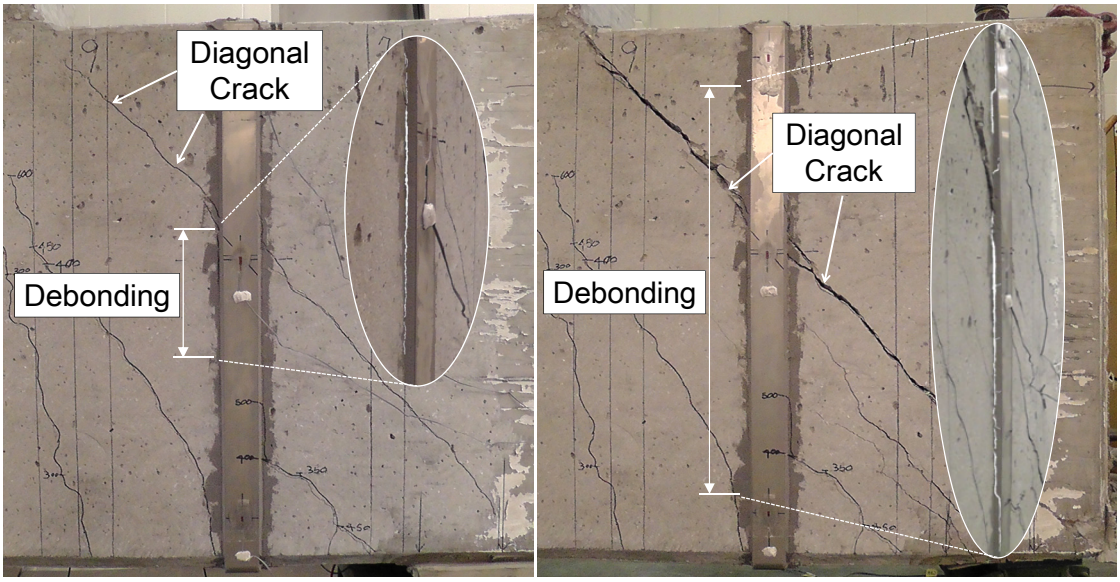

(a) Load at formation of diagonal crack (b) Load at failure

Figure 3.16- Progression of plate debonding for BSR008 specimen

3.6.2 Load - Deflection Behavior

The externally bonded stainless steel reinforcement system was shown to be an effective method for increasing the load carrying capacity of reinforced concrete pier caps. Load-carrying capacity of specimens with externally bonded stainless steel plates increased even after onset of the diagonal cracks. Load vs. deflection curves of tested specimens are presented in Fig. 3.17-(a), 3.17-(b), and 3.17-(c). Figure 3.18 shows the loads at which the diagonal crack was formed and failure occurred. The externally bonded stainless steel plates delayed failure of the specimens in Group A and B. The externally reinforced specimens in group C failed in flexure after yielding of longitudinal tension reinforcements. For this group of specimens, the amount of external reinforcement had an insignificant effect on increasing the load-carrying capacity. However, such reinforcements successfully altered the failure mode and formed yielding of the longitudinal tension reinforcement prior to the formation of the diagonal cracks that occurred in specimen CS00.

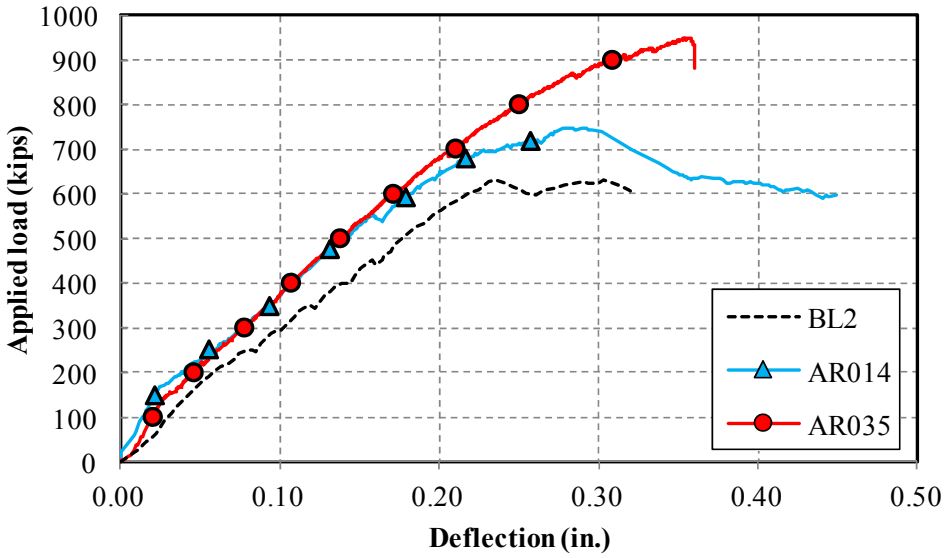

Figure 3.17-(a) Load vs. deflection curves for group A specimens

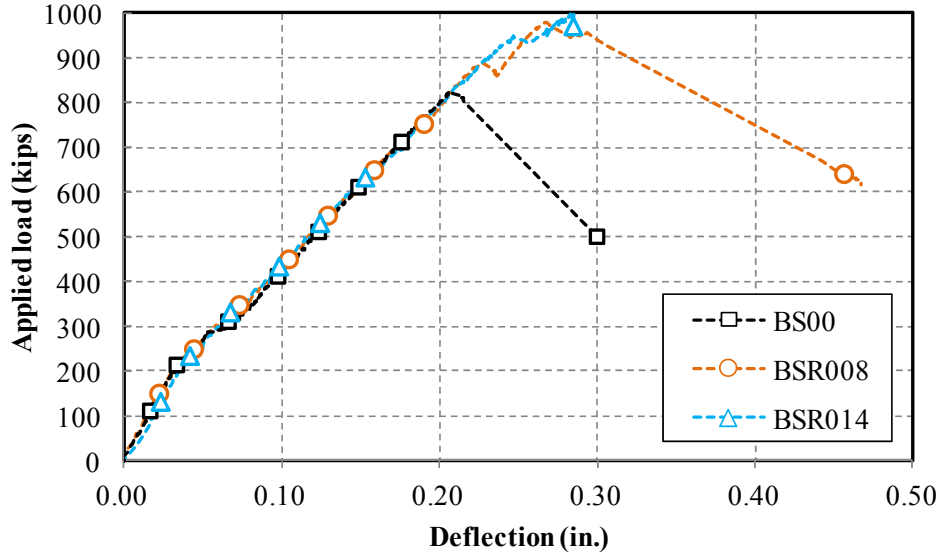

Figure 3.17-(b) Load vs. deflection curves for group B specimens

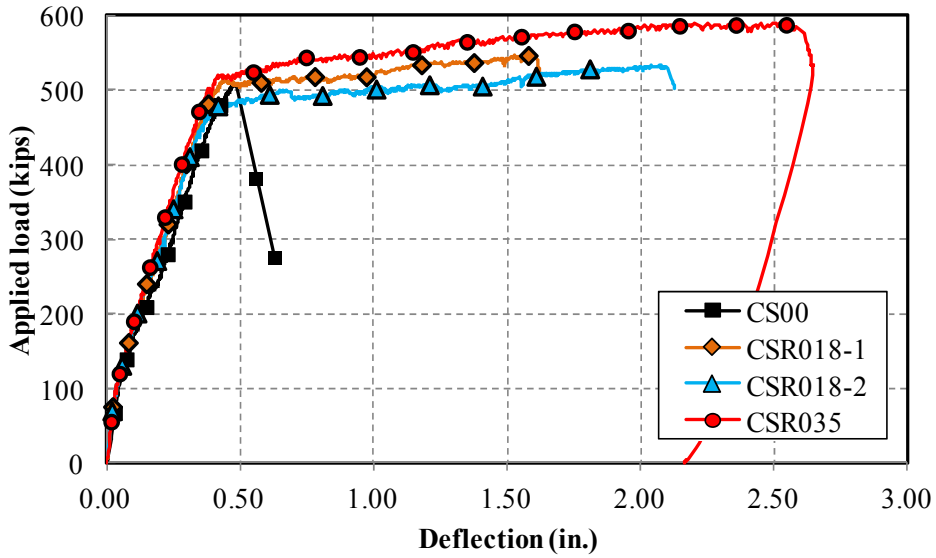

Figure 3.17-(c) Load vs. deflection curves for group C specimens

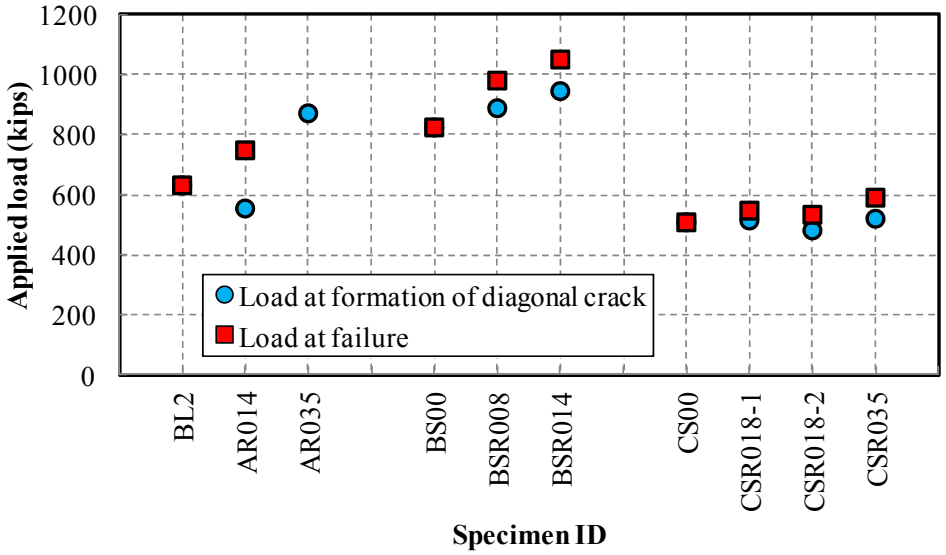

Figure 3.18- Loads at the formation of the diagonal crack and failure

3.6.3 Strains in the Stainless Steel External Reinforcement

Strains in the externally bonded stainless steel plates were measured using vertically mounted LVDTs. The vertical strains within the shear span increased as the applied load increased. Larger strain values were measured near the middle of the shear

span than near the supports and column. Cao et al. (2005), who examined reinforced concrete beams strengthened with externally bonded FRP composites, reported strain variations having the maximum value at mid-shear span. The larger strains near the mid-shear span demonstrated that the plates bonded in the middle of the shear span contributed the most to load-carrying capacity of the pier cap specimen. This is due to the initiation of a diagonal crack that initiated near the middle of the web and propagated toward the column and the support. Figure 3.19 shows the variation of vertical strains for BSR008 specimen. The externally bonded stainless steel plates started to resist the applied load when concrete tied arch behavior became dominant. An increase in the vertical strains was observed at a load greater than 300 kips at which the tied arch mechanism initiated. The plots for the variation of vertical strains in the stainless steel plates of the all test specimens are shown in Appendix C.

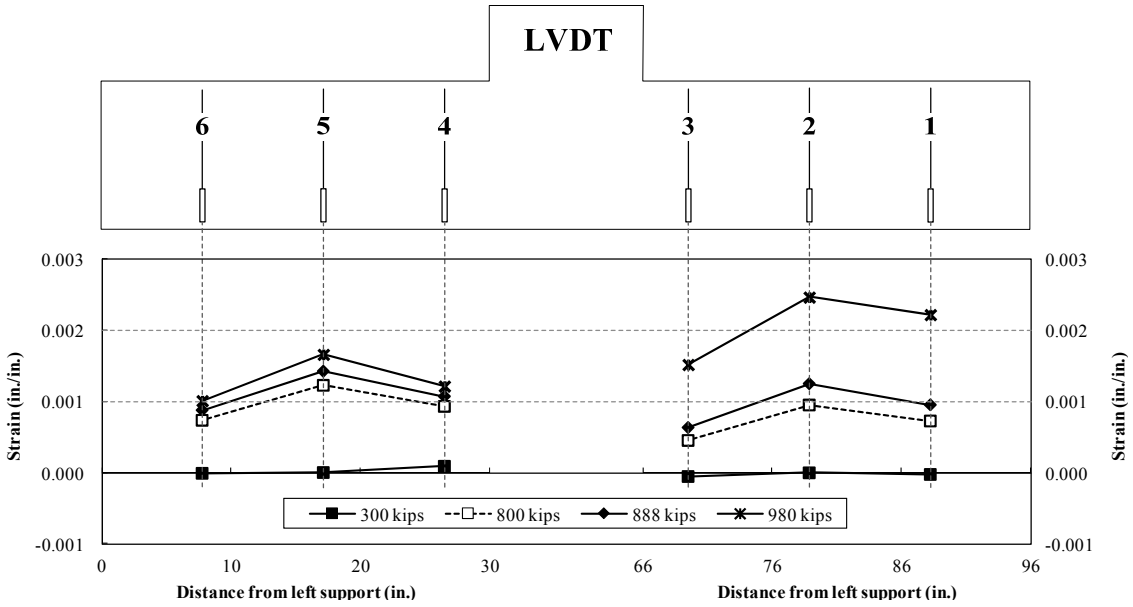

Figure 3.19- Variation of vertical strains in stainless steel plates for BSR008 specimen

Maximum vertical strains within the shear span at the load where the diagonal crack formed and when failure occurred are listed in Table. 3.9. It is to be noted that the vertical strains in the stainless steel plates did not reach the yield strain of the stainless

steel material throughout the entire duration of the tests. Strains in the stainless steel plates bonded near the column exhibited larger values than those in the plates near the support. The maximum strains in the stainless steel plates within the shear span at the formation of diagonal crack and failure are shown in Fig. 3.20. The average value of the maximum strains at failure, ε_{vER}, was 0.003.

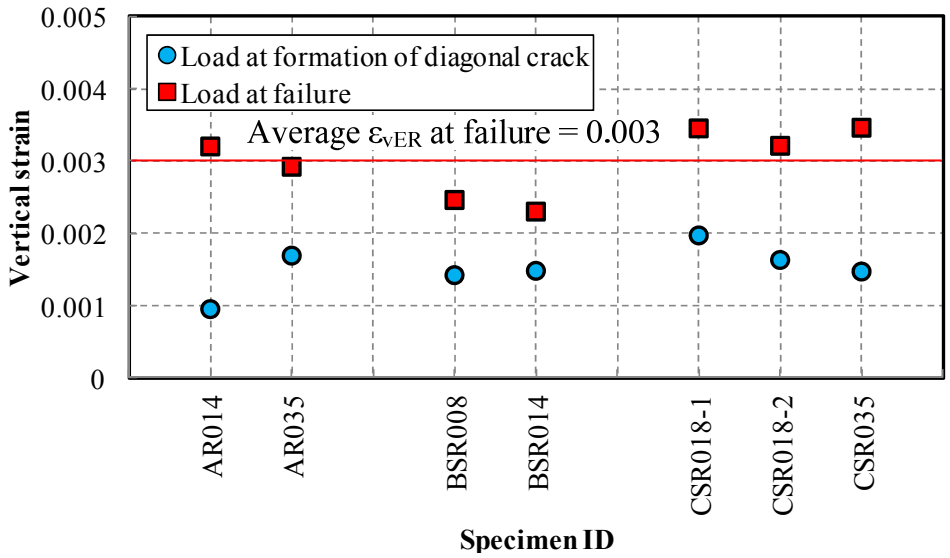

Figure 3.20- Strains in the externally bonded transverse reinforcement

Table 3.9- Maximum strains in the externally bonded reinforcement

Group	Specimen ID	Maximum strains	
		Load at the formation of the diagonal crack	Load at failure
A	BL2*	Not recorded	Not recorded
	AR014	0.00095	0.00320**
	AR035	0.00169	0.00292
B	BS00	0.00122	0.00122
	BSR008	0.00142	0.00246
	BSR014	0.00148	0.00230
C	CS00	0.00418	0.00418
	CSR018-1	0.00197	0.00345
	CSR018-2	0.00163	0.00321
	CSR035	0.00147	0.00346**

* BL2 is the reference test specimen reported by Zureick et al. (2013)
** The maximum vertical strain occurred at external reinforcement near the column

Throughout the tests of group specimens A, B, and C having externally bonded stainless steel strips, the maximum vertical strains in the strips were plotted with respect to the applied load. Figure 3.21-(a), 3.21-(b), and 3.21-(c) show the maximum vertical strains vs. applied load for the specimens in group A, B and C respectively. Specimen BSR014 having $\rho_{vER} = 0.14\%$ showed smaller strains in the stainless steel strips than specimen BSR008 having $\rho_{vER} = 0.08\%$. This behavior was also observed from specimens in groups A and C. Vertical deformation of the pier cap specimens was resisted by the externally bonded reinforcement system, thus little strain variation was observed.

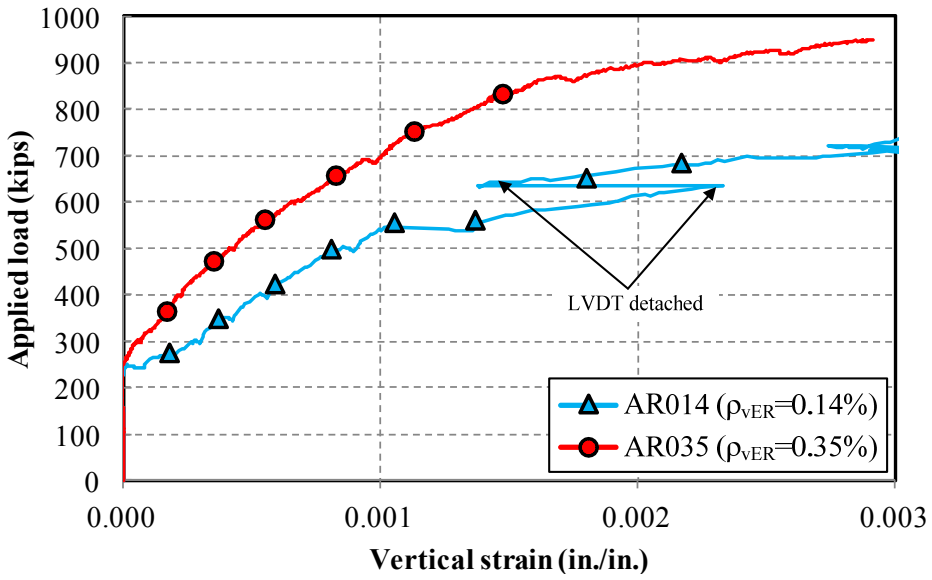

Figure 3.21-(a) Maximum vertical strain vs. applied load for Group A specimens

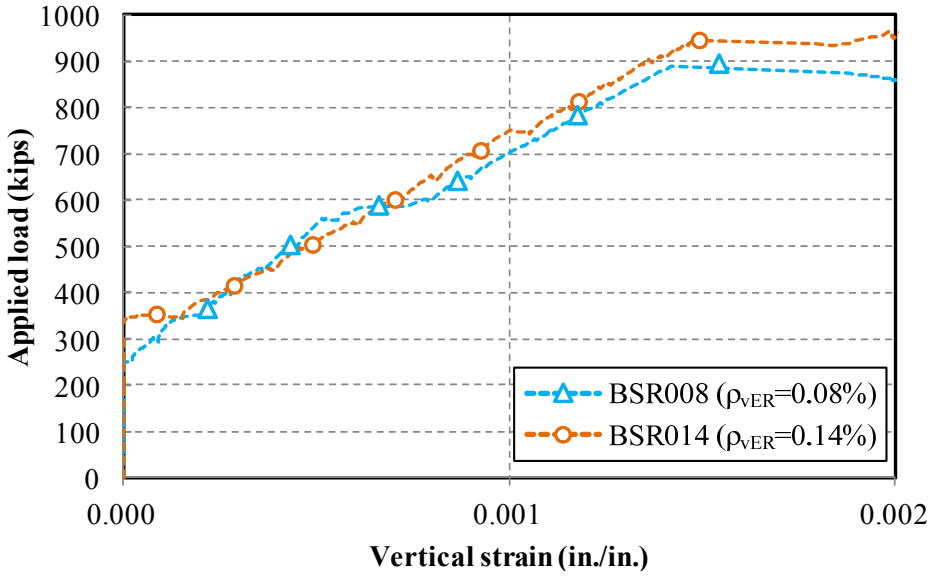

Figure 3.21-(b) Maximum vertical strain vs. applied load for Group B specimens

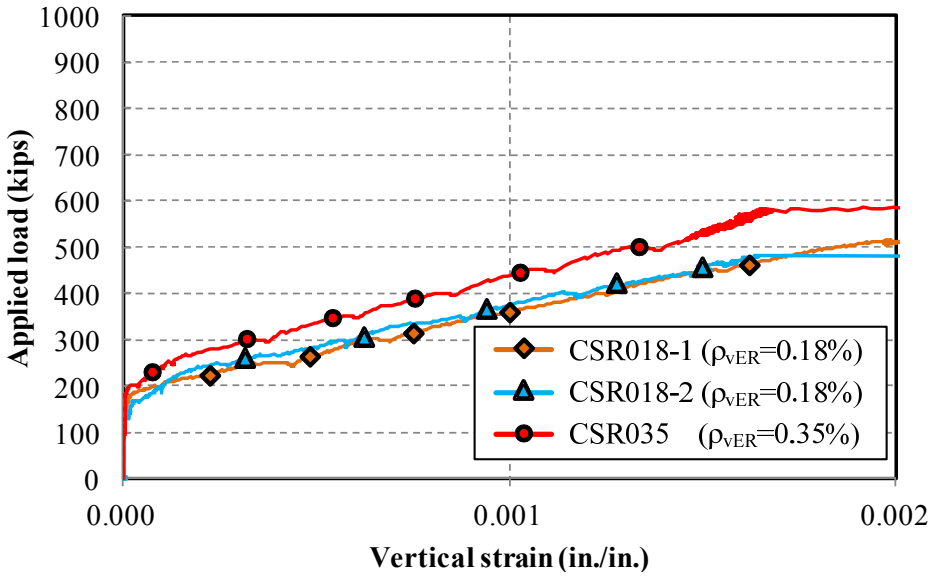

Figure 3.21-(c) Maximum vertical strain vs. applied load for Group C specimens

3.6.4 Strains in the Longitudinal Steel Reinforcement

Strains in the longitudinal tension reinforcement when the diagonal cracks formed and when failure occurred are shown in Table 3.10. The variation of the applied load vs. strain in longitudinal tension reinforcement is shown in Fig. 3.22-(a) and 3.22-(b) for specimens BSR008 and CSR035 respectively.

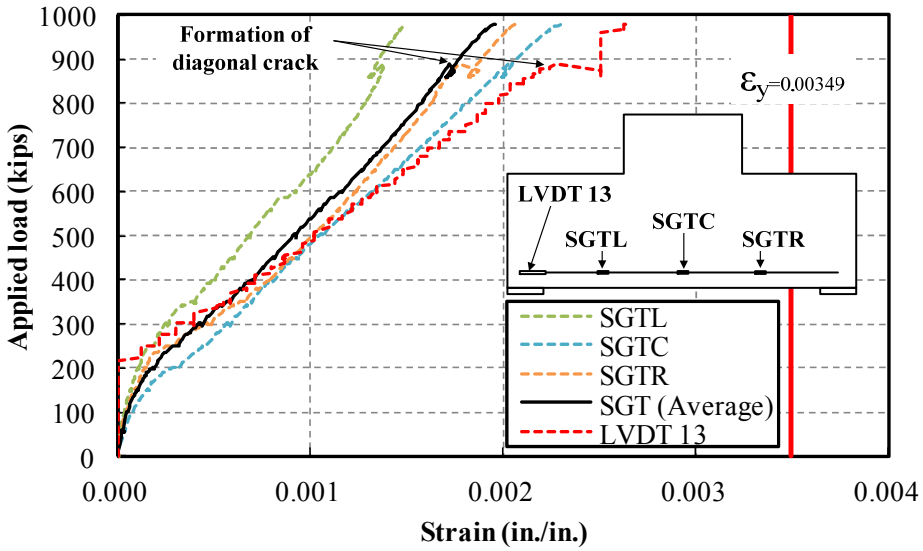

Figure 3.22-(a) Applied load vs. strain in longitudinal tension reinforcement for specimen BSR008

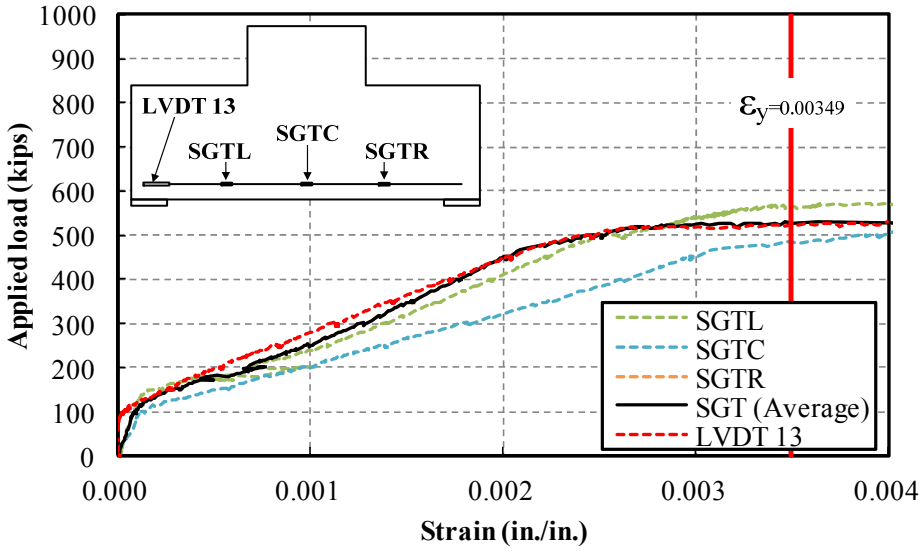

Figure 3.22-(b) Applied load vs. strain in longitudinal tension reinforcement for specimen CSR035

Table 3.10- Strains in longitudinal tension reinforcements

Group	Specimen ID	Load at the formation of diagonal crack		Load at failure	
		SGT (Average)	LVDT 13	SGT (Average)	LVDT 13
A	BL2*	0.00202	-	0.00202	-
	AR014	0.00132	0.00151	0.00187	0.00255
	AR035	0.00231	0.00250	0.00264	0.00301
B	BS00	0.00144	0.00197	0.00144	0.00197
	BSR008	0.00173	0.00228	0.00195	0.00263
	BSR014	0.00200	0.00265	0.00221	0.00317
C	CS00	0.00255	0.00313	0.00255	0.00313
	CSR018-1	0.00244	0.00286	$\varepsilon > \varepsilon_y$ (0.00349)	$\varepsilon > \varepsilon_y$ (0.00349)
	CSR018-2	0.00142	0.00268	$\varepsilon > \varepsilon_y$ (0.00349)	$\varepsilon > \varepsilon_y$ (0.00349)
	CSR035	0.00271	0.00286	$\varepsilon > \varepsilon_y$ (0.00349)	$\varepsilon > \varepsilon_y$ (0.00349)

* BL2 is the reference test specimen reported by Zureick et al. (2013)

When examining the measured strain data of specimens in group A and B, one would note that 1) the maximum strain in longitudinal reinforcing bars did not exceed the yield strains of steel reinforcing bars when the specimens reached their ultimate load-carrying capacities and 2) the strain values in the longitudinal reinforcing bars of the strengthened specimens were higher than those of the reference specimens. For specimens CSR018-1, CSR018-2 and CSR035, flexural failure occurred after yielding of the steel reinforcing bars at mid-span. The externally bonded reinforcement system increased contribution of longitudinal tension reinforcement by increasing the resistance of vertical deformation within the shear span.

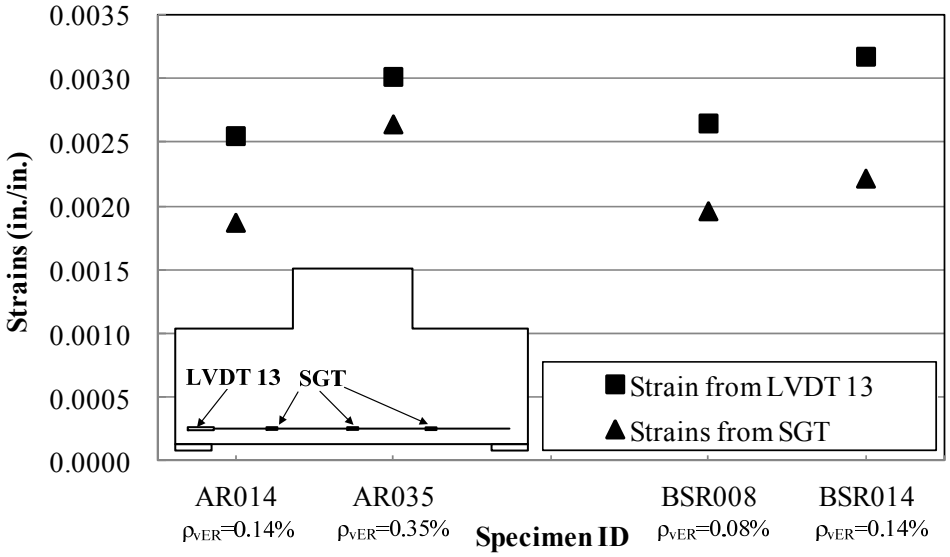

Figure 3.23-(a) Maximum strain in the longitudinal tension reinforcement at failure

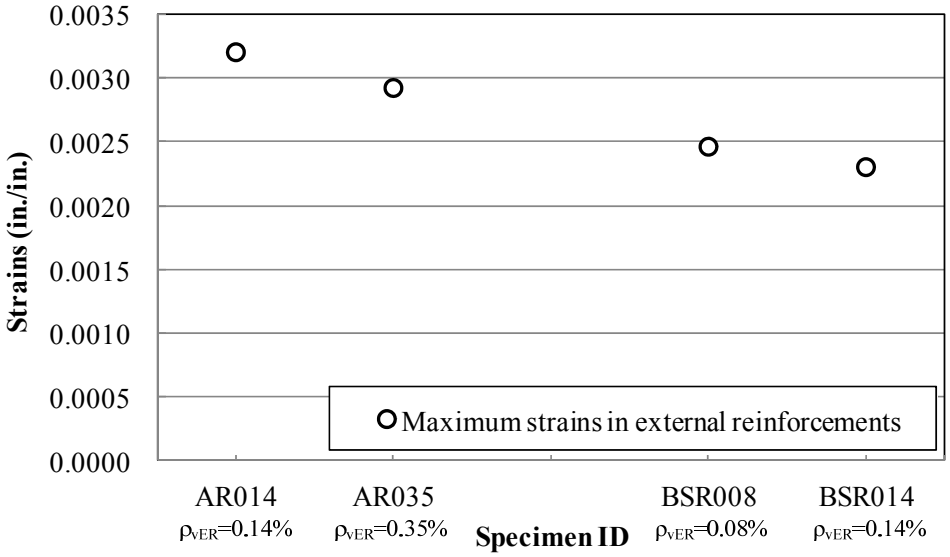

Figure 3.23-(b) Maximum strain in the externally bonded reinforcement at failure

3.6.5 Strut Angles

The strut angle of the pier cap specimens with externally bonded stainless steel systems was calculated from the vertical reaction force (R_v) at the support, and horizontal tension force of the longitudinal tension reinforcement (R_h) as shown in Figure 3.24. The

calculated strut angles at the load when the diagonal crack formed are shown in Table. 3.11.

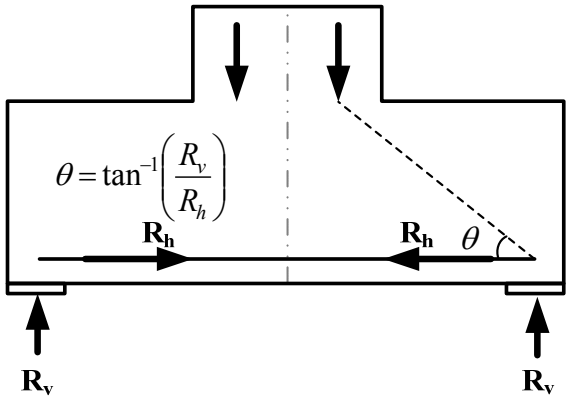

Figure 3.24-Calculation of strut angle

Table 3.11- Strut angles at limit state load

Group	Specimen ID	Strut angle at the load of formation of diagonal crack	
		SGT	LVDT 13
A	AR014	41.7˚	37.9˚
	AR035	40.0˚	38.3˚
B	BS00	56.5˚	47.4˚
	BSR008	53.4˚	44.9˚
	BSR014	50.9˚	43.5˚
C	CS00	38.1˚	34.9˚
	CSR018-1	-	-
	CSR018-2	-	-
	CSR035	-	-

The strut angles of CSR018-1, CSR018-2, and CSR035 are not reported in Table 3.11 because failure of these specimens occurred in flexure prior to the formation of the diagonal cracks. When calculating the strut angles using the strain measurements obtained from LVDT 13, it was found that the strut angles are in the range between α_1 and α_2 shown in Fig. 3.25. Thus, the load applied through the column can be resolved into two components, each of which is located within region R shown in Fig. 3.25.

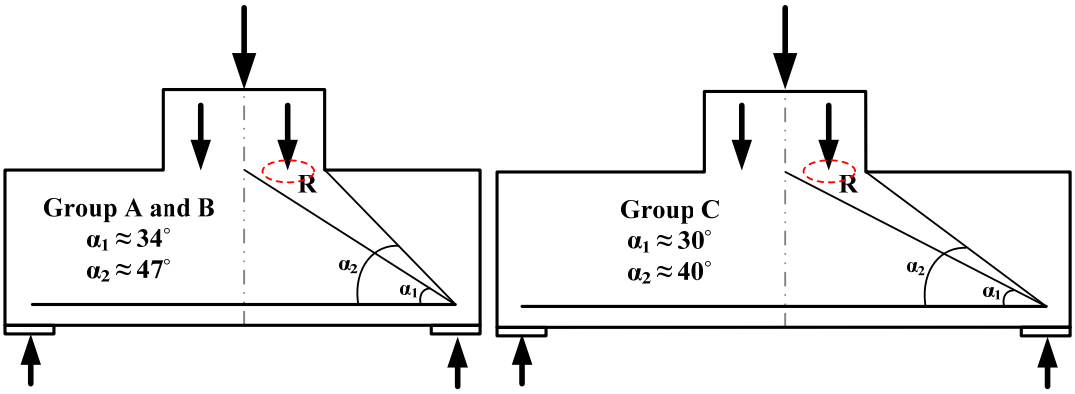

Figure 3.25- Estimated ranges of strut angles

The variation of strut angle with respect to the applied load for specimen AR014 is shown in Fig. 3.26. For group A and B specimens, the strut angle decreased at an approximate load of 300 kips. For group C specimens, a decrease in strut angle was shown at an approximate load of 200 kips. Thus, concrete tied arch mechanism formed at the load of 200 kips and became dominant load-carrying mechanism until failure.

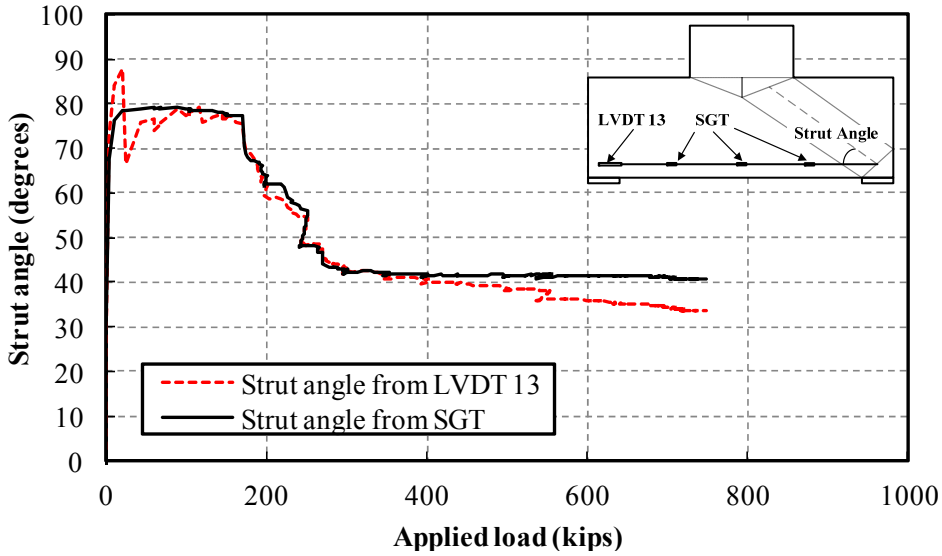

Figure 3.26-Strut angle vs. applied load for specimen AR014

3.6.6 Compressive strains in the compression zone

Compressive strains in the compression zone were measured by six strain gauges mounted in the compression reinforcing bars and four horizontal LVDTs mounted on the

surface of the specimens. Throughout the tests, the strains measured by strain gauges mounted on the longitudinal compression steel reinforcement indicated that the strain values near the pier cap-column corner were greater than those at mid-span. Figure 3.27-(a), 3.27-(b), 3.27-(c), and 3.27-(d) show the compressive strain variations with respect the applied load for specimens BS00, BSR008, BSR014 and CS00, respectively. The specimens, BSR008, BSR014 and CS00 which showed the failure mode of the formation of diagonal cracks and concrete crushing, had larger compressive strains at SGCL and SGCR than SGCC. However, specimen BS00, which failed due to the formation of a diagonal crack, showed negligible strain variations were observed among SGCL, SGCR, and SGCC. Stress concentration near column-pier cap corner was experimentally shown by strain measurements in the compression steel reinforcement.

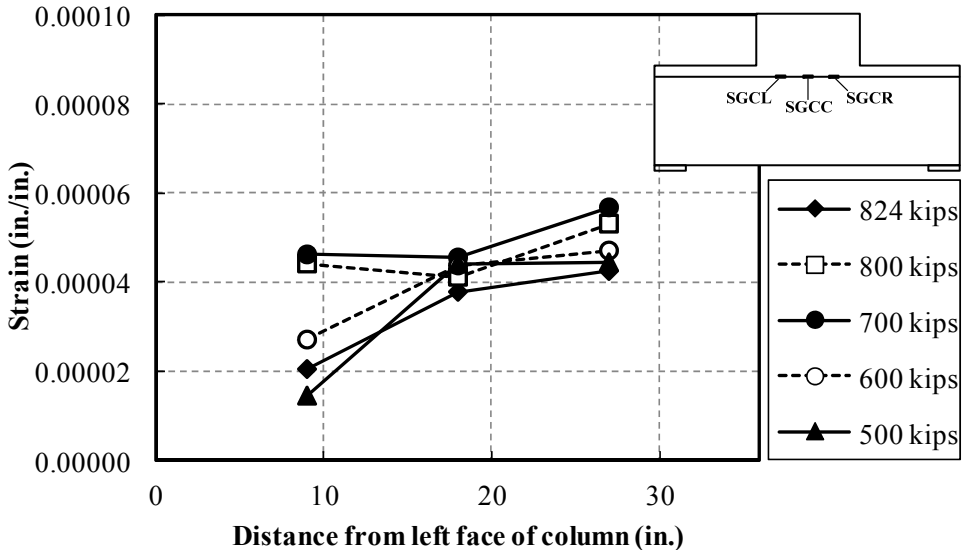

Figure 3.27-(a) Compressive strains in compression steel reinforcements for specimen BS00

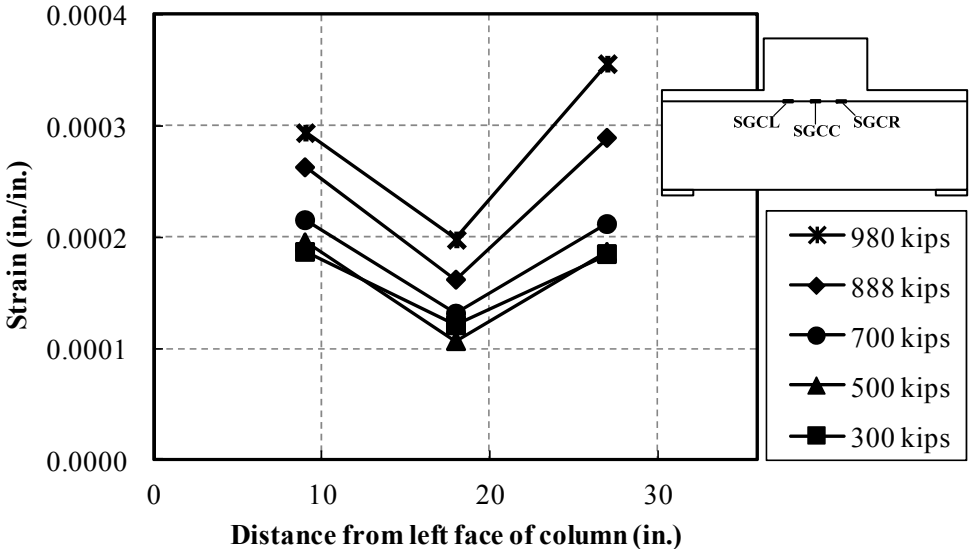

Figure 3.27-(b) Compressive strains in compression steel reinforcements for specimen BSR008

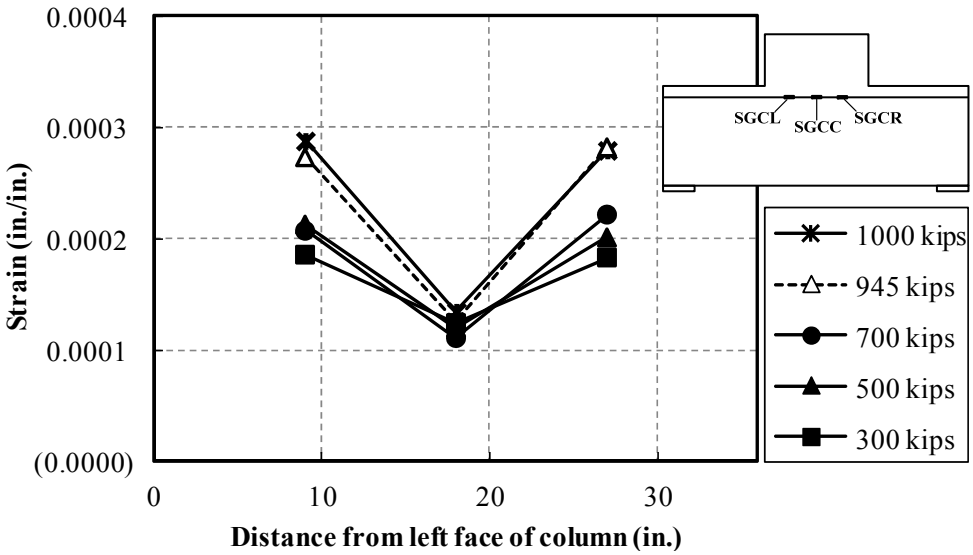

Figure 3.27-(c) Compressive strains in compression steel reinforcements for specimen BSR014

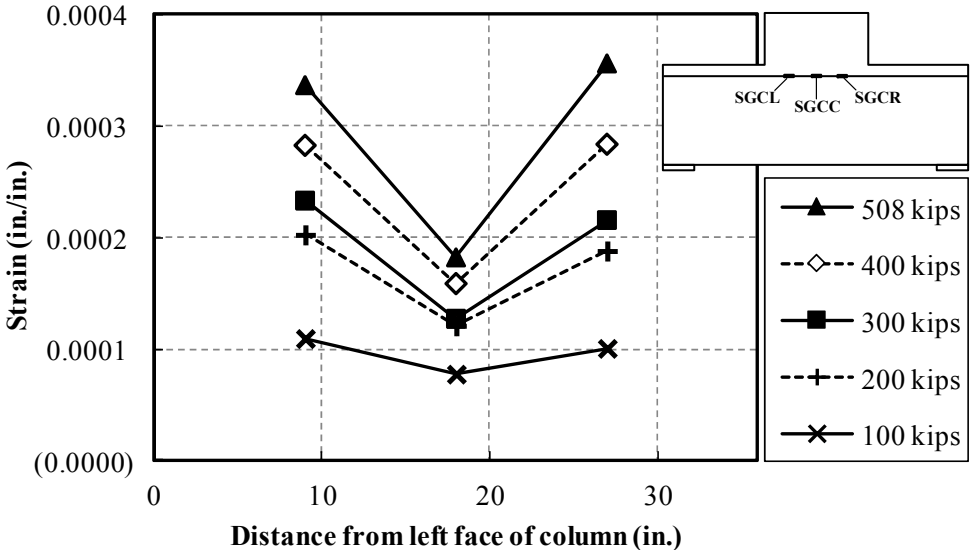

Figure 3.27-(d) Compressive strains in compression steel reinforcements for specimen CS00

Horizontal strains in the compression zone were measured by the four horizontal LVDTs to estimate the depth of the compression zone. For specimen AR014 that showed a diagonal crack failure mode, strain variations in the compression zone as a function of applied load are shown in Fig. 3.28. Compressive strain variations for AR035, BS00, BSR008, BSR014, and CS00 specimens are presented in Appendix F.

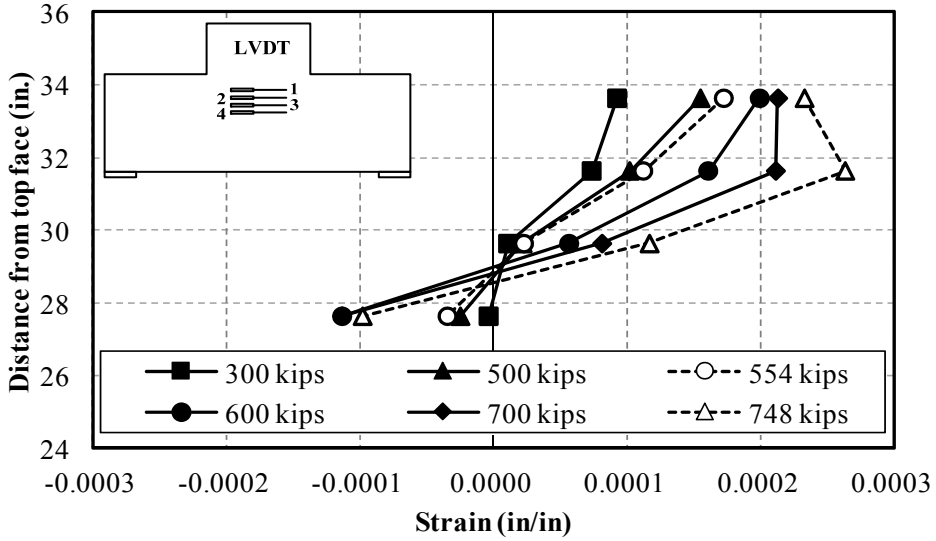

Figure 3.28- Strain variation at compression zone

CHAPTER 4

ANALYTICAL APPROACHES

In this chapter, two new proposed analytical models for shear strength of reinforced concrete bridge pier caps with externally bonded reinforcement systems are described. The first analytical model was developed based on the Zararis' approach, and the second analytical procedure is based on the superposition of two strut-and-tie models.

4.1 Proposed Mechanics-Based Approach

A mechanic-based analytical model for shear strength of reinforced concrete bridge pier caps externally bonded reinforcement system was developed from the work by Zararis (2003). Zararis' analytical model is advantageous, in that it takes into account the concrete tied-arch behavior. This model was modified and extended to cover reinforced concrete components with externally bonded reinforcement systems.

4.1.1 Development of Proposed Mechanics-Based Approach

To derive an analytical method for a reinforced concrete bridge pier cap with external reinforcement systems, a reinforced concrete cantilever pier cap shown in Fig. 4.1 is considered.

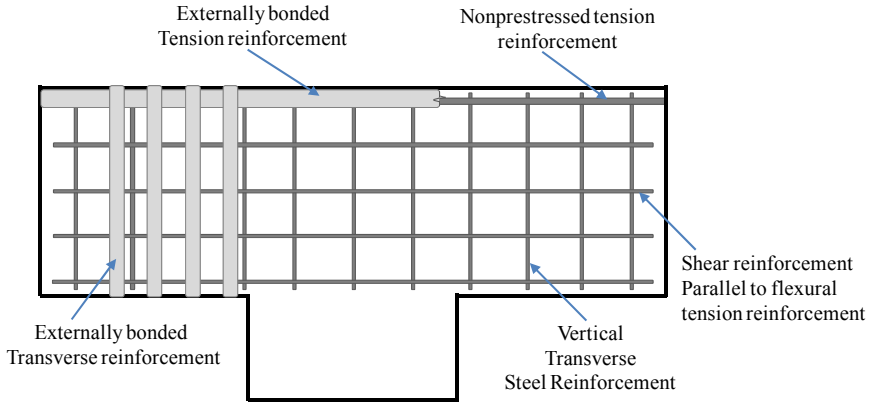

Figure 4.1- Details of a reinforced concrete pier cap with externally bonded reinforcement system

The concrete pier cap member contains internal tension, compression and transverse steel reinforcement as well as externally bonded vertical, horizontal, and longitudinal reinforcement. In the successive sections, the following notations are adopted.

a = Shear span

a_s = Effective shear span

c_s = The distance between the compression face and tip of diagonal crack

c = The distance between the compression face and tip of flexural crack

d_e = Effective depth of the component

L_c = Width of the column

A_s = Cross-sectional area of the longitudinal tension reinforcement

A'_s = Cross-sectional area of the longitudinal compression reinforcement

f_t = Tensile stress of the longitudinal tension reinforcement

f_c = Compressive stress of concrete

Development of the proposed mechanics-based approach will be established based on the following assumptions:

1- Stress distribution in the compression zone

For computation of the depth of compression zone at the onset of a diagonal crack, linear elastic stress distribution of concrete was assumed, and the location of the neutral axis was determined from the transformed section due to flexural cracks.

2- Effective shear span

In Zararis' work, shear span was defined as the distance between the resultant forces at a support and column. In accordance to the experimental work presented

in section 3.6.5, the effective shear span was assumed to be $a_s = a + L_c/4$ as shown in Fig. 4.2.

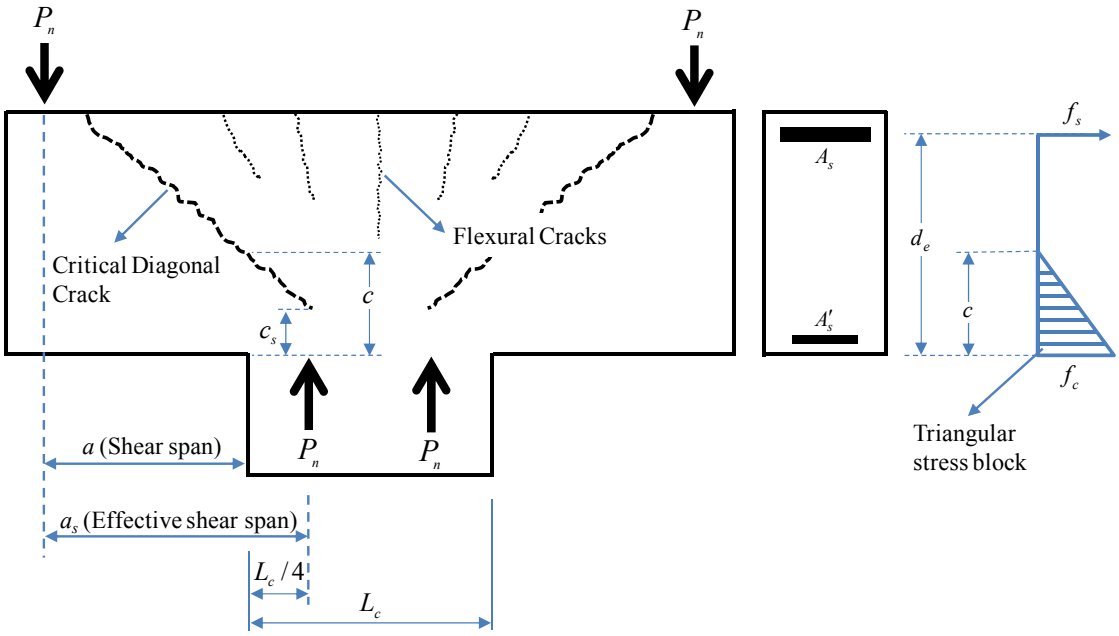

Figure 4.2- Reinforced concrete pier cap with the rectangular stress block

State of Stress in a Pier Cap after Formation of Diagonal Crack

As shown in Fig. 4.3, once a diagonal crack occurs, orthogonal reinforcing bars will be strained to resist a deformation or rupture of the member. The strain in steel reinforcement at the crack location ε_{cr} can be written as the mean crack width w_m divided by the mean crack spacing s_m as written in the form:

$$\varepsilon_{cr} = w_m / s_m \tag{4.1}$$

Similarly, the longitudinal strain in the x-direction can be written as the horizontal mean crack width divided by the mean horizontal crack spacing as follows:

$$\varepsilon_x = \frac{w_x}{s_x} = \frac{w_m \cos\theta}{s_m / \cos\theta} \tag{4.2}$$

From Eq. 4.1 and 4.2, ε_x can be written as

$$\varepsilon_x = \varepsilon_{cr} \cos^2 \theta \tag{4.3}$$

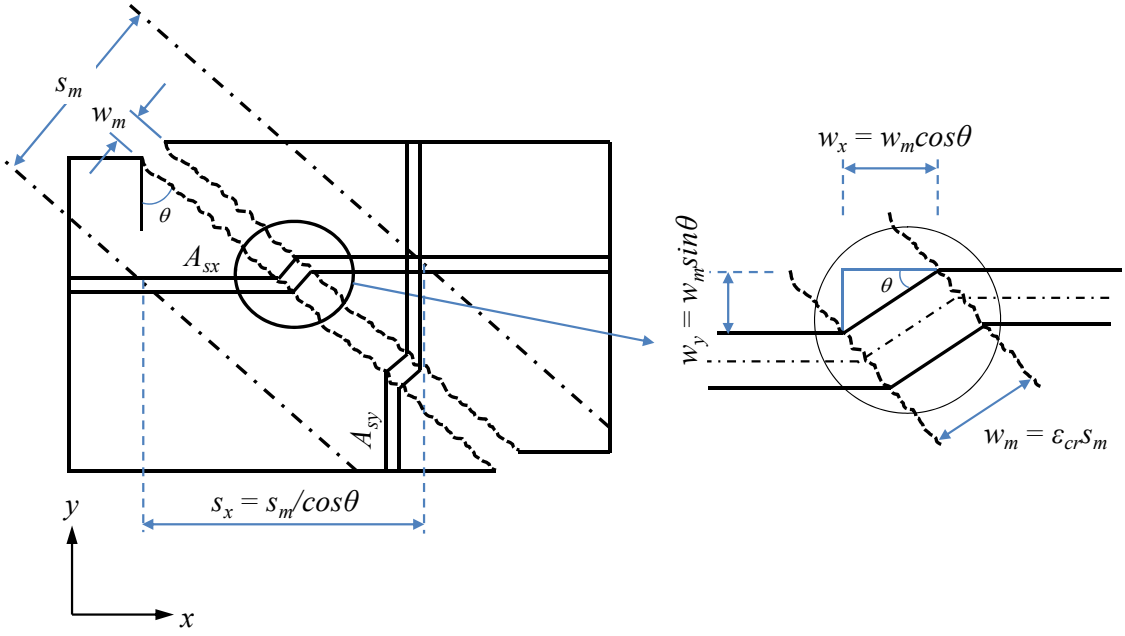

Figure 4.3- Cracked Reinforced Concrete Member (*Zararis, 1988*)

For the cracked reinforced concrete member shown in Fig. 4.3, the shear strain at the crack location can also be expressed as follows:

$$\frac{1}{2}\gamma_{xy} = \frac{w_y}{s_x} = \frac{w_x \sin\theta}{s_m / \cos\theta} = \varepsilon_{cr} \sin\theta\cos\theta \tag{4.4}$$

Therefore, the state of strain can be written as follows:

$$\varepsilon = \begin{bmatrix} \varepsilon_x & \frac{1}{2}\gamma_{xy} \\ \frac{1}{2}\gamma_{xy} & \varepsilon_y \end{bmatrix} = \varepsilon_{cr} \begin{bmatrix} \cos^2\theta & \sin\theta\cos\theta \\ \sin\theta\cos\theta & \sin^2\theta \end{bmatrix} \tag{4.5}$$

Thus, for the steel reinforcement

$$\varepsilon_s = \begin{bmatrix} \varepsilon_{sx} & \gamma_{sxy} \\ \gamma_{sxy} & \varepsilon_{sy} \end{bmatrix} = \varepsilon_{cr} \begin{bmatrix} \cos^2\theta & \sin\theta\cos\theta \\ \sin\theta\cos\theta & \sin^2\theta \end{bmatrix} \tag{4.6}$$

The normal and shear stresses of the steel reinforcement can be established as follows:

$$\sigma_s = \begin{bmatrix} \sigma_{sx} & \tau_{sxy} \\ \tau_{sxy} & \sigma_{sy} \end{bmatrix} = E_s \varepsilon_{cr} \begin{bmatrix} \cos^2\theta & \frac{1}{2(1+\nu)}\sin\theta\cos\theta \\ \frac{1}{2(1+\nu)}\sin\theta\cos\theta & \sin^2\theta \end{bmatrix} \tag{4.7}$$

By assuming a Poisson's ratio of the steel reinforcement equal to 0.3, Eq. 4.7 becomes:

$$\sigma_s = \begin{bmatrix} \sigma_{sx} & \tau_{sxy} \\ \tau_{sxy} & \sigma_{sy} \end{bmatrix} = E_s \varepsilon_{cr} \begin{bmatrix} \cos^2\theta & 0.4\sin\theta\cos\theta \\ 0.4\sin\theta\cos\theta & \sin^2\theta \end{bmatrix} \tag{4.8}$$

Regarding the externally bonded reinforcement, the state of stress is assumed to have the form:

$$\sigma_{ER} = \begin{bmatrix} \sigma_{ERx} & \tau_{ERxy} \\ \tau_{ERxy} & \sigma_{ERy} \end{bmatrix} = \begin{bmatrix} E_{ER}\varepsilon_{cr}\cos^2\theta & \tau_{ERxy} \\ \tau_{ERxy} & E_{ER}\varepsilon_{cr}\sin^2\theta \end{bmatrix} \tag{4.9}$$

The depth of the compression zone between the compression face and the tip of the diagonal crack can be determined from the force equilibrium of a diagonally-cracked reinforced concrete element. After the formation of the diagonal crack, the cracked reinforced concrete component can be considered as two elements, an arch element below the diagonal crack and a flexural element above the diagonal crack. The two elements after the formation of the diagonal crack are shown in Fig. 4.4. The depth of the compression zone below the tip of the diagonal crack can now be determined from the consideration of equilibrium of forces.

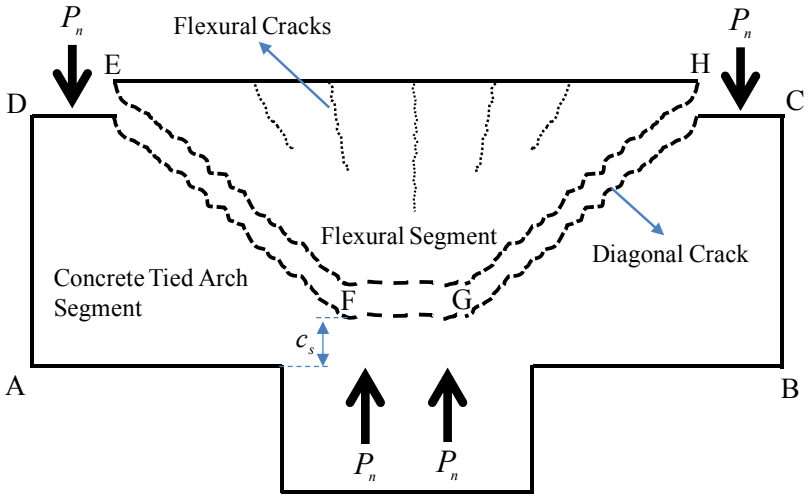

Figure 4.4- Two segments after the formation of diagonal crack

Figure 4.5 presents a free-body diagram of the flexural segment E F G H, and concrete tied arch segment A B C D, shown in Fig. 4.4. Moment equilibriums of the both segments will be considered to derive the equation for the depth of compression zone after the formation of the diagonal crack.

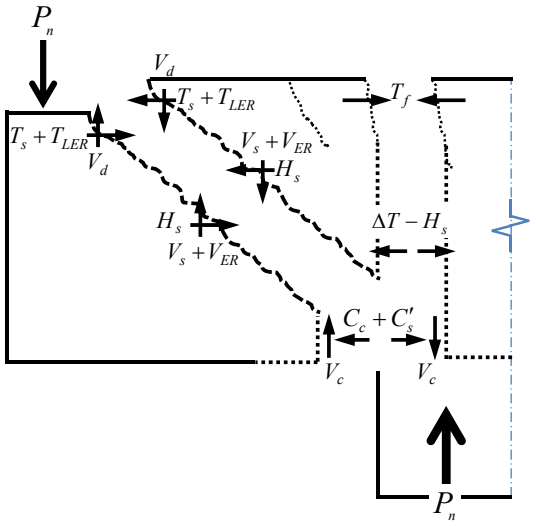

where,

T_s = Tension force of longitudinal steel reinforcement
T_{LER} = Tension force of longitudinal external reinforcement
T_f = Tension force in the flexural region
ΔT = Difference between T_f and resultant tension force ($T_s + T_{LER}$)
C_c = Resultant compression force of concrete
C'_s = Compression force of compression steel reinforcement
V_c = Shear force of concrete tied arch
V_d = Shear force in longitudinal steel reinforcement due to dowel action
V_s = Force of vertical transverse reinforcement
V_{ER} = Force of vertical external reinforcement
H_s = Force due to the shear reinforcement parallel to flexural tension reinforcement

Figure 4.5- Free-body diagram of flexural and concrete tied arch segments

Moment equilibrium for Flexural Segment

After the formation of a diagonal crack, the free-body diagram of the flexural concrete element is shown in Fig. 4.6.

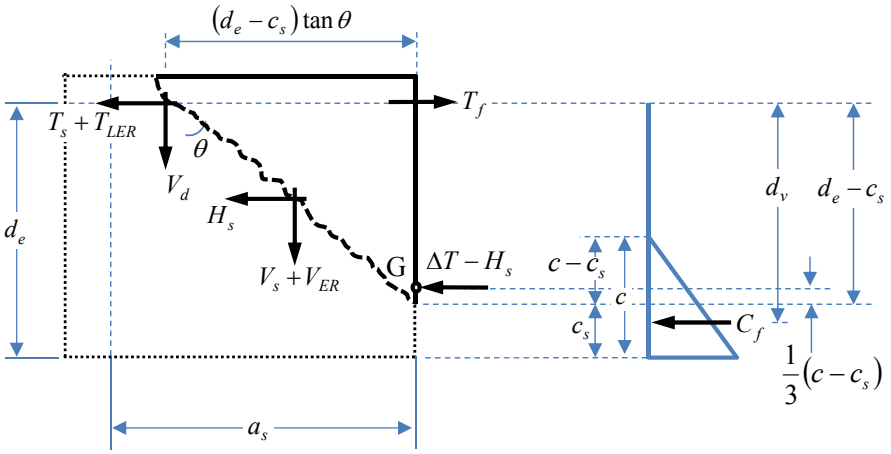

Figure 4.6- Free-body diagram of the flexural concrete element

Zararis (2003) assumed that the stress distribution in the concrete compression zone is parabolic with a maximum compressive strain of 0.002. In the present work, the stress distribution in the concrete compression zone was assumed to be triangular-shape. It is to be noted that any different shapes of distributions yield negligible difference in the depth of compression zone, provided that the beam is under-reinforced. Using the triangular-shaped distribution of concrete stress, the location of the neutral axis can be computed from a transformed section of the pier cap.

The tension force in the flexural region, T_f is:

$$T_f = V_n \frac{a_s}{d_v} \tag{4.10}$$

where d_v, the distance between resultant tension and compression forces, is

$$d_v = d_e - \frac{1}{3}c \tag{4.11}$$

Taking moment of forces about point G shown in Fig. 4.6, the following equation is obtained:

$$\begin{aligned} &V_d(d_e - c_s)\tan\theta + (V_s + V_{ER})\frac{(d_e - c_s)\tan\theta}{2} \\ &= (T_f - T_{LER} - T_s)\left(1 - \frac{c - c_s}{3(d_e - c_s)}\right)(d_e - c_s) - H_s\left(0.5 - \frac{c - c_s}{3(d_e - c_s)}\right)(d_e - c_s) \end{aligned} \tag{4.12}$$

Moment equilibrium for Concrete Tied Arch Segment

Considering now the concrete tied arch segment shown in Fig. 4.7. The shape of the stress distribution of concrete was assumed to be triangular having the distance from the face of compression zone to the centroid of the distribution is $c_s/3$. The moment arm between the force of compression steel reinforcement, C_s' and the resultant compressive force of concrete, C_c is very small. Thus, it is reasonable to assume for simplification purposes, that C_s' coincides with C_c.

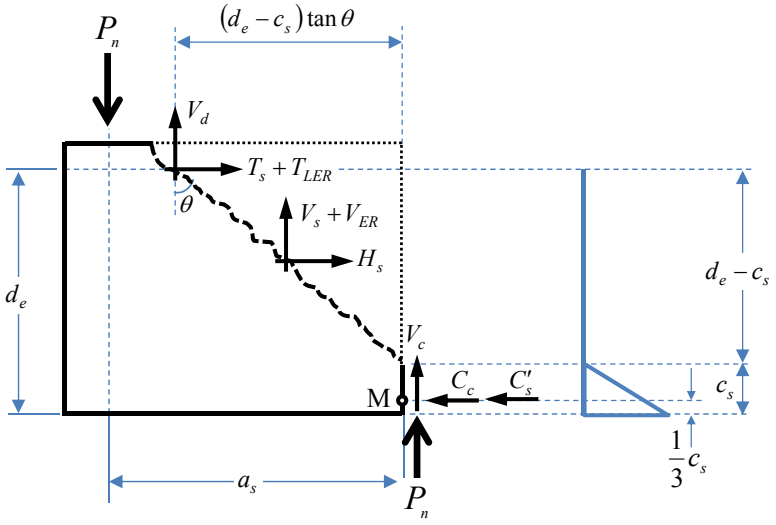

Figure 4.7- Free-body diagram of an arch segment after the formation of diagonal crack

By summing moment of forces about point M shown in Fig. 4.7, the following equation is obtained.

$$(T_s + T_{LER})\left(d_e - \frac{1}{3}c_s\right) + V_d(d_e - c_s)\tan\theta + 0.5(V_s + V_{ER})(d_e - c_s)\tan\theta + H_s\left(0.5(d_e - c_s) + \frac{2}{3}c_s\right) = P_n a_s \tag{4.13}$$

The tension forces in the longitudinal steel reinforcement, T_s and longitudinal external reinforcement, T_{LER} are

$$T_s = A_s \sigma_{sx} \tag{4.14}$$

$$T_{LER} = A_{LER} \sigma_{ERx} \tag{4.15}$$

The shear force in longitudinal steel reinforcement due to dowel action, V_d is:

$$V_d = A_s \tau_{sxy} \tag{4.16}$$

With $\tau_{sxy} = 0.4 E_s \varepsilon_{cr} \sin\theta \cos\theta$, V_d becomes:

$$V_d = 0.4 A_s E_s \varepsilon_{cr} \sin\theta \cos\theta \tag{4.17}$$

From Eq. 4.8, $\sigma_{sx} = E_s \varepsilon_{cr} \cos^2\theta$, then

$$V_d = 0.4 A_s \sigma_{sx} \tan\theta \tag{4.18}$$

or

$$\sigma_{sx} = \frac{2.5 V_d}{A_s \tan\theta} \tag{4.19}$$

From Eq. 4.9, the average stress in the externally bonded reinforcement in the *x*-direction, σ_{ERx} is:

$$\sigma_{ERx} = E_{ER} \varepsilon_{cr} \cos^2\theta \tag{4.20}$$

With $\varepsilon_{cr} \cos^2\theta = \frac{\sigma_{sx}}{E_s}$ from Eq. 4.8, σ_{ERx} becomes:

$$\sigma_{ERx} = \frac{E_{ER}}{E_s} \sigma_{sx} = \frac{2.5 n V_d}{A_s \tan\theta} \tag{4.21}$$

where $n = \frac{E_{ER}}{E_s}$

Substituting Eq. 4.19 and 4.21 into 4.14 and 4.15 yields:

$$T_s = A_s \sigma_{sx} = \frac{2.5 V_d}{\tan\theta} \tag{4.22}$$

$$T_{LER} = A_{LER} \sigma_{ERx} = \frac{A_{LER}}{A_s} \frac{2.5 n V_d}{\tan\theta} \tag{4.23}$$

The force in the vertical transverse reinforcement, V_s is:

$$V_s = A_v \sigma_{sy} n_v \tag{4.24}$$

in which n_v is:

$$n_v = \frac{(d_e - c_s)\tan\theta}{s_v} \tag{4.25}$$

Substituting Eq. 4.25 into 4.24 yields

$$V_s = \frac{A_v}{s_v}\sigma_{sy}(d_e - c_s)\tan\theta \tag{4.26}$$

After substituting the expressions, $\sigma_{sy} = E_s \varepsilon_{cr} \sin^2\theta$ and $\varepsilon_{cr} = \sigma_{sx}/(E_s \cos^2\theta)$ into Eq. 4.26, V_s becomes:

$$V_s = \frac{A_v}{s_v}\sigma_{sx}(d_e - c_s)\tan^3\theta \tag{4.27}$$

Substituting the expressions, σ_{sx} from Eq. 4.19 into Eq. 4.27, V_s becomes:

$$V_s = 2.5V_d \frac{A_v}{s_v A_s}(d_e - c_s)\tan^2\theta \tag{4.28}$$

The force in the vertical external reinforcement V_{ER} can be written as follows:

$$V_{ER} = A_{vER}\sigma_{ERy} n_{vER} \tag{4.29}$$

in which

$$n_{vER} = \frac{(d_e - c_s)\tan\theta}{s_{vER}} \tag{4.30}$$

With $\sigma_{ERy} = E_{ER}\varepsilon_{cr}\sin^2\theta$ and $\varepsilon_{cr} = \sigma_{ERx}/(E_{ER}\cos^2\theta)$ (see Eq. 4.8), V_{ER} becomes:

$$V_{ER} = A_{vER}\sigma_{ERx}\frac{(d_e - c_s)}{s_{vER}}\tan^3\theta \tag{4.31}$$

Noting that $\sigma_{ERx} = \dfrac{2.5nV_d}{A_s \tan\theta}$ (Eq.4.21), the force in the vertical external reinforcement V_{ER} can be written in the following form:

$$V_{ER} = 2.5nV_d \frac{A_{vER}}{s_{vER}A_s}(d_e - c_s)\tan^2\theta \tag{4.32}$$

The force (H_s) due to the shear reinforcement parallel to flexural tension reinforcement is:

$$H_s = A_h \sigma_{sx} n_h \tag{4.33}$$

$$n_h = \frac{(d_e - c_s)}{s_h} \tag{4.34}$$

$$H_s = \frac{A_h}{s_h}\sigma_{sx}(d_e - c_s) \tag{4.35}$$

$$H_s = 2.5V_d \frac{A_h}{s_h A_s}(d_e - c_s)\frac{1}{\tan\theta} \tag{4.36}$$

Depth of Compression Zone between Compression Face and Tip of Diagonal Crack

The shear force in the longitudinal steel reinforcement present in the flexural segment can be obtained from Eq. 4.12 as:

$$V_d = \frac{\left(P_n \dfrac{a_s}{d_e}\right)\tan\theta}{\left(1 - \dfrac{c}{3d_e}\right)\left[2.5\left(1 + n\dfrac{A_{LER}}{A_s}\right) + \dfrac{1 + 0.5\dfrac{(V_s + V_{ER})}{V_d} + \left(0.5 - \dfrac{c - c_s}{3(d_e - c_s)}\right)\dfrac{H_s}{V_d}\dfrac{1}{\tan\theta}}{\left(1 - \dfrac{c - c_s}{3(d_e - c_s)}\right)}\tan^2\theta\right]} \tag{4.37}$$

Similarly, moment of equilibrium (Eq. 4.13) yields the following equation.

$$V_d = \frac{\left(P_n \frac{a_s}{d_e}\right)\tan\theta}{2.5\left(1+n\frac{A_{LER}}{A_s}\right)\left(1-\frac{c_s}{3d_e}\right)+\left(1-\frac{c_s}{d_e}\right)\left(1+0.5\frac{V_s+V_{ER}}{V_d}\right)\tan^2\theta+\left(0.5\left(1-\frac{c_s}{d_e}\right)+\frac{2c_s}{3d_e}\right)\frac{H_s}{V_d}\tan\theta} \tag{4.38}$$

The depth of compression zone, c_s is derived from equating Eqs. 4.37 and 4. 38. The equations for V_s, V_{ER} and H_s shown in Eq. 4.28, 4.32 and 4.36 are substituted into Eq. 4.37 and 4.38, and the following cubic equation is obtained:

$$\begin{aligned}
&\left(\frac{1}{3.6}\right)(3V\tan^4\theta - H)\left(\frac{c_s}{d_e}\right)^3 + \\
&\left(\frac{1}{3.6}\right)\left[\left(1-\frac{c}{d_e}\right)H - 2.4\left(1+2.5V\tan^2\theta\right)\tan^2\theta - 2ER\right]\left(\frac{c_s}{d_e}\right)^2 + \\
&\left(\frac{1}{3.6}\right)\left[H\frac{c}{d_e}\left(4-\frac{c}{d_e}\right)+ER\left(3+\frac{c}{d_e}\right)+\left(2.4+3V\tan^2\theta\right)\tan^2\theta\right]\left(\frac{c_s}{d_e}\right)+ \\
&\left(\frac{1}{3.6}\right)\left[\frac{c}{d_e}\left(\frac{c}{d_e}-3\right)(H+ER)\right]=0
\end{aligned} \tag{4.39}$$

From the analysis of test results reported in Appendix G, the computed values of $(c_s/d_e)^3$ were negligible, thus $(c_s/d_e)^3$ was ignored for simplification purposes. Therefore, c_s can now be determined by solution of which is expressed as follows:

$$c_s = \frac{d_e}{3.6}\left(\frac{-B+\sqrt{B^2-4AC}}{2A}\right) \tag{4.40}$$

$$A = \left(1-\frac{c}{d_e}\right)H - 2.4\left(1+2.5V\tan^2\theta\right)\tan^2\theta - 2ER \tag{4.41}$$

$$B = H\frac{c}{d_e}\left(4-\frac{c}{d_e}\right)+ER\left(3+\frac{c}{d_e}\right)+\left(2.4+3V\tan^2\theta\right)\tan^2\theta \tag{4.42}$$

$$C = \frac{c}{d_e}\left(\frac{c}{d_e}-3\right)(H+ER) \tag{4.43}$$

$$V = d_e\left(\frac{A_v}{s_v A_s} + n\frac{A_{ER}}{s_{ER}A_s}\right) \tag{4.44}$$

$$H = d_e\left(\frac{A_h}{s_h A_s}\right) \tag{4.45}$$

$$ER = 1 + n\frac{A_{LER}}{A_s} \tag{4.46}$$

$$n = \frac{E_{ER}}{E_s} \tag{4.47}$$

For a small number of tests, it was found that the computed value of c_s from Eq. 4.40 is less than d'_s. This implies that the diagonal crack penetrates the compression steel reinforcement. For such cases, it is reasonable to assume that the shear strength limit state is reached when

$$c_s = \frac{d_e}{3.6}\left(\frac{-B + \sqrt{B^2 - 4AC}}{2A}\right) \geq d'_s \tag{4.48}$$

Shear Strength Determination

The nominal shear strength of the pier cap, V_n, is derived from the condition of the concrete tied arch segment, shown in Fig. 4.8. The shear strength is computed from moment equilibrium about B as follows. The nominal shear strength, V_n, of the pier cap is obtained from the condition of equilibrium of forces in the concrete tied arch segment. By taking moments about B, the equation for, V_n, is:

$$V_n = \frac{1}{a_s}\left[(T_s + T_{LER})\left(d_e - \frac{1}{2}c_s\right) + \frac{1}{2}(V_s + V_{ER})(d_e - c_s)\tan\theta + \frac{1}{2}H_s(d_e - c_s) + C'_s\left(\frac{1}{2}c_s - d'_s\right)\right] \quad \text{if } c_s > d'_s \tag{4.49-a}$$

$$V_n = \frac{1}{a_s}\left[(T_s + T_{LER})\left(d_e - \frac{1}{2}c_s\right) + \frac{1}{2}(V_s + V_{ER})(d_e - c_s)\tan\theta + \frac{1}{2}H_s(d_e - c_s)\right] \quad \text{if } c_s \leq d'_s \tag{4.49-b}$$

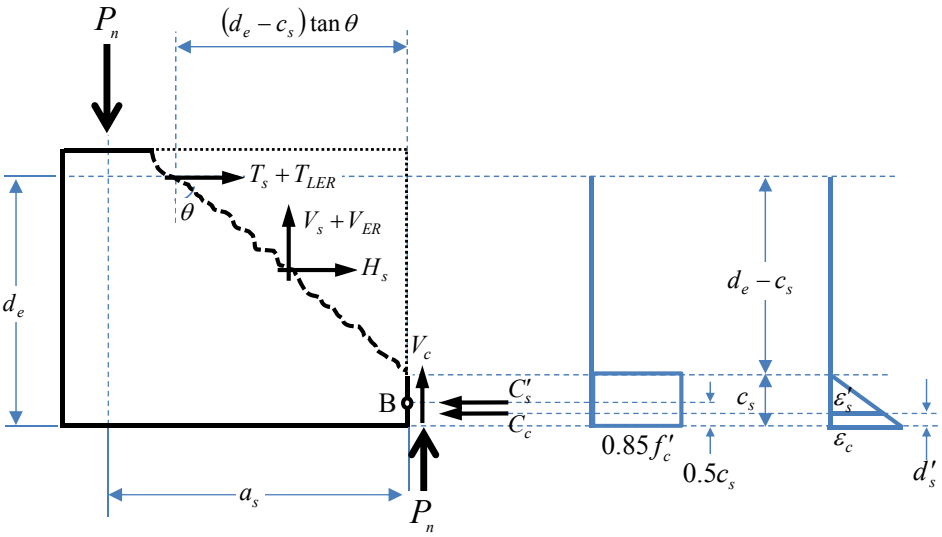

Figure 4.8- Forces on a free-body diagram of arch segment at failure

Adopting a uniform stress distribution in the concrete of $0.85\,f'_c$, the compression force of concrete (C_c) over the depth of compression zone below a diagonal crack is shown as follows.

$$C_c = 0.85 f'_c c_s b \tag{4.50}$$

The compression force of compression steel reinforcement (C'_s) can be written as follows:

$$C'_s = A'_s E_s \varepsilon'_y \quad \text{if} \quad \varepsilon'_s = \varepsilon_c \left(\frac{c_s - d'_s}{c_s} \right) \geq \varepsilon'_y \tag{4.51-a}$$

$$C'_s = A'_s E_s \varepsilon'_s \quad \text{if} \quad \varepsilon'_s = \varepsilon_c \left(\frac{c_s - d'_s}{c_s} \right) < \varepsilon'_y \tag{4.51-b}$$

Following the customary practice of assuming that the internal transverse reinforcement crosses at least one diagonal crack yields, V_s becomes:

$$V_s = \frac{A_v}{s_v} f_{yv} (d_e - c_s) \tan\theta \tag{4.52}$$

For the stress in the vertical externally bonded reinforcement, f_{vER}, is taken as the value corresponding to a strain of 0.003 (see section 3.6.3). The force in the vertical external reinforcement, V_{ER} can be written in the following form.

$$V_{ER} = \frac{A_{vER}}{s_{vER}} f_{vER}(d_e - c_s)\tan\theta \tag{4.53}$$

The forces in the reinforcement parallel to the flexural tension reinforcement (H_s), the longitudinal tension reinforcement (T_s), and the longitudinal external reinforcement (T_{LER}) are calculated as follows:

$$H_s = \frac{A_h}{s_h}\sigma_{sx}(d_e - c_s) \tag{4.54}$$

$$T_s = A_s\sigma_{sx} \tag{4.55}$$

$$T_{LER} = nA_{LER}\sigma_{sx} \tag{4.56}$$

Equilibrium of forces shown in Fig. 4.8 in the horizontal direction yields:

$$C_c + C_s' = T_s + T_{LER} + H_s \tag{4.57}$$

Substituting Eq. 4.54, 4.55 and 4.56 into Eq. 4.57, the average stress in the steel reinforcement in the *x*-direction, σ_{sx}, becomes:

$$\sigma_{sx} = \frac{C_c + C_s'}{A_s + nA_{LER} + \frac{A_h}{s_h}(d_e - c_s)} \quad \text{if} \quad c_s > d_s' \tag{4.58-a}$$

$$\sigma_{sx} = \frac{C_c}{A_s + nA_{LER} + \frac{A_h}{s_h}(d_e - c_s)} \quad \text{if} \quad c_s \le d_s' \tag{4.58-b}$$

The angle of the diagonal crack, $\tan\theta$ can be approximated as a_s / d_e.

4.1.2 Experimental Validation of the Analytical Work

Results from Eq. 4.49-a and 4.49-b were compared with available results from 294 experiments conducted on reinforced concrete beams with a/d ratios ranging from 1 and 2 (see Appendix G). The analytical results from Eq. 4.49-a and 4.49-b were also compared with those resulted from testing pier cap specimens with externally bonded stainless steel reinforcement, described in Chapter 3.

Reinforced Concrete Deep Beams

Regarding the 294 experiments conducted on the reinforced concrete deep beams, Fig. 4.9 and Table 4.1 present the mean, standard deviation and coefficient of variation of $P_{experiment}/P_{analysis}$. The analytical model yielded smaller values of $P_{experiment}/P_{analysis}$ for the beams containing transverse reinforcement than those not containing transverse reinforcement.

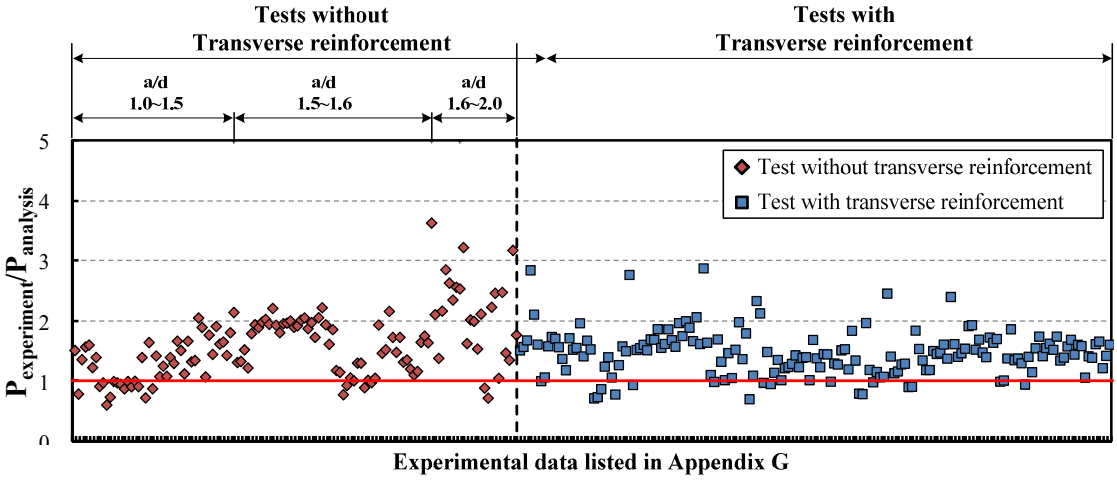

Figure 4.9- Comparison of analytical results with experimental results

Table 4.1- Comparison of analytical results with experimental results

	Sample size	$P_{experiment}/P_{analysis}$				
		Max	Min	Mean	Std.	COV (%)
Present Mechanics-based Approach	294	3.64	0.61	1.52	0.46	30.5
Present Mechanics-based Approach (Beams tested without transverse reinforcement)	126	3.64	0.61	1.59	0.55	34.8
Present Mechanics-based Approach (Beams tested with transverse reinforcement)	168	2.88	0.70	1.47	0.38	25.6

Figure 4.10 shows the computed values of $P_{experiment}/P_{analysis}$ as a function of the a/d ratio. Regardless of the amount of transverse reinforcement, it was shown that the value of $P_{experiment}/P_{analysis}$ increases as the a/d ratio increases. According to Kani's work, concrete tied-arch becomes dominant load-carrying mechanism for beams having a/d ratio less than 2.5. As the a/d ratio increases, the contribution of concrete tied-arch mechanism decreases. This is illustrated in Fig. 4.10 showing larger $P_{experiment}/P_{analysis}$ values as a/d ratio increases.

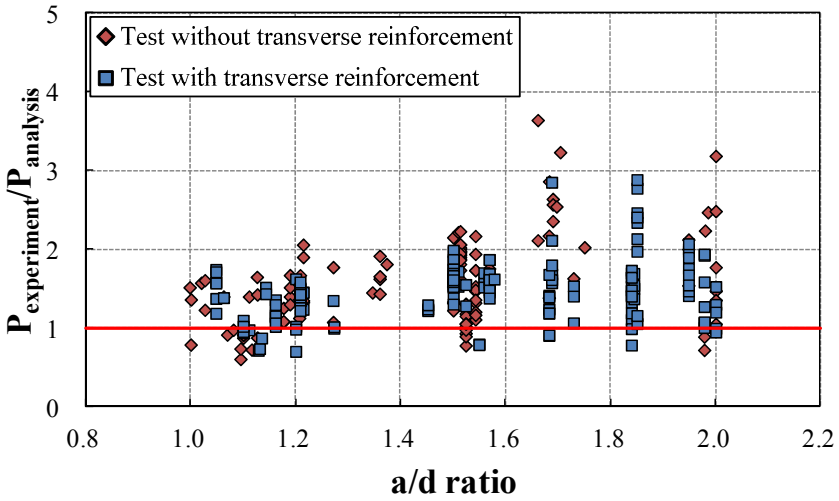

Figure 4.10- $P_{experiment}/P_{analysis}$ vs. a/d ratio

The computed values of $P_{experiment}/P_{analysis}$ as a function of the effective depth of the members, are plotted in Fig. 4.11. Due to the limited number of testes on the beams

having the effective depth greater than 40 in., size effect of the analytical model was not able to be estimated.

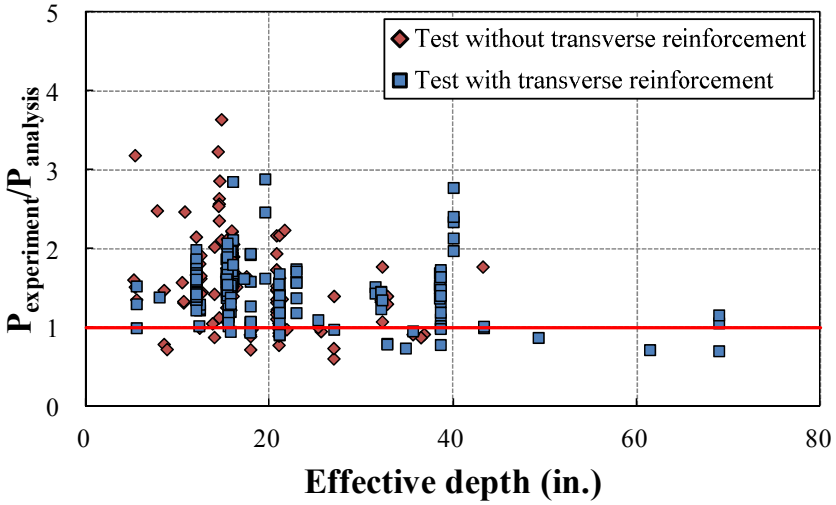

Figure 4.11- $P_{experiment}/P_{analysis}$ vs. effective depth

The depth of compression zone representing the distance between the tip of the diagonal crack and the face of compression zone is an important parameter to determine the strength of the tied arch mechanism. The value of c_s/d_e was estimated from the experimental data of Smith and Vantsiotis (1982) to be $c_s/d_e \approx 0.2$. Using the Proposed Mechanics-based Approach, the values of c_s/d_e for the specimens tested by Smith and Vantsiotis were computed according to Eq. 4.49-a and 4.49-b. Figure 4.12 presents comparison of computed values of c_s/d_e with the experimentally estimated value of c_s/d_e. The Proposed Mechanics-based approach yielded mean value of $c_s/d_e = 0.164$.

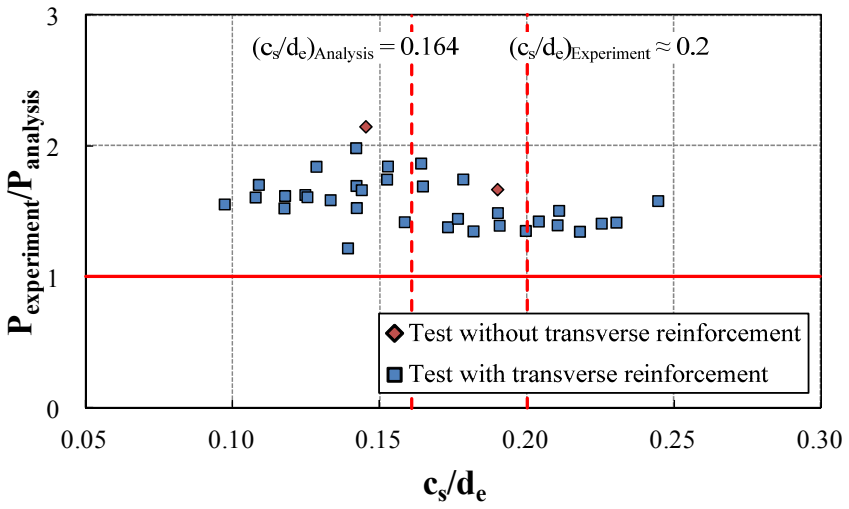

Figure 4.12- Computed c_s/d_e for the work by Smith and Vantsiotis (1982)

For 294 experimental data, the values of c_s / d_e were computed and the results are shown in Fig. 4.13. The mean value of computed c_s / d_e was equal to 0.13. As shown in Fig. 4.14 presenting the value of c_s / d_e as a function of a/d ratio, the value of c_s / d_e decreases when a/d ratio increases. This is due to the fact that the strength of concrete tied arch varies with respect to c_s / d_e, and the influence of the concrete tied arch mechanism decreases as a/d ratio increases.

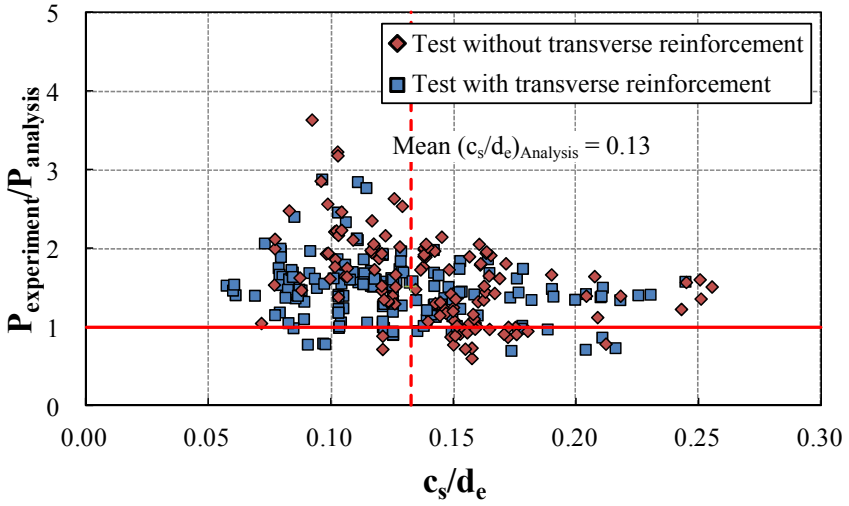

Figure 4.13- $P_{experiment}/P_{analysis}$ vs. computed c_s/d_e

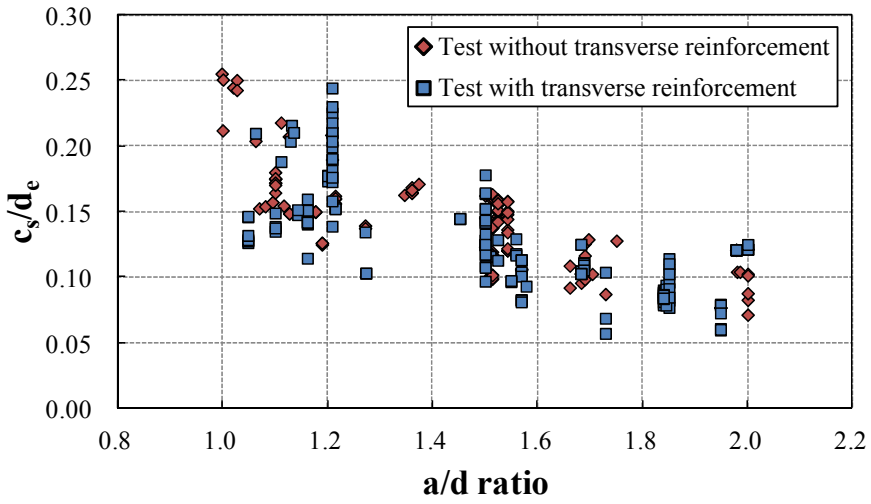

Figure 4.14- Computed c_s/d_e vs. a/d ratio

Comparison of Analytical Models for Reinforced Concrete Deep Beams

To compare the results of analysis among all analytical models presented in Chapter 2 and the Proposed Mechanics-based approach, the 156 experimental tests of reinforced concrete deep beams presented in Appendix A were analyzed. The mean, standard deviation and coefficient of variation of $P_{experiment}/P_{analysis}$ are listed in Table. 4.2. The Proposed Mechanics-based Model yielded the mean $P_{experiment}/P_{analysis}$ of 1.44 and COV of 29.5 %. When comparing the analytical results among the Zararis' Approach, Modified Zararis' Approach Proposed Mechanics-based Model, the greatest mean value of $P_{experiment}/P_{analysis}$ was obtained by the Proposed Mechanics-based Model. Although the mean and standard deviation values of $P_{experiment}/P_{analysis}$ are greater than those computed in the original Zararis' and Modified Zararis' methods, the Proposed Mechanics-based Model is justified as on the grounds that the Zararis' Approach contained assumptions which could not be verified analytically.

Table 4.2- Comparison of analytical and experimental results

	$P_{experiment}/P_{analysis}$		
	Mean	Std.	COV (%)
AASHTO Simplified Procedure	3.48	1.61	48.1
AASHTO General Procedure	2.60	1.17	44.9
AASHTO Strut-and-Tie Model	2.02	0.58	28.7
ACI Strut-and-Tie Model	1.60	0.43	26.8
FIP Strut-and-Tie Model	1.76	0.56	31.8
Zararis' Approach	1.00	0.25	25.1
Modified Zararis' Approach	1.26	0.29	23.3
Proposed Mechanics-based Model	1.44	0.42	29.5

Sample size : 156
Note: AASHTO Simplified Procedure was used for analyzing experimental data from tests conducted on beams having depths greater than 16 in.

Reinforced Concrete Pier Caps with Externally Bonded Reinforcement System

The Proposed Mechanics-based approach was used to calculate the strength of the specimens tested in the experimental work reported in Chapter 3. Regarding the material properties of the stainless steel, the tensile strength was taken at a strain value of 0.003 and the secant modulus defined between zero and yield strength were used. Stress-strain curve for the stainless steel plate is shown in Fig. 4.15. For this strength computation, the actual material properties determined by experiments were used. Table 4.3 shows the material properties used in this strength computation.

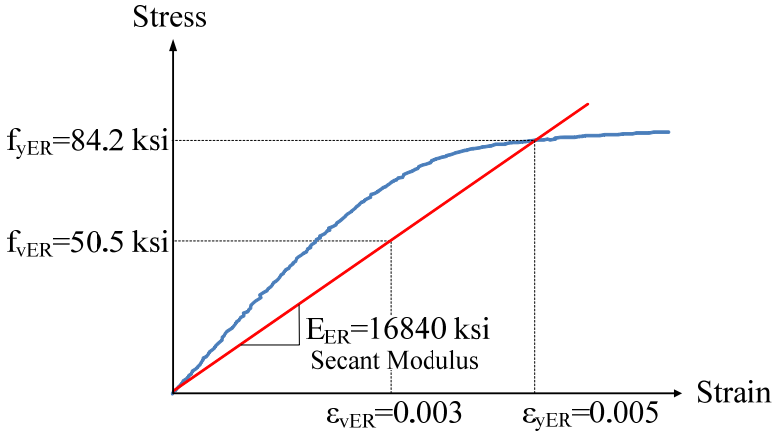

Figure 4.15- Stress vs. strain for stainless steel plate

Table 4.3- Material properties for strength computation

Group	Specimen ID	f_c' (psi)	f_y (ksi)	f_{yv} (ksi)	f_{vER} (ksi)	E_{ER} (ksi)
A	BL2*	3353	80.0	-	-	-
	AR014	3402	80.0	-	50.5	16840
	AR035	3599	80.0	-	50.5	16840
B	BS00	6164	74.6	89.4	-	-
	BSR008	6085	74.6	89.4	50.5	16840
	BSR014	6024	74.6	89.4	50.5	16840
C	CS00	6655	74.6	89.4	-	-
	CSR018-1	6258	74.6	89.4	50.5	16840
	CSR018-2	6008	74.6	89.4	50.5	16840
	CSR035	6419	74.6	89.4	50.5	16840

* BL2 is the reference test specimen reported by Zureick et al. (2013)

Table 4.4 shows the comparison between the experimental and analytical strength values. The values of c_s / d_e are also calculated. The Proposed Mechanics-based approach yielded reasonable shear strength predictions for the bridge pier caps with externally bonded stainless steel reinforcement. The computed strengths of the specimens in group B showed that the externally bonded reinforcement system had an insignificant influence on the analytical results. However, it would be due to the influence on the compressive strength of concrete. The values of $P_{analysis} / f_c' b d_e$ presented in Table 4.4 show the computed shear strengths excluding the effect of the concrete strength. Figure 4.16 and 4.17 show the ratios of $P_{experiment}/P_{analysis}$ and c_s / d_e for each specimen respectively. The specimens that failed due to the formation of diagonal cracks are presented in the table.

Table 4.4- Comparison between experimental and analytical results

Group	Specimen ID	$P_{experiment}$ (kips)	$P_{analysis}$ (kips)	$\frac{P_{analysis}}{f'_c b d_e}$	$\frac{P_{experiment}}{P_{analysis}}$	c_s/d_e
A	BL2*	632	468	0.241	1.35	0.16
	AR014	748	486	0.247	1.54	0.15
B	BS00	824	734	0.206	1.12	0.14
	BSR008	980	731	0.208	1.34	0.13
	BSR014	1050	729	0.209	1.44	0.13
C	CS00	508	355	0.089	1.43	0.07

* BL2 is the reference test specimen reported by Zureick et al. (2013)

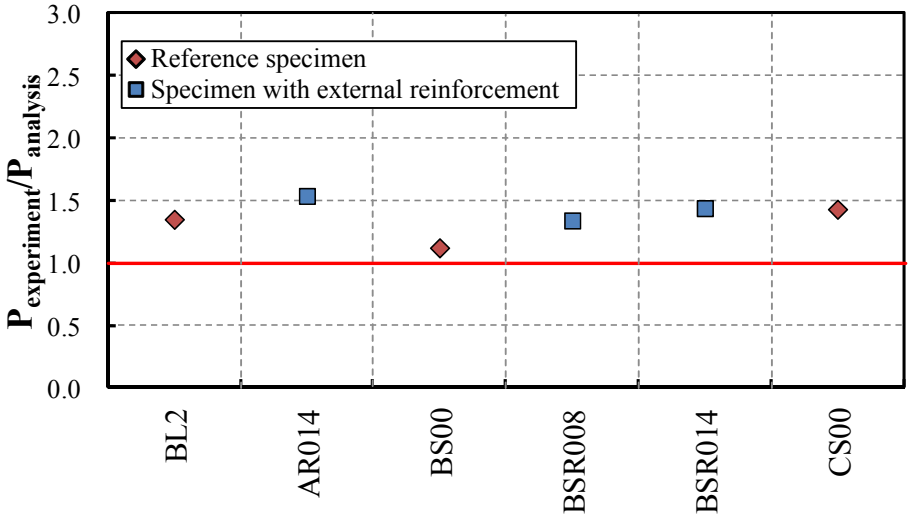

Figure 4.16- $P_{experiment}$ / $P_{analysis}$ computed by Proposed Mechanics-based Model

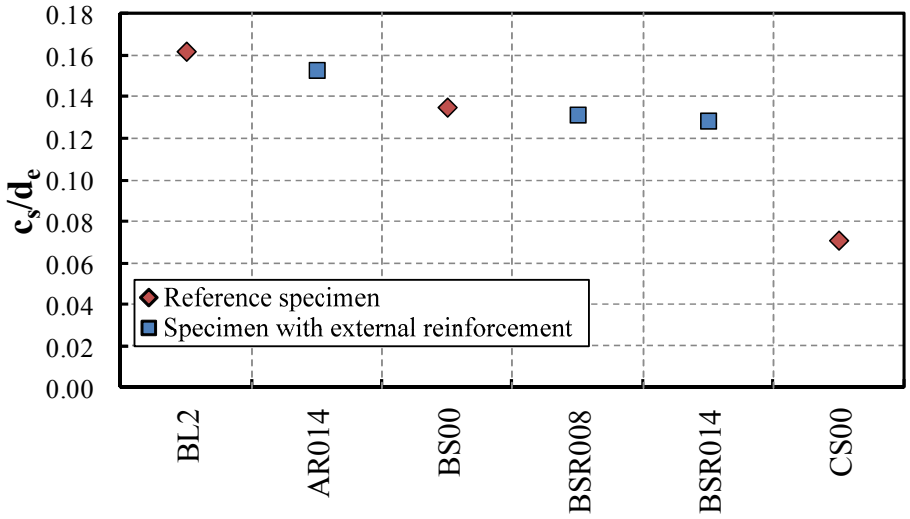

Figure 4.17- c_s/d_e computed by Proposed Mechanics-based Model

4.2 Proposed Procedure for the application of a Combined Strut-and-Tie Model for Determining the Strength of Reinforced Concrete Bridge Pier Caps

The mechanics-based approached presented in Section 4.1 is limited to calculating only the shear strength of reinforced concrete deep beams and bridge pier caps and must be used in conjunction with other equations capable of predicting the strength limit states associated with yielding of the tension reinforcement, bearing in regions subjected to compressive forces, or regions anchoring the tension reinforcement. This section describes a procedure for calculating the strength of a reinforced concrete bridge pier cap with externally bonded reinforcement. This procedure requires the analysis of a structural model constructed by superimposing a strut-and-tie model and a truss model, which was proposed originally by Schlaich and Schäfer (1991) and adopted in the FIP (1999) recommendation. The application of the superposition of these two models to reinforced concrete bridge pier caps strengthened with externally bonded reinforcement is validated experimentally and is shown to be capable of predicting reasonably well the failure modes due to the formation of a diagonal crack or flexure. The procedures for calculating the strength of compressive strut, node regions and nominal strength of the bridge pier cap are described in this section.

4.2.1 Superposition of Strut-and-Tie Models

An elasticity-based combined strut-and-tie model for the bridge pier cap test specimens with externally bonded reinforcement is constructed by combining the traditional strut-and tie- model representing the concrete tied arch mechanism and a truss model representing the externally bonded reinforcement (Figure 4.18). The strength of the combined strut-and-tie model is computed by summing the individual strengths of each separate model.

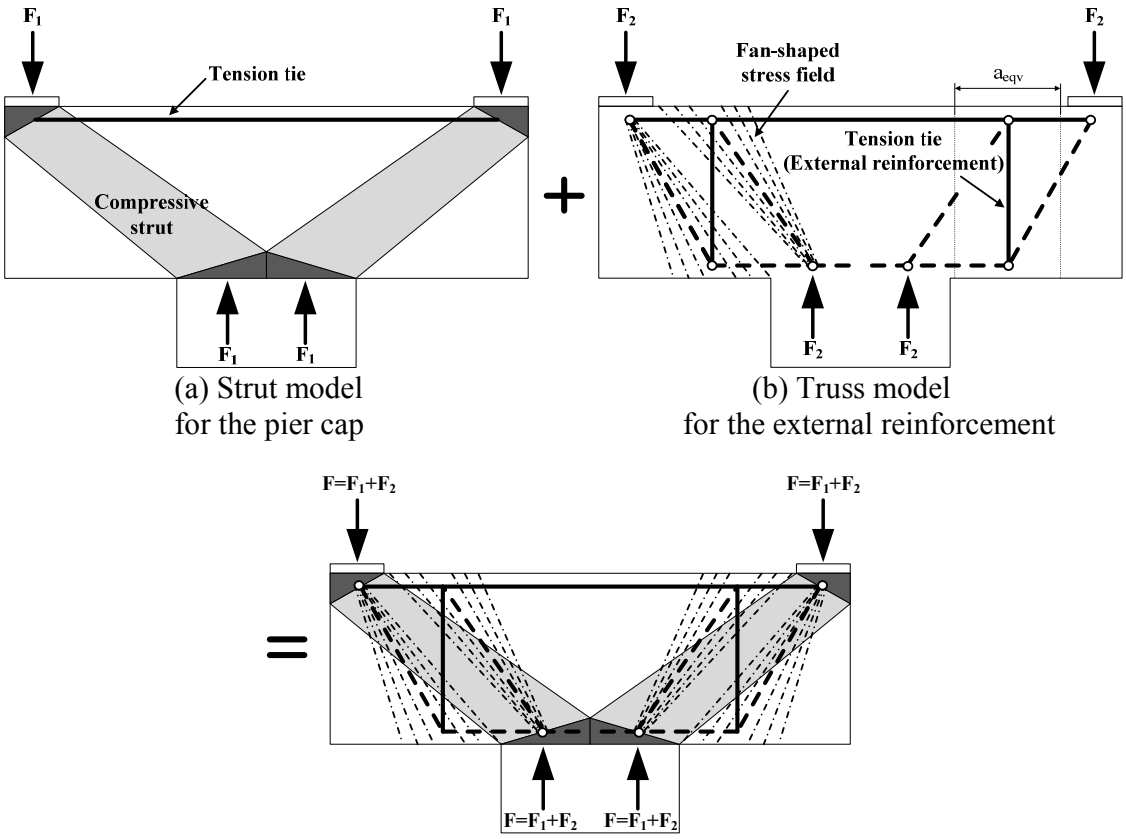

(a) Strut model for the pier cap

(b) Truss model for the external reinforcement

(c) Combined strut-and-tie model

Figure 4.18- Combined strut-and-tie model for bridge pier caps

The truss model shown in Fig. 4.18-b contains a vertical tension tie representing vertically bonded external reinforcements and fan-shaped compression stress fields. Stress check for the fan-shaped compression stress fields shown in Fig. 4.18-b are unnecessary since the stress field does not develop transverse stresses (*Schlaich, 1991*).

4.2.2 Contribution of Externally Bonded Reinforcement System

The externally bonded reinforcement system is treated as a vertical tie of the truss model shown in 4.18-b. To estimate the effective number of the externally bonded reinforcement system, the equation for a_w, provided in FIP (1999) is adopted. a_w can be computed as follows:

$$a_w = (0.85a_s - z/4) \tag{4.59}$$

where,

a_s = shear span

z = inner lever arm

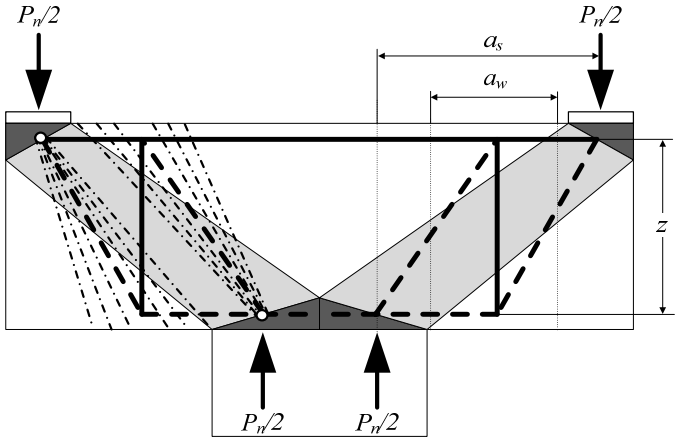

Figure 4.19- Effective region for vertical tension tie

4.2.3 Strain Calculation

The procedure for calculating the strains in the externally bonded reinforcement system and longitudinal tension reinforcement is necessary to compute the strength of the combined strut-and-tie model. Regarding the strut model shown in 4.18-a, current design specifications, AASHTO LRFD Bridge Design Specifications (2012), ACI 318 (2008) and FIP (1999) are used. The procedure of strain calculation is presented below.

1. Strain in the longitudinal tension reinforcement, ε_s of the reinforced concrete bridge pier cap without the externally bonded reinforcement system is computed in accordance with current strut-and-tie provisions by AASHTO (2012), ACI (2008) and FIP (1999). The specific procedures for the strain computation using AASHTO Strut-and-Tie Model are presented in section 4.2.4.

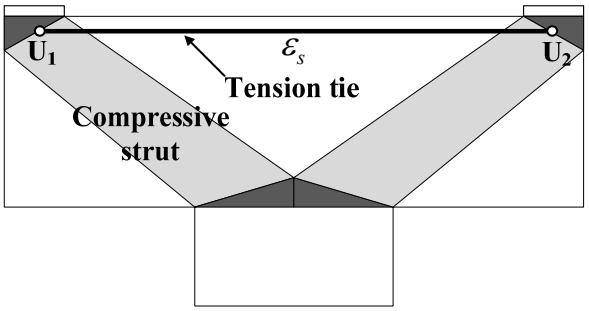

Figure 4.20- Direct strut model in combined strut-and-tie model

2. Assume a value of the tensile strain in the vertical tension tie of the truss member representing the externally bonded reinforcement system, ε_{vER} , shown in Fig. 4.21. When the limit state of the reinforced concrete pier cap is assumed to be the failure mode involving formation of a diagonal crack, the value of ε_{vER} is assumed to be 0.003. It should be noted that the value of ε_{vER} should be limited to 0.003 in accordance with the experimental observation presented in section 3.6.3.

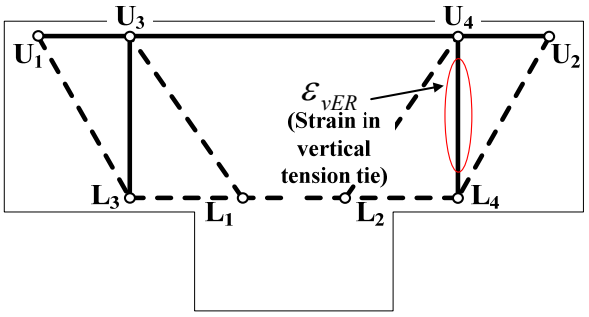

Figure 4.21- Truss model in combined strut-and-tie model

3. Determine the stress in the externally bonded reinforcement system corresponding to the strain assumed in step 2. The stress is determined from experiment on the material property or material models. The force in the externally bonded reinforcement system can be calculated by multiplying the determined stress by

the cross sectional area of the plates within the equivalent shear span which will be presented in the following section. The member forces of the truss model shown in Fig.4.21 can be computed by a truss analysis.

4. Strains in the longitudinal tension reinforcement of the truss model shown in Fig. 4.22 can be computed by dividing the member forces calculated in the previous step by the modulus of elasticity and the cross sectional area of the reinforcement.

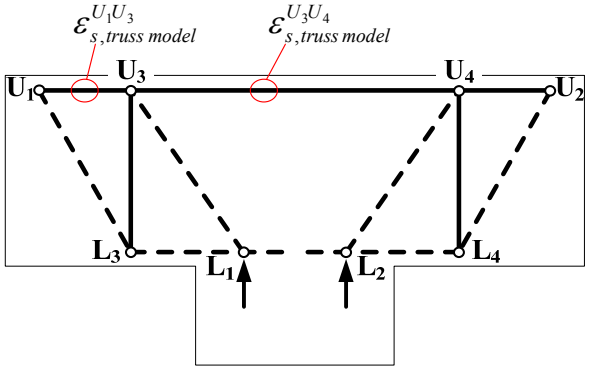

Figure 4.22- Strains in the longitudinal tension reinforcement of truss model

Since the computed strains are additionally induced strains by the externally bonded reinforcement system, the strains, $\varepsilon^{U_1U_3}_{s,truss\ model}$ and $\varepsilon^{U_3U_4}_{s,truss\ model}$ are added to the strain in the longitudinal tension reinforcement, ε_s calculated in the step 1 to compute the strains of combined strut-and-tie model. The strains in the longitudinal tension reinforcements of the combined strut-and-tie model can be determined using the following equations.

$$\varepsilon^{U_1U_3}_{s,combined\ model} = \varepsilon_s + \varepsilon^{U_1U_3}_{s,truss\ model} \tag{4.60}$$

$$\varepsilon^{U_3U_4}_{s,combined\ model} = \varepsilon_s + \varepsilon^{U_3U_4}_{s,truss\ model} \tag{4.61}$$

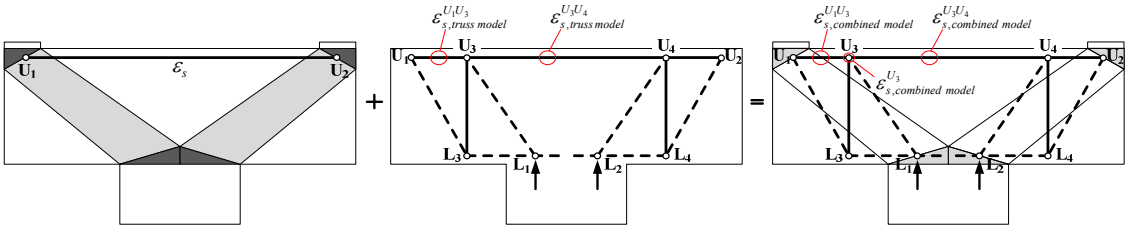

Figure 4.23- Combined strut-and-tie model

The strain at node U_3 of the combined strut-and-tie model is:

$$\varepsilon_{s,combined\,model}^{U_3} = \frac{1}{2}(\varepsilon_{s,combined\,model}^{U_1U_3} + \varepsilon_{s,combined\,model}^{U_3U_4}) \tag{4.62}$$

5. Check if the strain in the longitudinal tension reinforcement, $\varepsilon_{s,combined\ model}^{U_3U_4}$ of the combined strut-and-tie model reaches yield strain. When the strain reaches yield strain of the longitudinal tension reinforcement, the flexural failure mode controls the reinforced concrete pier cap. In this case, the strain in the longitudinal tension reinforcement of the truss model, $\varepsilon_{s,truss\,model}^{U_3U_4}$, can be calculated as follows:

$$\varepsilon_{s,truss\,model}^{U_3U_4} = \varepsilon_y - \varepsilon_s \tag{4.63}$$

Member forces of the truss mode shown in Fig. 4.21 are calculated from the member force U_3U_4 by a truss analysis.

4.2.4 Analysis Procedure

This section describes step-by-step procedure for the Proposed Strut-and-Tie Model for the cases in which bridge pier caps show both the failure modes by yielding of longitudinal tension reinforcement and those by the formation of a diagonal crack.

1. Compute the distance, c, from the extreme compression face to the location of the neutral axis, and depth of rectangular stress block, a, shown in Fig. 4.24.

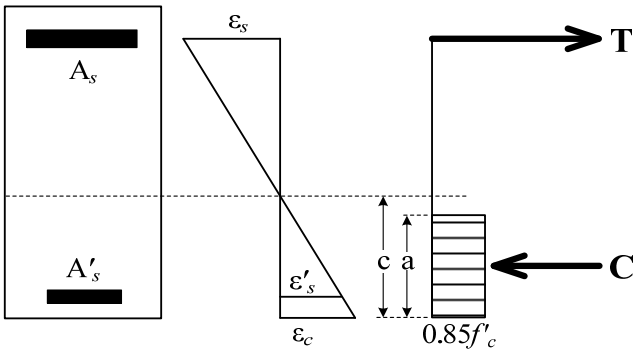

Figure 4.24- Stress and strain diagram

2. Select a preliminary strut-and-tie model for the bridge pier cap specimen excluding the externally bonded reinforcement system as shown in Fig. 4.25.

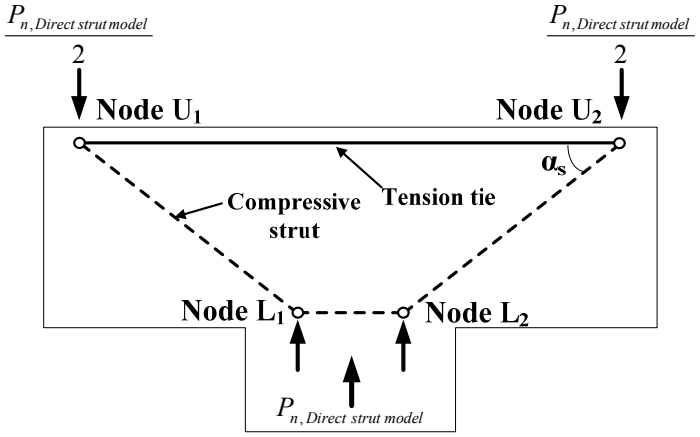

Figure 4.25- Direct strut model

3. Compute dimensions of node U_1 ($L_b^{L_1}$, $h_a^{L_1}$, and $w_s^{L_1}$), and strut angle, α_s using the following equations.

$$L_b^{L_1} = L_c / 2 \tag{4.64}$$

$$h_a^{L_1} = \beta_1 c \tag{4.65}$$

$$w_s^{L_1} = L_b^{L_1} \sin(\alpha_s) + h_a^{L_1} \cos(\alpha_s) \tag{4.66}$$

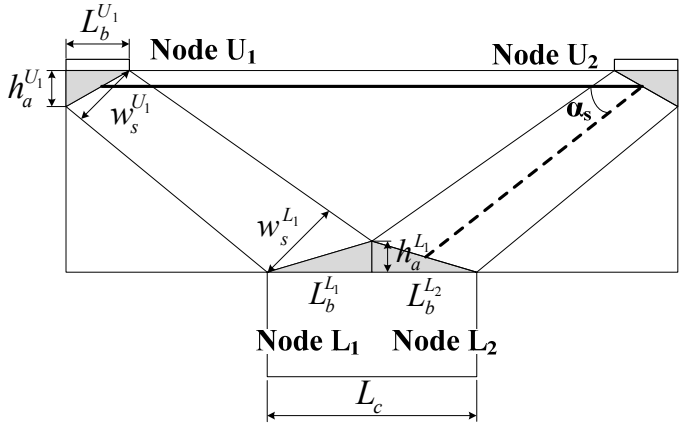

Figure 4.26- Dimensions of direct strut model

4. Compute dimensions of node U_1 ($L_b^{U_1}$, $h_a^{U_1}$, and $w_s^{U_1}$), shown in Fig. 4.30. The height, $h_a^{U_1}$, can be computed by assuming the strain in the longitudinal tension reinforcement ε_s as follows:

$$h_a^{U_1} = \frac{A_s E_s \varepsilon_s}{0.75 \phi f_c' b_w} \tag{4.67}$$

The height of the node U_1, $h_a^{U_1}$, should not exceed the effective concrete area of the node shown in the Figure 5.6.3.3.2-1-(b) of AASHTO LRFD Bridge Specifications (2012). Width of the node U_1, $w_s^{U_1}$ can be calculated as follows:

$$w_s^{U_1} = L_b^{U_1} \sin(\alpha_s) + h_a^{U_1} \cos(\alpha_s) \tag{4.68}$$

5. Compute the limiting stress in the compressive strut using the equation shown below.

$$f_{cu} = \frac{f_c'}{0.8 + 170\varepsilon_1} \le 0.85 f_c' \tag{4.69}$$

$$\varepsilon_1 = \varepsilon_s + (\varepsilon_s + 0.002)\cot^2 \alpha_s \tag{4.70}$$

6. Compute the nominal stress in the compressive strut at the node U_1 using the following equation.

$$f_n^{U_1} = \frac{A_s E_s \varepsilon_s}{w_s^{U_1} b_w \cos\alpha_s} \tag{4.71}$$

Check the calculated nominal stress. If $f_n^{U_1} > f_{cu}$, the strain in the longitudinal tension reinforcement, ε_s, should be reassumed. Repeat step 4 through 6 until $f_n^{U_1} = f_{cu}$ is satisfied.

7. Compute areas of the compressive strut at node L_1 and U_1 as follows:

$$A_{cs}^{L_1} = w_s^{L_1} b_w \tag{4.72}$$

$$A_{cs}^{U_1} = w_s^{U_1} b_w \tag{4.73}$$

For the area of the compressive strut $A_{cs}^{U_1 L_1}$ shown in Fig. 4.30, the minimum of $A_{cs}^{L_1}$ and $A_{cs}^{U_1}$ should be taken.

8. Compute strength of the bridge pier cap excluding the externally bonded reinforcement. The nominal strengths of compressive strut, $F^{U_1 L_1}$ and tension tie, $F^{U_1 U_2}$ are:

$$F^{U_1 L_1} = A_{cs}^{U_1 L_1} f_{cu} \tag{4.74}$$

$$F^{U_1 U_2} = A_s E_s \varepsilon_s \tag{4.75}$$

The nominal strength of the bridge pier cap is:

$$P_{n,\,Direct\,strut\,model}^{Compressive\,strut} = 2F^{U_1 L_1} \sin(\alpha_s) \tag{4.76}$$

$$P_{n,\,Direct\,strut\,model}^{Tension\,tie} = 2F_{U_1 U_2} \tan(\alpha_s) \tag{4.77}$$

$$P_n = Min(P_{n,\,Direct\,strut\,model}^{Compressive\,strut}, P_{n,\,Direct\,strut\,model}^{Tension\,tie}) \tag{4.78}$$

9. Determine a truss model representing the externally bonded reinforcement system. The vertical tension tie shown in Fig. 4.27 should be placed at the location of the resultant vertical force of the external reinforcement system. Compute the strut angles $\alpha_{s,\,truss\,model}^{U_1}$ and $\alpha_{s,\,truss\,model}^{U_3}$ shown in Fig. 4.27.

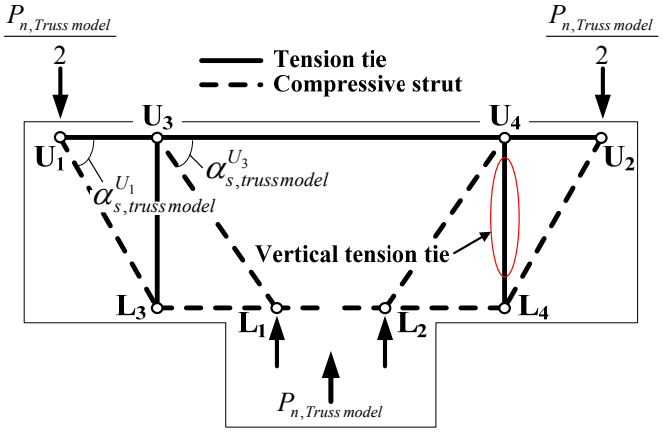

Figure 4.27- Truss model

10. Compute a_w and effective numbers of the external reinforcement as follows.

$$a_w = (0.85a_s - z/4) \tag{4.79}$$

The effective number of the external reinforcement, n_{ER}, can be determined by dividing a_w, by a spacing of the externally bonded reinforcement, s_{vER}.

11. Compute the member forces of the truss model. From the stress computed in the previous step, the force in the externally bonded reinforcement is:

$$F_{truss\ model}^{U_3L_3} = n_{ER} A_{ER} \sigma_{vER} \tag{4.80}$$

The other member forces of the truss model shown in Fig. 4.27 can be determined from a truss analysis.

12. Compute the strains in the truss members U_1U_3 and U_3U_4 as follows:

$$\varepsilon_{s,truss model}^{U_1U_3} = \frac{F_{truss model}^{U_1U_3}}{A_s E_s} \tag{4.81}$$

$$\varepsilon_{s,truss model}^{U_3U_4} = \frac{F_{truss model}^{U_3U_4}}{A_s E_s} \tag{4.82}$$

The strains in the truss members, $\varepsilon_{s,truss\ model}^{U_1U_3}$ and $\varepsilon_{s,truss\ model}^{U_3U_4}$, are added to the strain in the tension tie of direct strut model determined in step 4. Thus, the strains in

the members, U_1U_3 and U_3U_4 of the combined strut-and-tie model shown in Fig. 4.28 are:

$$\varepsilon_{s,combined\ model}^{U_1U_3} = \varepsilon_{s,truss\ model}^{U_1U_3} + \varepsilon_s \tag{4.83}$$

$$\varepsilon_{s,combined\ model}^{U_3U_4} = \varepsilon_{s,truss\ model}^{U_3U_4} + \varepsilon_s \tag{4.84}$$

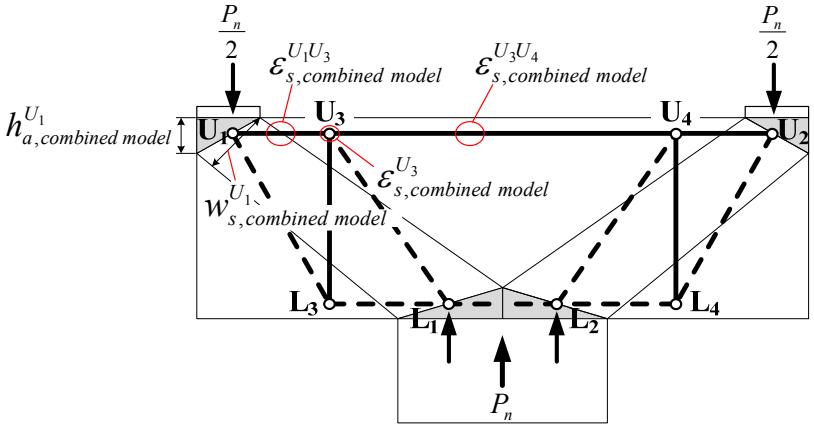

Figure 4.28- Combined strut-and-tie model

For the combined strut-and-tie model shown in Fig. 4.28, compute the strain in the tension tie at the node U_3 as follows:

$$\varepsilon_{s,combined\ model}^{U_3} = \frac{1}{2}\left(\varepsilon_{s,combined\ model}^{U_1U_3} + \varepsilon_{s,combined\ model}^{U_3U_4}\right) \tag{4.85}$$

13. Check if the longitudinal tension reinforcement of the combined strut-and-tie model yields. For the case in which $\varepsilon_{s,combined\ model}^{U_3U_4} < \varepsilon_y$, the strength of the pier cap is controlled by a failure mode due to the formation of a diagonal crack. When $\varepsilon_{s,combined\ model}^{U_3U_4} \geq \varepsilon_y$, flexural capacity controls the failure mode. In that case, the analytical procedure should skip to step 16.

14. Compute the height of node U_1 shown in Fig. 4.28 as follows:

$$h_{a,combined\ model}^{U_1} = \frac{A_s E_s \varepsilon_{s,combined\ model}^{U_3}}{f_{cu,combined\ model} b_w \cos^2(\alpha_s)} - L_b^{U_1} \tan(\alpha_s) \tag{4.86}$$

$$f_{cu,combined\,model} = \frac{f_c'}{0.8 + 170\varepsilon_{1,combined\,model}} \le 0.85 f_c' \tag{4.87}$$

$$\varepsilon_{1,combined\ model} = \varepsilon_{s,combined\ model}^{U_3} + (\varepsilon_{s,combined\ model}^{U_3} + 0.002)\cot^2 \alpha_s \tag{4.88}$$

The width of the compressive strut at node U_1 is:

$$w_{s,combined\,model}^{U_1} = L_b^{U_1} \sin(\alpha_s) + h_{a,combined\,model}^{U_1} \cos(\alpha_s) \tag{4.89}$$

The areas of compressive strut at node U_1 and L_1 are:

$$A_{cs,combined\,model}^{U_1} = w_{s,combined\,model}^{U_1} b_w \tag{4.90}$$

$$A_{cs,combined\,model}^{L_1} = A_{cs}^{L_1} \tag{4.91}$$

For the area of the compressive strut $A_{cs,combined\ model}^{U_1L_1}$, the minimum area between $A_{cs,combined\ model}^{U_1}$ and $A_{cs,combined\ model}^{L_1}$ shall be taken.

15. Compute strength of the bridge pier cap with externally bonded reinforcement system. The nominal strength of the compressive strut, $F_{combinedmodel}^{U_1L_1}$ and tension tie $F_{combined\,model}^{U_1U_2}$ are:

$$F_{combinedmodel}^{U_1L_1} = A_{cs,combinedmodel}^{U_1L_1} f_{cu,combinedmodel} \tag{4.92}$$

$$F_{combinedmodel}^{U_1U_2} = A_s E_s \varepsilon_{s,combinedmodel}^{U_3} \tag{4.93}$$

The nominal strength of the bridge pier cap with externally bonded reinforcement system is:

$$P_n = \min(F_{combinedmodel}^{U_1L_1}, F_{combinedmodel}^{U_1U_2}) + F_{trussmodel}^{U_3L_3} \tag{4.94}$$

The following steps are for the case in which $\varepsilon_{s,combined\ model}^{U_3U_4} \ge \varepsilon_y$.

16. Compute the strain in the member U_3U_4 of the combined model shown in Fig. 4.28 as follows:

$$\varepsilon_{s,combined\ model}^{U_3U_4} = \varepsilon_y - \varepsilon_s \tag{4.95}$$

The strain in the tension reinforcement, ε_s, is computed by the iterative procedure from the step 4 through step 6.

17. Compute member forces of the truss model shown in Fig. 4.27. The member force $F_{truss\ model}^{U_3U_4}$ is:

$$F_{truss\ model}^{U_3U_4} = A_s E_s \varepsilon_{s,combined\ model}^{U_3U_4} \tag{4.96}$$

The other member forces of the truss model can be computed by a truss analysis.

18. Compute the strains at the member U_1U_3 and node U_3 as follows:

$$\varepsilon_{s,combined\ model}^{U_1U_3} = \frac{F_{truss\ model}^{U_1U_3}}{A_s E_s} \tag{4.97}$$

$$\varepsilon_{s,combined\ model}^{U_3} = \frac{1}{2}(\varepsilon_{s,combined\ model}^{U_1U_3} + \varepsilon_{s,combined\ model}^{U_3U_4}) \tag{4.98}$$

The remained procedures for shear strength of the bridge pier cap can be conducted by step 14 and 15.

4.2.5 Experimental Validation of Proposed Strut-and-Tie Procedure

For the specimens with externally bonded reinforcement system, the proposed strut-and-tie procedure yielded the values of $P_{experiment}/P_{analysis}$ ranged from 1.03 to 1.33. Table 4.5 shows the comparison of analytical results by the proposed strut-and-tie procedure with the experimental results. Figure 4.29 shows the values of $P_{experiment}/P_{analysis}$. The proposed strut-and-tie model yielded strengths of the test specimens as well as failure modes. Although CSR018-1 and CSR018-2 specimens exhibited the flexural failure mode, the failure mode due to the formation of a diagonal crack was predicted by the proposed strut-and-tie procedure. It is because the proposed strut-and tie procedure is

based on the lower bound theorem of AASHTO Strut-and-Tie Model and the proposed strut-and-tie procedure gives a safe prediction.

Table 4.5- Analytical results by the proposed strut-and-tie procedure

Group	Specimen ID	$P_{experiment}$ (kips)	$P_{analysis}$ (kips)	$\frac{P_{analysis}}{f'_c b d_e}$	$\frac{P_{experiment}}{P_{analysis}}$	Predicted failure mode
A	BL2*	632	443	0.229	1.43	Diagonal crack
	AR014	748	563	0.286	1.33	Diagonal crack
	AR035	871	809	0.389	1.08	Diagonal crack
B	BS00	824	747	0.210	1.10	Diagonal crack
	BSR008	980	796	0.226	1.23	Diagonal crack
	BSR014	1050	848	0.243	1.24	Diagonal crack
C	CS00	508	310	0.078	1.64	Diagonal crack
	CSR018-1	514***	478	0.125	1.09	Flexural failure
	CSR018-2	481***	477	0.130	1.03	Flexural failure
	CSR035	520***	479	0.122	1.10	Flexural failure

* BL2 is the reference test specimen reported by Zureick et al. (2013)
*** Load at yielding of the longitudinal tension reinforcement

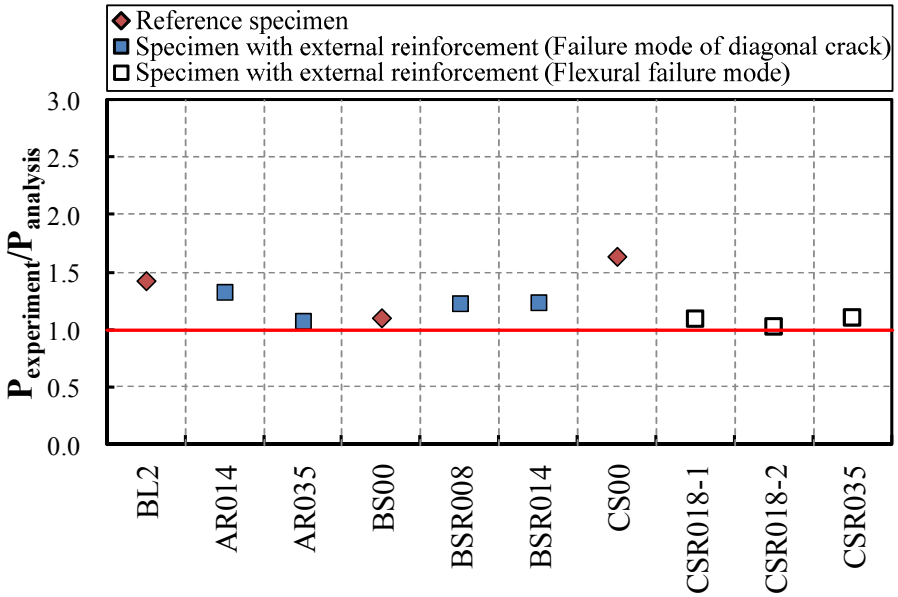

Figure 4.29- $P_{experiment}$ / $P_{analysis}$ computed by proposed strut-and-tie procedure

CHAPTER 5

SUMMARY, CONCLUSIONS, AND FUTURE WORK

This chapter summarizes the work conducted in this thesis and presents conclusions and recommendations for further studies.

5.1 Summary

The research presented in this thesis consisted of experimental and analytical studies aimed at examining the behavior of reinforced concrete bridge pier caps with externally bonded reinforcement. In the experimental part of this work, nine full-scale reinforced concrete bridge pier caps were built, externally strengthened with stainless reinforcement, and tested to failure. In the analytical part of this work, two methods were proposed for the analysis and design of reinforced concrete bridge pier caps strengthened with externally bonded reinforcement. In the first analytical method, a closed-form mechanics-based solution was derived for computing the shear of the reinforced concrete bridge pier caps. The second analytical method is based on the application of strut-and-tie models that can predict the overall strength and the corresponding strength limit state of reinforced concrete pier caps with externally bonded reinforcement. Both analytical methods were experimentally validated from the experimental study.

5.2 Conclusions

Based on the results of this study, the following conclusions are made:

1. The use of externally bonded stainless steel reinforcement, for increasing the shear strength of reinforced concrete bridge pier caps has shown to be effective. An increase of up to 28% in the shear strength has been realized in this study.

2. The use of externally bonded stainless steel reinforcement to strengthen reinforced concrete bridge pier caps containing low ratio of longitudinal tension reinforcement (e.g. less than 1%) can alter the failure mode from diagonal shear cracks to yielding of longitudinal tension reinforcement.
3. When calculating the shear strength of the reinforced concrete bridge pier caps, the strain of the externally bonded transverse reinforcement system should be limited to 0.003.
4. The Mechanics-based approach is a direct and efficient method for computing the shear strength of reinforced concrete bridge pier caps with externally bonded reinforcement. Equations for determining the shear strength are presented in closed-form where the solution does not require iteration.
5. The strut-and-tie procedure consisting of two separate models is time-consuming and requires iteration. However, it has the advantage of calculating the strength and identifying the governing strength limit state of reinforced concrete bridge pier caps with externally bonded reinforcement system.

5.3 Recommended Future Work

Based on the results and limitations of this work, the following topics are recommended for further studies:

1. A single strut-and-tie model to account for the arching mechanism as well as the internal and external reinforcements should be developed. Such an approach can be developed in a manner similar to that in AASHTO LRFD Bridge Specifications (2012) and ACI 318 (2008).
2. The analytical expressions (Eq. 4.49-a and 4.49-b) developed in this study have been validated experimentally only for the case of externally bonded transverse reinforcement. It is recommended that Eq. 4.49-a and 4.49-b be validated from

experiments on reinforced concrete pier caps having externally bonded longitudinal reinforcement as well as combination of longitudinal and transverse reinforcement.

APPENDIX A

REINFORCED CONCRETE DEEP BEAM DATABASE (156 SAMPLES)

Table A.1- Reinforced concrete deep beams database (156 samples)

Specimen ID	a (in.)	b	d_e (in.)	a/d	f_c' (psi)	f_y (ksi)	ρ (%)	ρ_v (%)
Clark (1954)								
C1-1	24.00	8.00	15.30	1.57	3720	47	2.075	0.344
C1-2	24.00	8.00	15.30	1.57	3820	47	2.075	0.344
C1-3	24.00	8.00	15.30	1.57	3475	47	2.075	0.344
C1-4	24.00	8.00	15.30	1.57	4210	47	2.075	0.344
C2-1	24.00	8.00	15.30	1.57	3430	47	2.075	0.688
C2-2	24.00	8.00	15.30	1.57	3625	47	2.075	0.688
C2-3	24.00	8.00	15.30	1.57	3500	47	2.075	0.688
C2-4	24.00	8.00	15.30	1.57	3910	47	2.075	0.688
D1-1	18.00	8.00	15.50	1.16	3800	49	1.613	0.458
D1-2	18.00	8.00	15.50	1.16	3790	49	1.613	0.458
D1-3	18.00	8.00	15.50	1.16	3560	49	1.613	0.458
D2-1	18.00	8.00	15.50	1.16	3480	49	1.613	0.611
D2-2	18.00	8.00	15.50	1.16	3755	49	1.613	0.611
D2-3	18.00	8.00	15.50	1.16	3595	49	1.613	0.611
D2-4	18.00	8.00	15.50	1.16	3550	49	1.613	0.611
D3-1	18.00	8.00	15.50	1.16	4090	49	2.419	0.917
D4-1	18.00	8.00	15.50	1.16	3350	49	1.613	1.222
C0-1	24.00	8.00	15.30	1.57	3580	54	0.980	
C0-2	24.00	8.00	15.30	1.57	3405	54	0.980	
C0-3	24.00	8.00	15.30	1.57	3420	54	0.980	
D0-1	18.00	8.00	15.30	1.18	3750	54	0.980	
D0-2	18.00	8.00	15.30	1.18	3800	54	0.980	
D0-3	18.00	8.00	15.30	1.18	3765	54	0.980	
Moody et al. (1954)								
III-24a	32.00	7.00	21.00	1.52	2580	46	2.721	
III-24b	32.00	7.00	21.00	1.52	2990	46	2.721	
III-25a	32.00	7.00	21.00	1.52	3530	45	3.456	
III-25b	32.00	7.00	21.00	1.52	2500	45	3.456	
III-26a	32.00	7.00	21.00	1.52	3140	44	4.245	
III-26b	32.00	7.00	21.00	1.52	2990	44	4.245	
III-27a	32.00	7.00	21.00	1.52	3100	46	2.721	
III-27b	32.00	7.00	21.00	1.52	3320	46	2.721	
III-28a	32.00	7.00	21.00	1.52	3380	45	3.456	
III-28b	32.00	7.00	21.00	1.52	3250	45	3.456	
III-29a	32.00	7.00	21.00	1.52	3150	44	4.245	
III-29b	32.00	7.00	21.00	1.52	3620	44	4.245	
III-30	32.00	7.00	21.00	1.52	3680	44	4.245	0.524
III-31	32.00	7.00	21.00	1.52	3250	44	4.245	0.952
Moody et al. (1954)								
II-a	32.00	7.00	20.75	1.54	3820	46	0.551	

II-b	32.00	7.00	20.75	1.54	3720	44	0.854	
II-c	32.00	7.00	20.75	1.54	4040	42	1.212	
II-d	32.00	7.00	20.75	1.54	3440	42	1.652	
II-17a	32.00	7.00	20.75	1.54	2650	47	2.176	
II-17b	32.00	7.00	20.75	1.54	3000	47	2.176	
II-18a	32.00	7.00	20.75	1.54	2170	46	2.754	
II-18b	32.00	7.00	20.75	1.54	2700	46	2.754	
II-19a	32.00	7.00	20.75	1.54	3030	45	3.497	
II-19b	32.00	7.00	20.75	1.54	3240	45	3.497	
II-20a	32.00	7.00	20.75	1.54	2890	44	4.296	
II-20b	32.00	7.00	20.75	1.54	2960	44	4.296	
Morrow and Viest (1956)								
B21E2	24.50	12.00	14.75	1.66	1640	67	0.574	
B21E4R	24.50	12.00	14.50	1.69	4630	60	1.236	
B21F4	24.50	12.00	14.56	1.68	4560	66	1.118	
Watstein and Mathey (1958)								
B-18-1	24.00	8.00	15.90	1.51	3680	39	2.995	
B-18-2	24.00	8.00	15.90	1.51	3330	39	2.995	
C-18-2	24.00	8.00	15.90	1.51	3830	68	1.863	
D-18-1	24.00	8.00	15.90	1.51	3720	105	1.163	
D-18-2	24.00	8.00	15.90	1.51	3910	97	1.163	
E-18-1	24.00	8.00	15.90	1.51	3250	100	0.731	
E-18-2	24.00	8.00	15.90	1.51	3870	100	0.731	
Rodriguez et al. (1959)								
E6N1	17.00	6.00	12.50	1.36	3213	43	2.637	
E6N2	17.00	6.06	12.50	1.36	2627	45	2.611	
E6N3	17.00	6.06	12.50	1.36	3277	45	2.611	
C6N1	17.00	6.13	12.63	1.35	3640	47	2.555	
C6N2	17.00	6.00	12.50	1.36	2963	46	2.637	
C6N3	17.00	6.06	12.38	1.37	3153	46	2.637	
Mathey and Watstein (1963)								
I-1	24.00	8.00	15.86	1.51	3680	39	3.045	
II-4	24.00	8.00	15.86	1.51	3830	68	1.884	
IV-7	24.00	8.00	15.86	1.51	3500	65	1.861	
IV-8	24.00	8.00	15.86	1.51	3610	65	1.861	
V-9	24.00	8.00	15.86	1.51	3350	101	1.163	
V-10	24.00	8.00	15.86	1.51	3910	101	1.163	
VI-11	24.00	8.00	15.86	1.51	3680	105	1.166	
VI-12	24.00	8.00	15.86	1.51	3720	105	1.166	
V-13	24.00	8.00	15.86	1.51	3250	103	0.752	
V-14	24.00	8.00	15.86	1.51	3870	103	0.752	
VI-15	24.00	8.00	15.86	1.51	3700	101	0.750	
VI-16	24.00	8.00	15.86	1.51	3310	101	0.750	
Manuel (1974)								
11	17.00	4.00	16.00	1.06	4680	54	1.875	
Smith and Vantsiotis (1982)								
0B0-49	14.50	4.00	12.00	1.21	3145	61	1.938	
1B1-01	14.50	4.00	12.00	1.21	3200	63	1.938	0.233
1B3-29	14.50	4.00	12.00	1.21	2915	63	1.938	0.233
1B3-30	14.50	4.00	12.00	1.21	3020	63	1.938	0.233
1B6-31	14.50	4.00	12.00	1.21	2830	63	1.938	0.233
2B1-05	14.50	4.00	12.00	1.21	2780	63	1.938	0.408

2B3-06	14.50	4.00	12.00	1.21	2755	63	1.938	0.408
2B4-07	14.50	4.00	12.00	1.21	2535	63	1.938	0.408
2B4-52	14.50	4.00	12.00	1.21	3160	63	1.938	0.408
2B6-32	14.50	4.00	12.00	1.21	2865	63	1.938	0.408
3B1-08	14.50	4.00	12.00	1.21	2355	63	1.938	0.613
3B1-36	14.50	4.00	12.00	1.21	2960	63	1.938	0.754
3B3-33	14.50	4.00	12.00	1.21	2755	63	1.938	0.754
3B4-34	14.50	4.00	12.00	1.21	2790	63	1.938	0.754
3B6-35	14.50	4.00	12.00	1.21	2995	63	1.938	0.754
4B1-09	14.50	4.00	12.00	1.21	2480	63	1.938	1.225
1C4-15	18.00	4.00	12.00	1.50	3290	63	1.938	0.175
Subedi et al. (1986)								
1B2	27.17	3.94	17.22	1.58	5366	72	0.921	0.218
2D2	50.79	3.94	32.79	1.55	5714	44	1.179	0.199
Rogowsky et al. (1986)								
BM3/1.5 T1	35.43	7.87	21.06	1.68	2103	66	1.121	0.227
BM3/1.5 T2	35.43	7.87	21.06	1.68	2103	66	1.121	0.227
BM4/1.5 T1	35.43	7.87	21.06	1.68	4714	66	1.121	
BM4/1.5 T2	35.43	7.87	21.06	1.68	4714	66	1.121	
BM5/1.5 T1	35.43	7.87	21.06	1.68	5743	66	1.121	0.643
BM5/1.5 T2	35.43	7.87	21.06	1.68	5743	66	1.121	0.643
BM7/1.5 T1	35.43	7.87	21.06	1.68	4409	66	1.121	
BM7/1.5 T2	35.43	7.87	21.06	1.68	4409	66	1.121	
BM8/1.5 T1	35.43	7.87	21.06	1.68	5395	66	1.121	0.227
BM8/1.5 T2	35.43	7.87	21.06	1.68	5395	66	1.121	0.227
Xie et al.(1994)								
NNW-1	8.50	5.00	8.00	1.06	5470	61	3.200	0.490
Anguilar (2002)								
STM-H	36.00	12.00	31.50	1.14	4130	61	1.254	0.306
STM-M	36.00	12.00	31.50	1.14	4130	61	1.254	0.153
Yang et al. (2003)								
L10-40	15.75	6.30	13.98	1.13	4554	117	1.011	
L10-40R	15.75	6.30	13.98	1.13	4554	117	1.011	
L10-60	23.62	6.30	21.85	1.08	4554	117	0.970	
L10-75	29.53	6.30	26.97	1.09	4554	117	1.047	
L10-75R	29.53	6.30	26.97	1.09	4554	117	1.047	
L10-100	39.37	6.30	36.81	1.07	4554	88	0.901	
Tanimura and Sato (2005)								
9	23.62	11.81	15.75	1.50	3321	66	2.202	
10	23.62	11.81	15.75	1.50	3263	66	2.202	0.189
11	23.62	11.81	15.75	1.50	3336	66	2.202	0.525
12	23.62	11.81	15.75	1.50	3408	66	2.202	0.886
22	23.62	11.81	15.75	1.50	3800	66	2.202	0.525
23	23.62	11.81	15.75	1.50	3814	66	2.202	0.886
Brown et al (2006)								
I-CL-8.5-0	30.00	6.00	27.00	1.11	2580	68	1.951	0.431
I-CL-0-0	30.00	6.00	27.00	1.11	2370	68	1.951	
Zhang and Tan (2007)								
1DB35bw	13.56	3.15	12.32	1.10	3757	68	1.255	0.473
1DB50bw	19.66	4.53	17.87	1.10	3974	74	1.279	0.329
1DB70bw	27.80	6.30	25.28	1.10	4105	76	1.224	0.419

1DB100bw	39.15	9.06	35.59	1.10	4163	77	1.203	0.456
2DB35	13.60	3.15	12.36	1.10	3974	68	1.251	
2DB50	19.88	3.15	18.07	1.10	4699	72	1.152	
2DB70	28.15	3.15	25.59	1.10	3597	74	1.284	
2DB100	40.10	3.15	36.46	1.10	4438	74	1.259	
3DB35b	13.60	3.15	12.36	1.10	3974	68	1.251	
3DB50b	19.66	4.53	17.87	1.10	4105	74	1.279	
3DB70b	27.80	6.30	25.28	1.10	4163	76	1.224	
3DB100b	39.15	9.06	35.59	1.10	4250	77	1.203	
Alcocer and Uribe (2008)								
MT	55.12	13.78	43.31	1.27	5134	65	1.059	0.527
MR	55.12	13.78	43.31	1.27	5076	65	1.059	0.527
Birrcher et al. (2009)								
III-1.2-02	46.32	21.00	38.60	1.20	4100	66	2.309	0.201
III-1.2-03	46.32	21.00	38.60	1.20	4220	66	2.309	0.311
IV-2175-1.2-03	82.68	21.00	68.90	1.20	5010	68	2.372	0.207
IV-2123-1.2-02	23.40	21.00	19.50	1.20	4630	65	2.315	0.200
Bechtel (2011)								
AL1	39.00	18.00	32.80	1.19	3473	65	0.645	
BL1	39.00	18.00	32.80	1.19	3352	80	0.645	
AL2	39.00	18.00	32.12	1.21	3651	65	1.318	
BL2	39.00	18.00	32.12	1.21	3353	80	1.318	
BL3	39.00	18.00	32.12	1.21	3966	80	1.318	0.278
BL4	39.00	18.00	32.12	1.21	3874	80	1.318	0.278
BL5	39.00	18.00	32.12	1.21	3998	80	1.318	0.278
AS1	19.50	9.00	16.40	1.19	4123	79	0.630	
AS2	19.50	9.00	16.40	1.19	4226	79	0.630	
AS3	19.50	9.00	16.06	1.21	4036	76	1.384	
AS4	19.50	9.00	16.06	1.21	4650	85	1.384	
O'Malley (2011)								
1-S	41.00	12.00	32.25	1.27	3430	73	1.021	0.272
2-NS	41.00	12.00	32.25	1.27	3180	73	1.021	
6-NS	41.00	12.00	32.25	1.27	3460	73	1.021	

APPENDIX B

DETAILS OF PIER CAP SPECIMENS

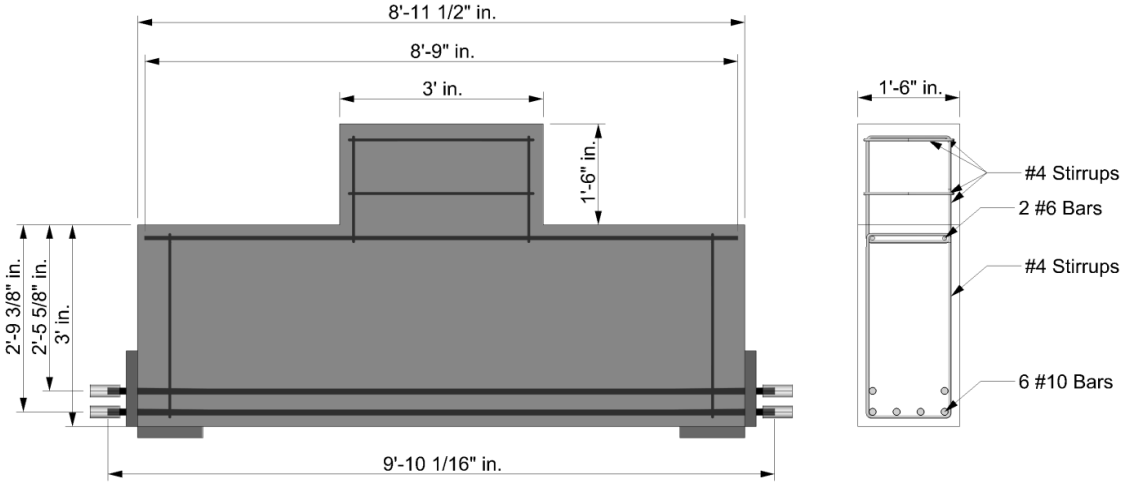

Figure B.1- BL2 specimen

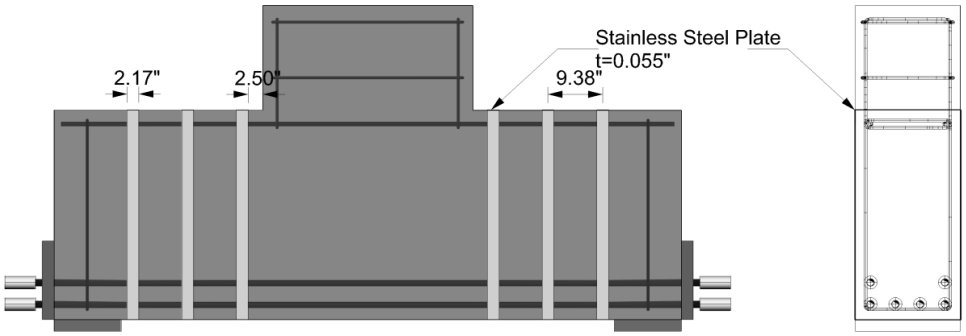

Figure B.2- AR014 specimen

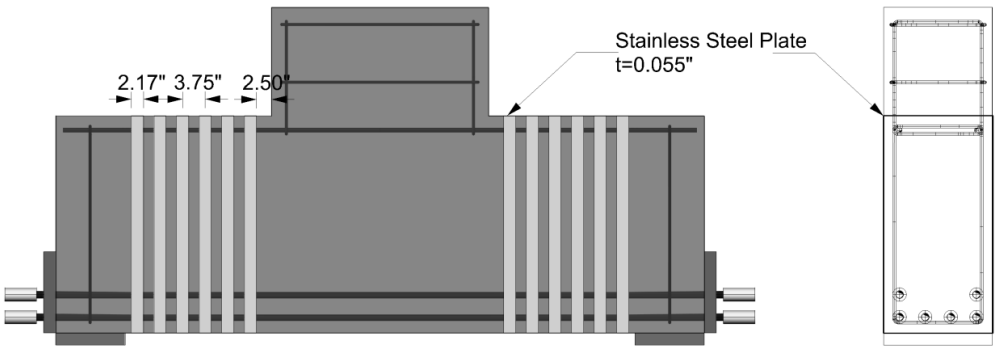

Figure B.3- AR035 specimen

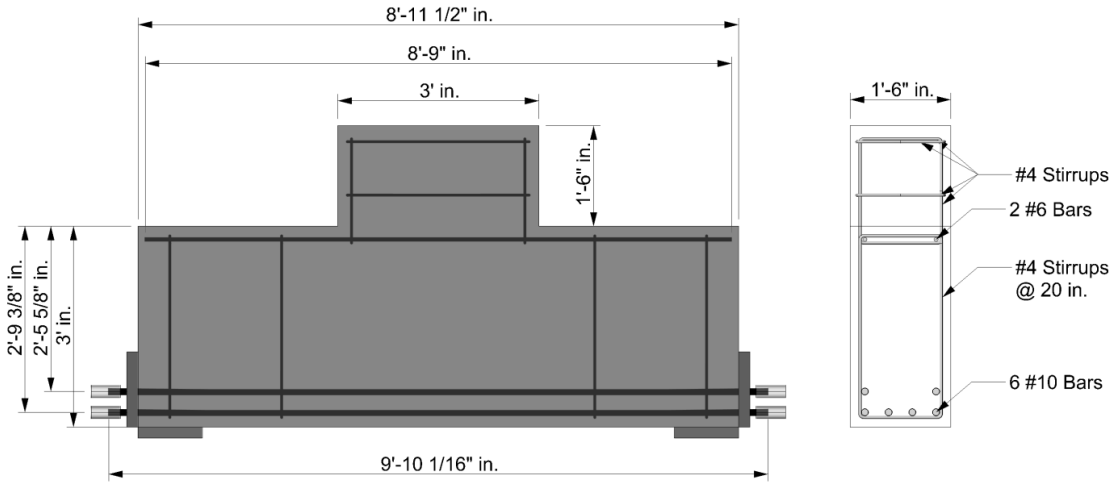

Figure B.4- BS00 Specimen

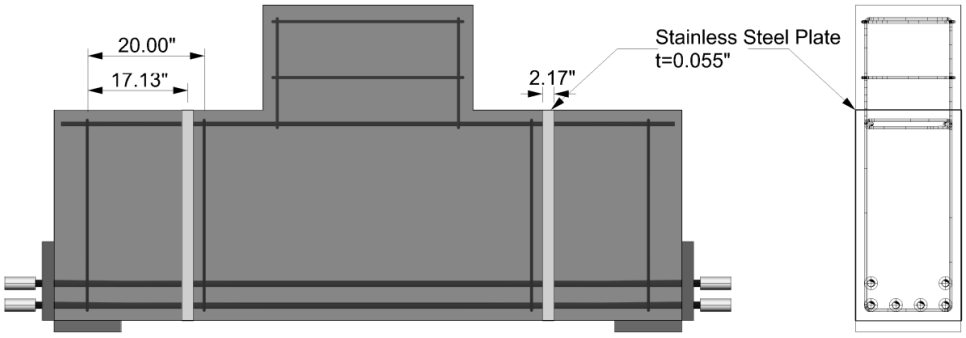

Figure B.5- BSR008 Specimen

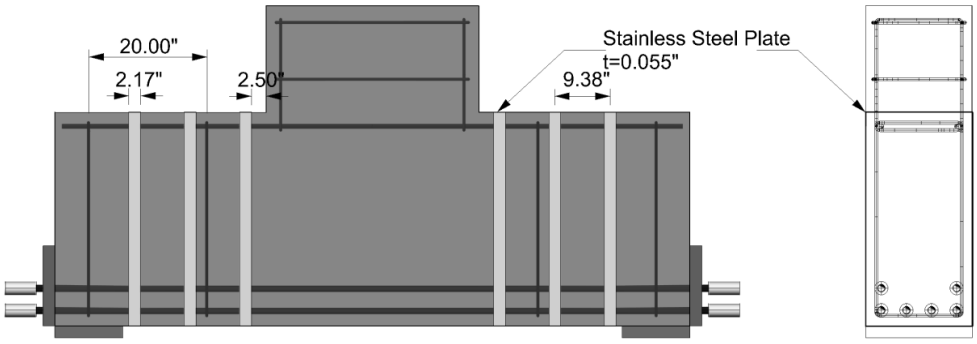

Figure B.6- BSR014 Specimen

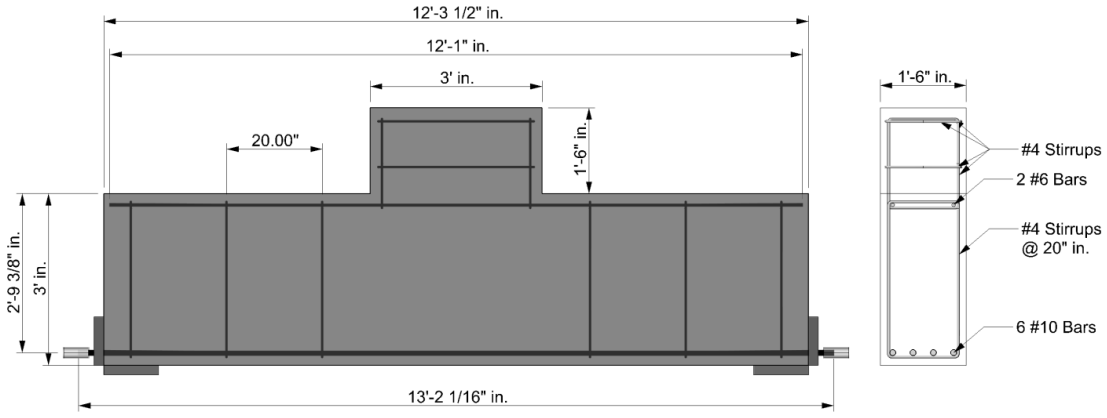

Figure B.7- CS00 Specimen

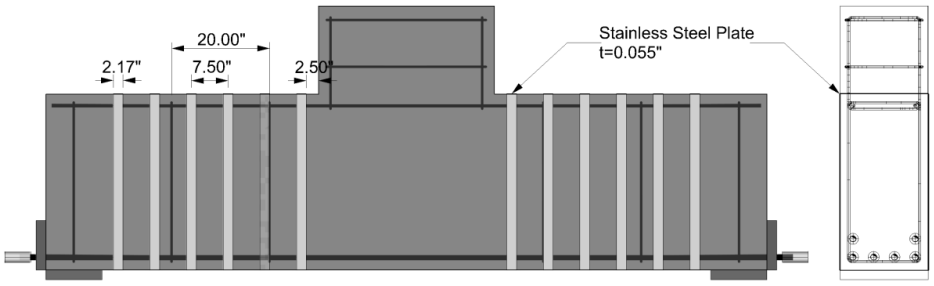

Figure B.8- CSR018-1 and CSR018-2 Specimen

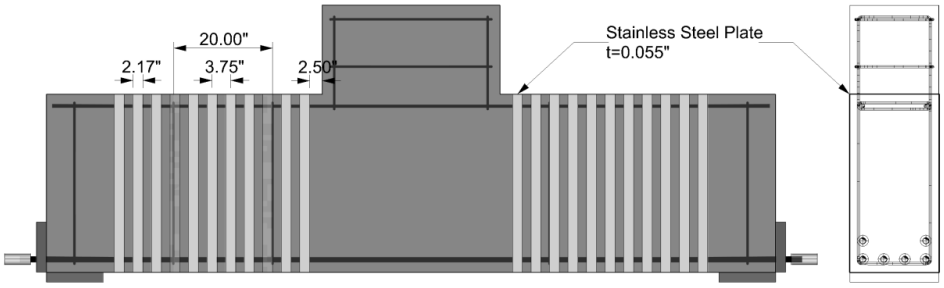

Figure B.9- CSR035 Specimen

APPENDIX C

PLOTS FOR STRAINS IN STAINLESS STEEL EXTERNAL REINFORCEMENT

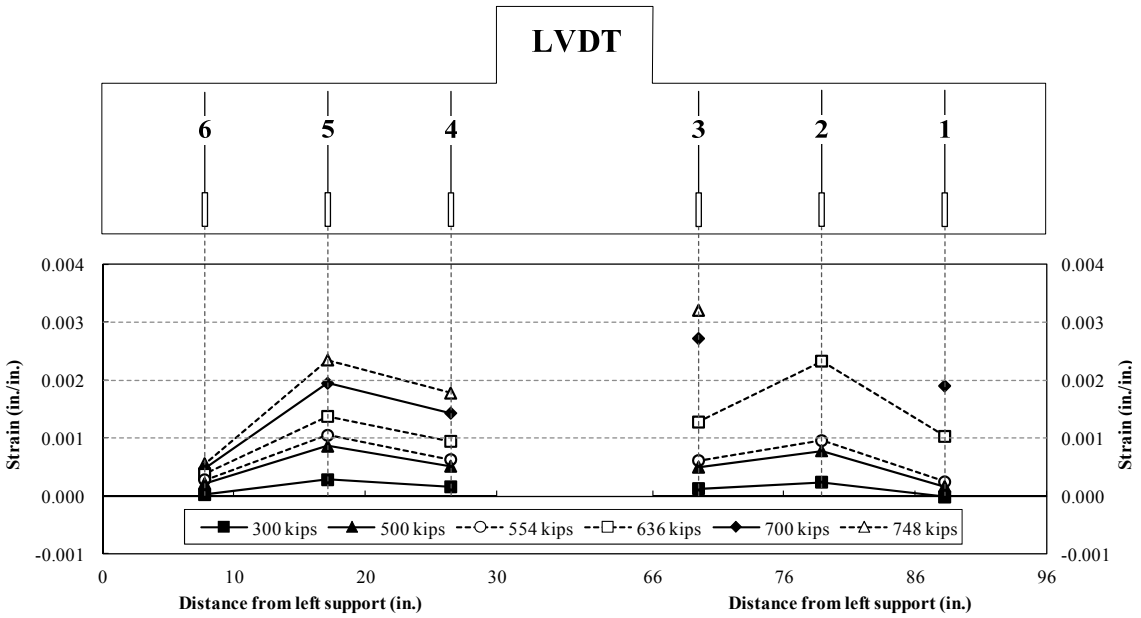

Figure C.1-Variations of vertical strains in stainless steel plates for AR014 specimen

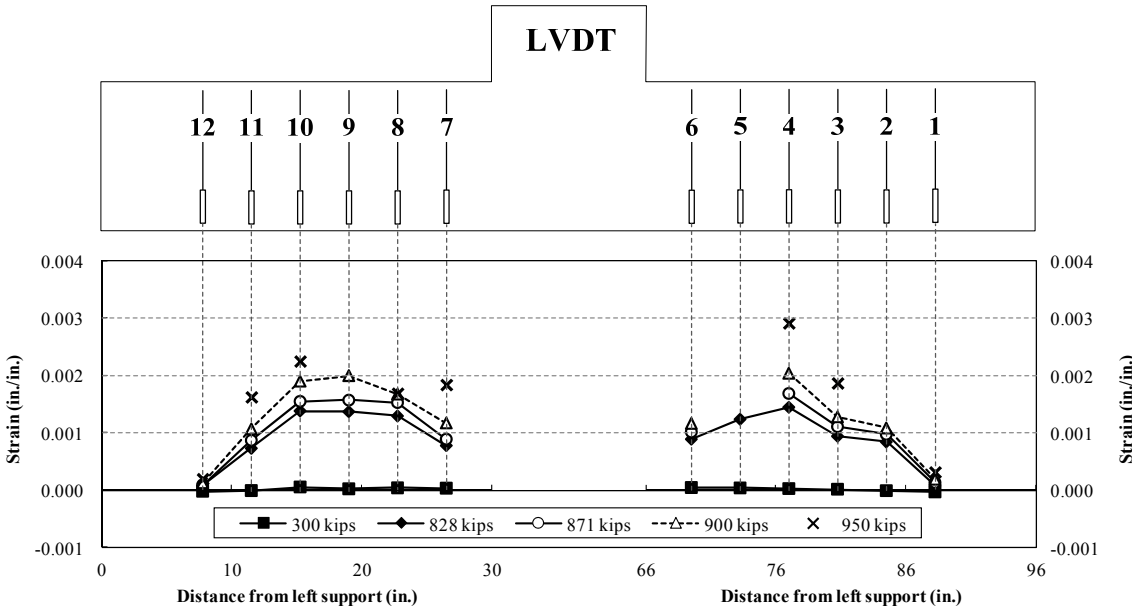

Figure C.2-Variations of vertical strains in stainless steel plates for AR035 specimen

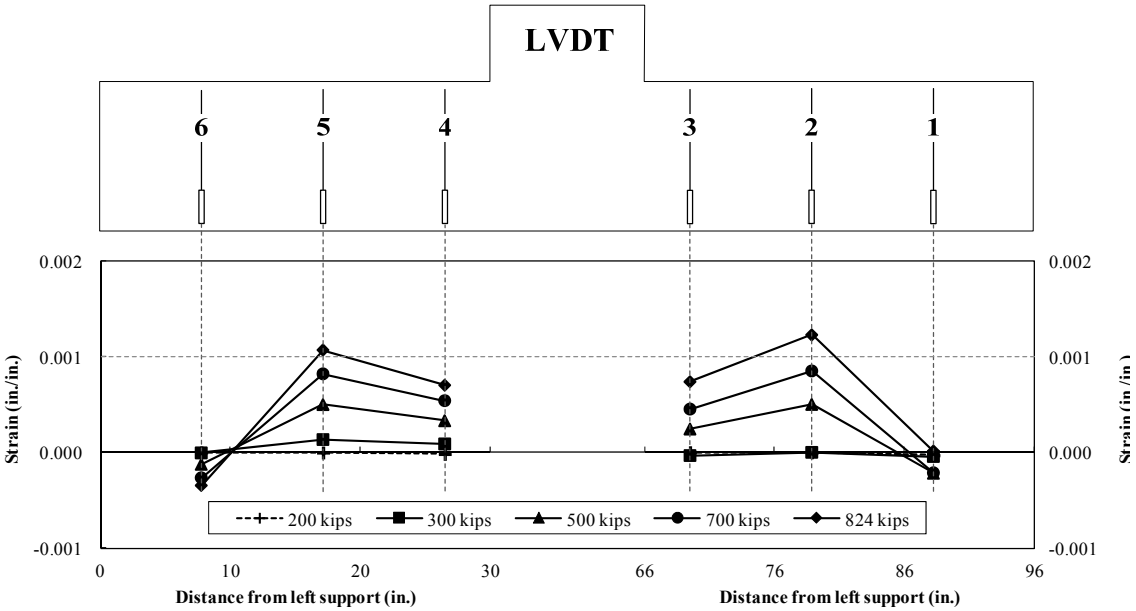

Figure C.3- Variations of vertical strains in stainless steel plates for BS00 specimen

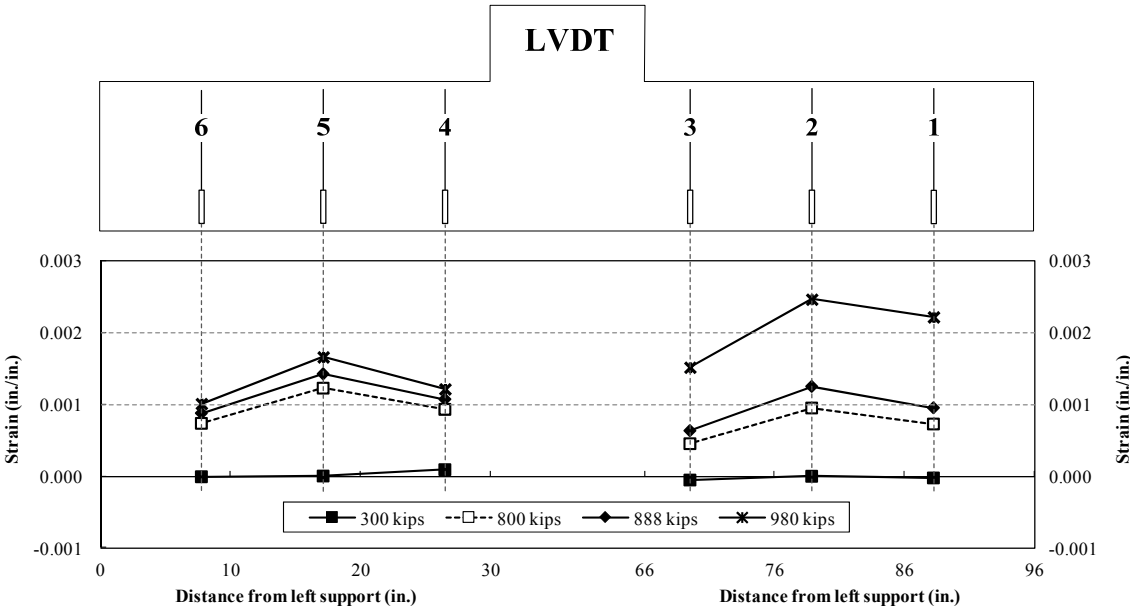

Figure C.4- Variations of vertical strains in stainless steel plates for BSR008 specimen

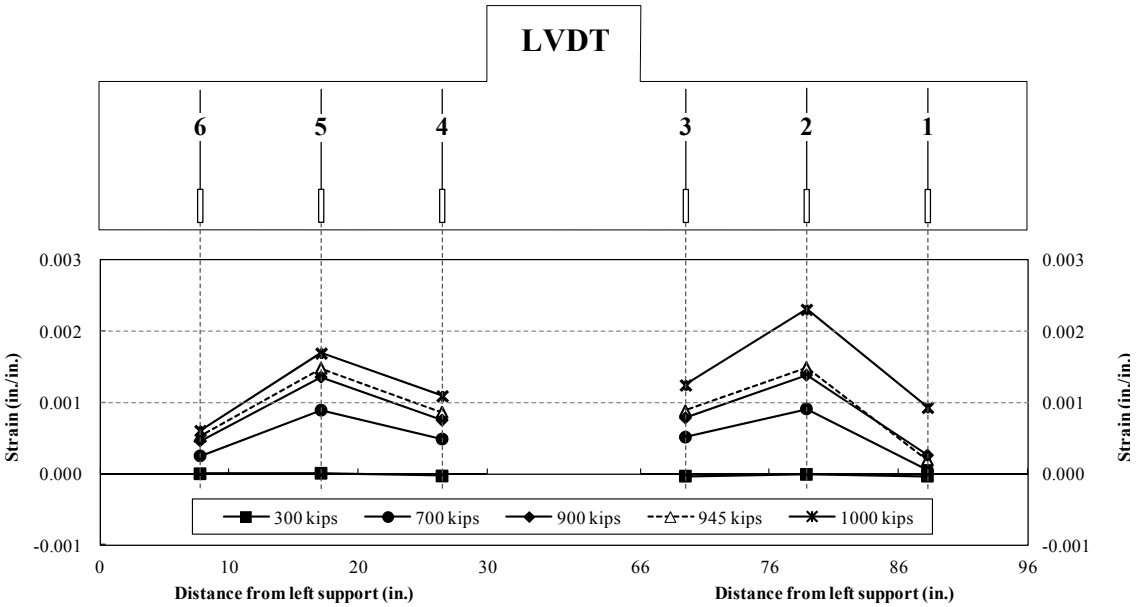

Figure C.5- Variations of vertical strains in stainless steel plates for BSR014 specimen

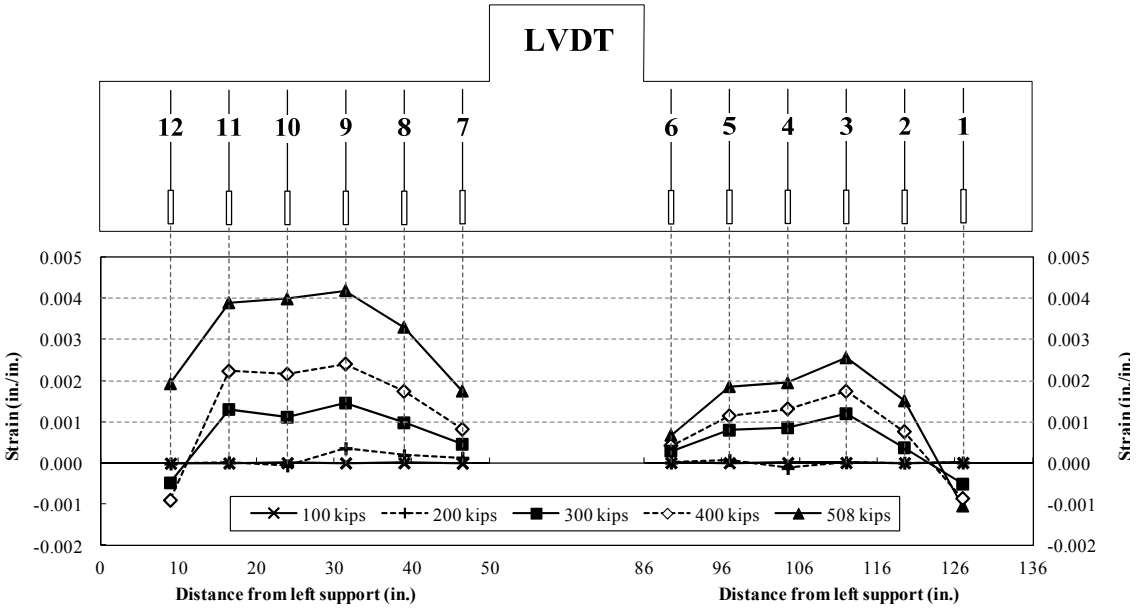

Figure C.6- Variations of vertical strains in stainless steel plates for CS00 specimen

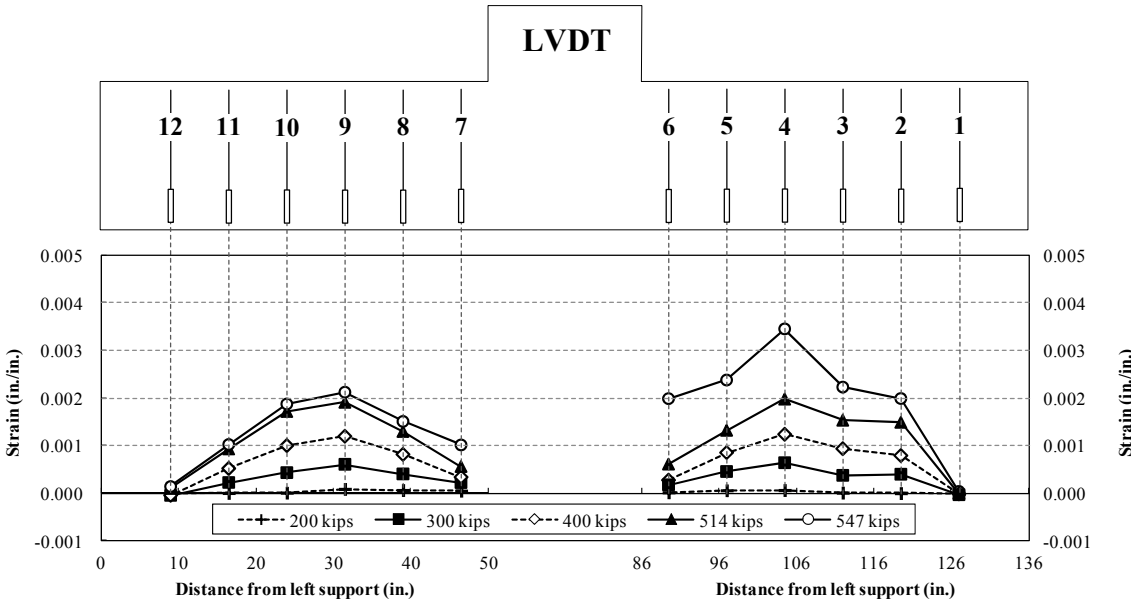

Figure C.7- Variations of vertical strains in stainless steel plates for CSR018-1 specimen

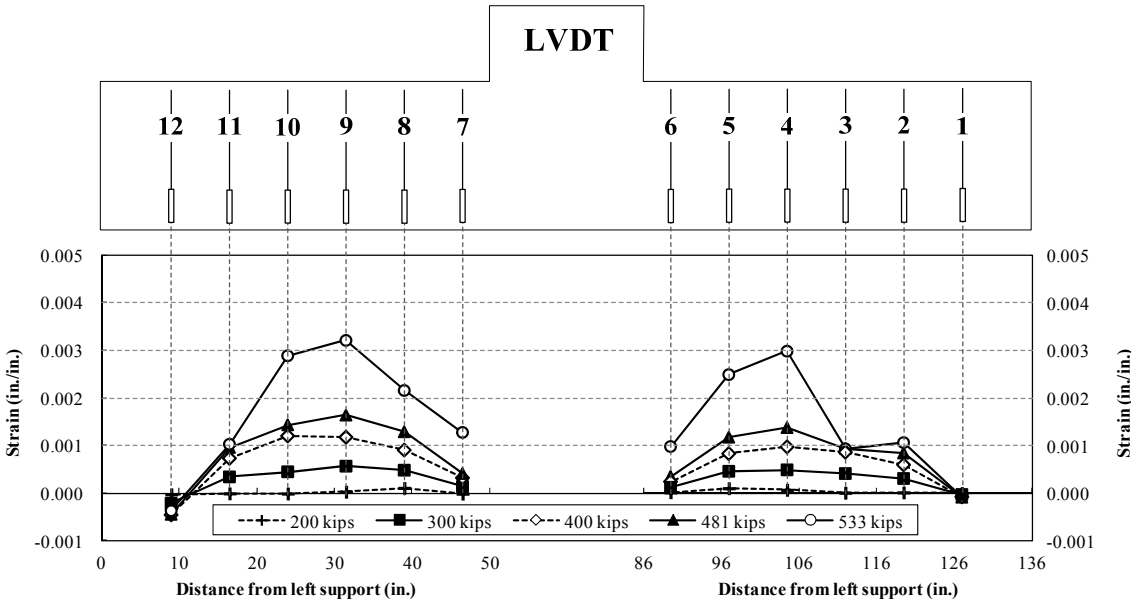

Figure C.8- Variations of vertical strains in stainless steel plates for CSR018-2 specimen

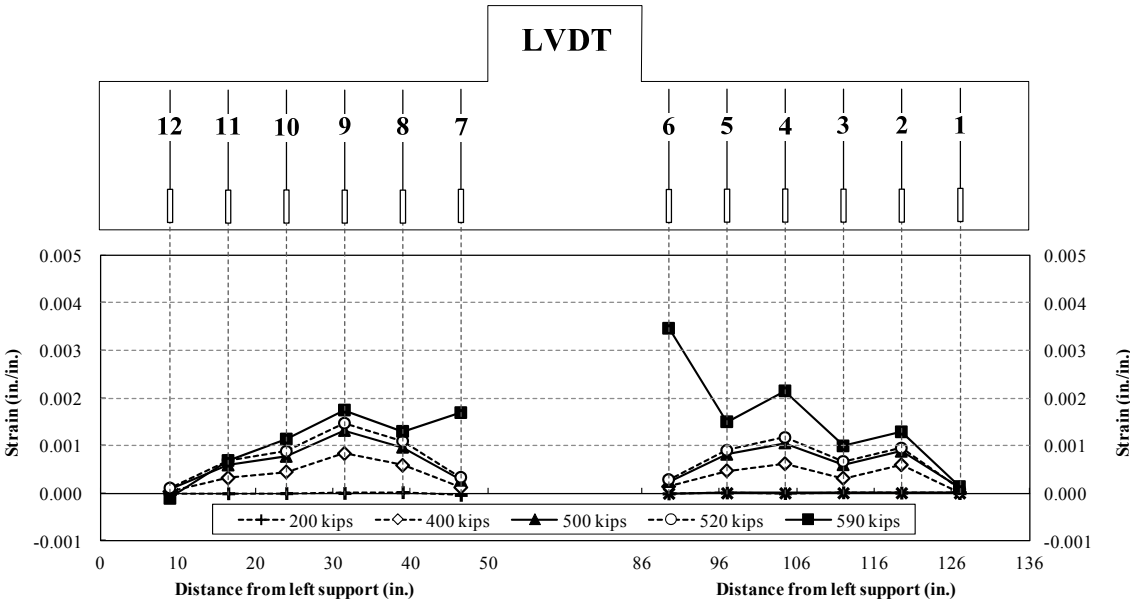

Figure C.9- Variations of vertical strains in stainless steel plates for CSR035 specimen

APPENDIX D

PLOTS FOR STRAINS IN LONGITUDINAL TENSION REINFORCEMENT

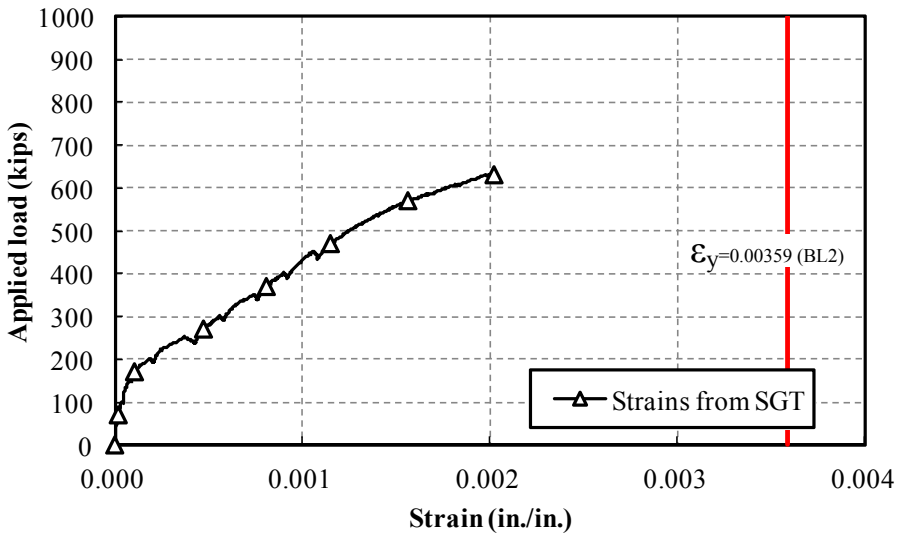

Figure D.1- Applied load vs. strain of longitudinal tension reinforcement for specimen BL2 (*Zureick et al., 2011*)

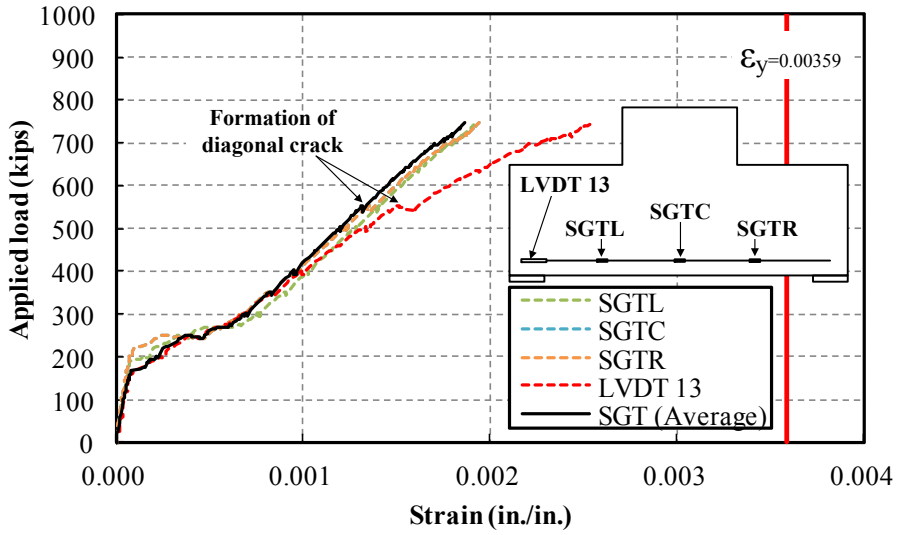

Figure D.2- Applied load vs. strain of longitudinal tension reinforcement for specimen AR014

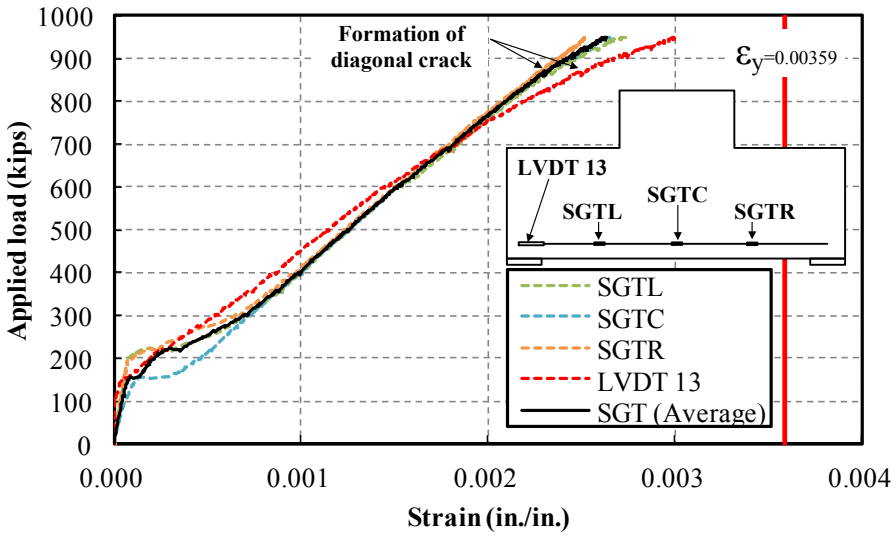

Figure D.3- Applied load vs. strain of longitudinal tension reinforcement for specimen AR035

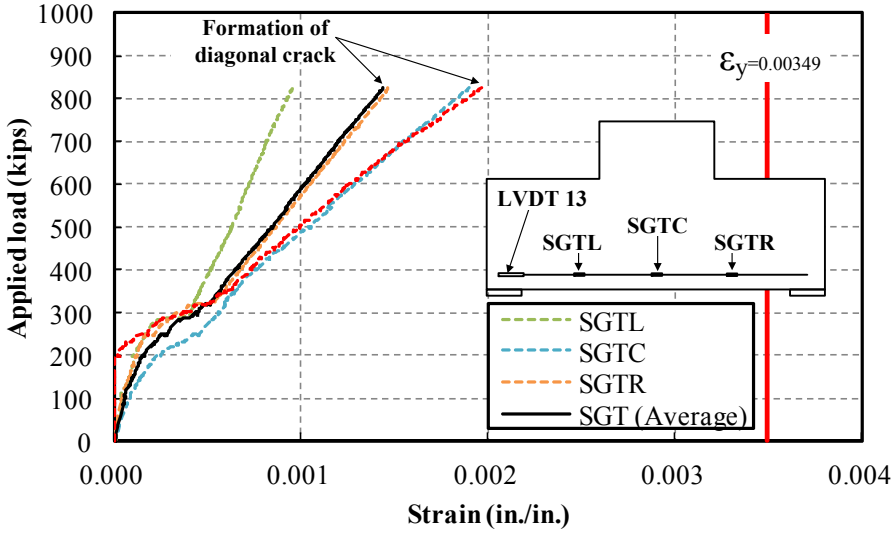

Figure D.4- Applied load vs. strain of longitudinal tension reinforcement for specimen BS00

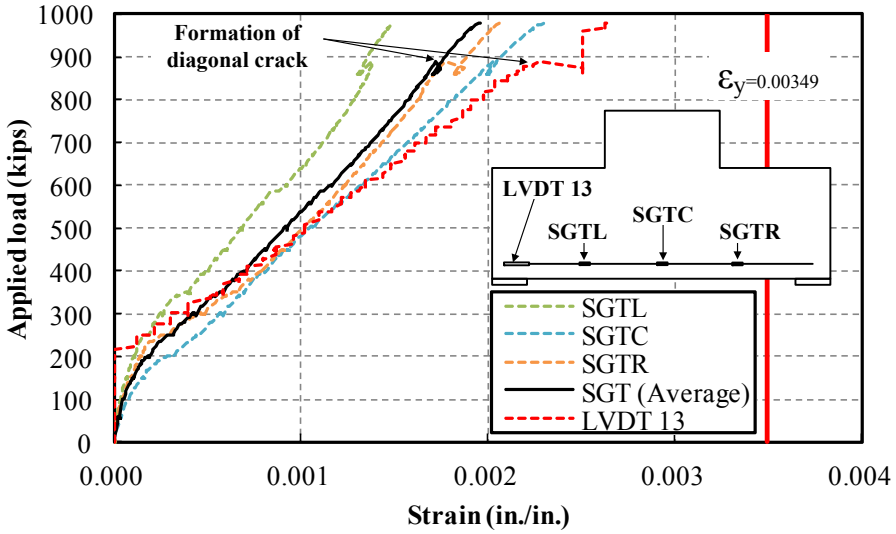

Figure D.5- Applied load vs. strain of longitudinal tension reinforcement for specimen BSR008

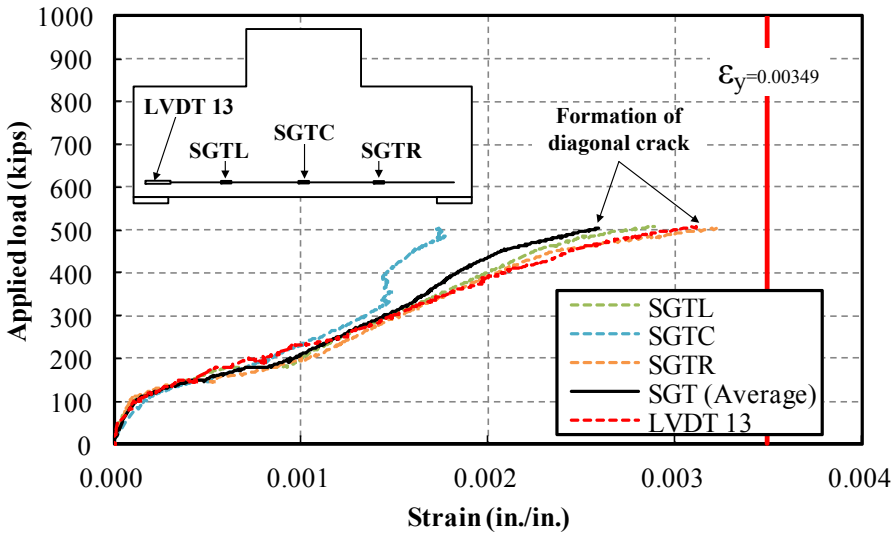

Figure D.6- Applied load vs. strain of longitudinal tension reinforcement for specimen BSR014

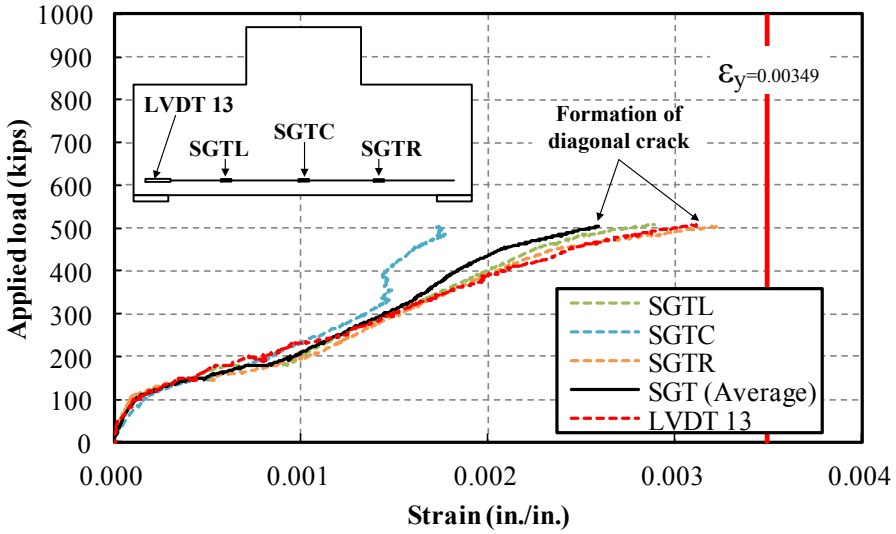

Figure D.7- Applied load vs. strain of longitudinal tension reinforcement for specimen CS00

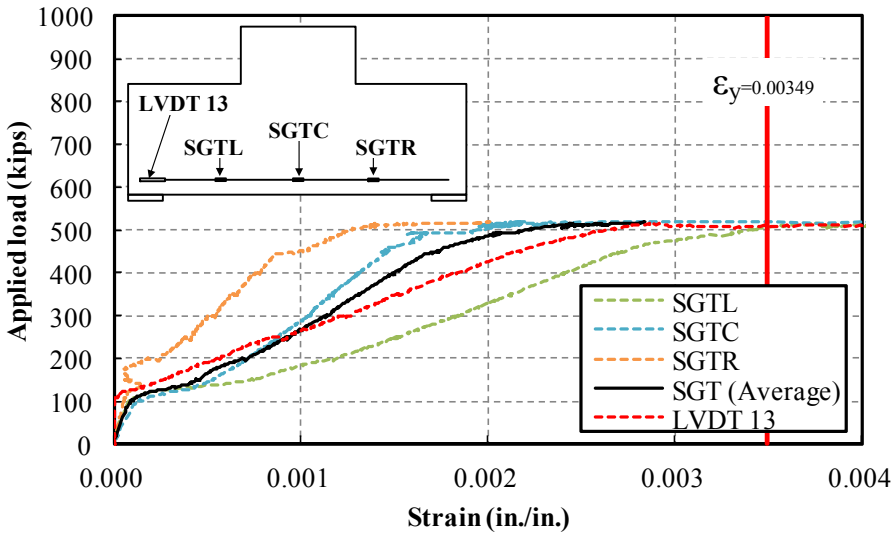

Figure D.8- Applied load vs. strain of longitudinal tension reinforcement for specimen CSR018-1

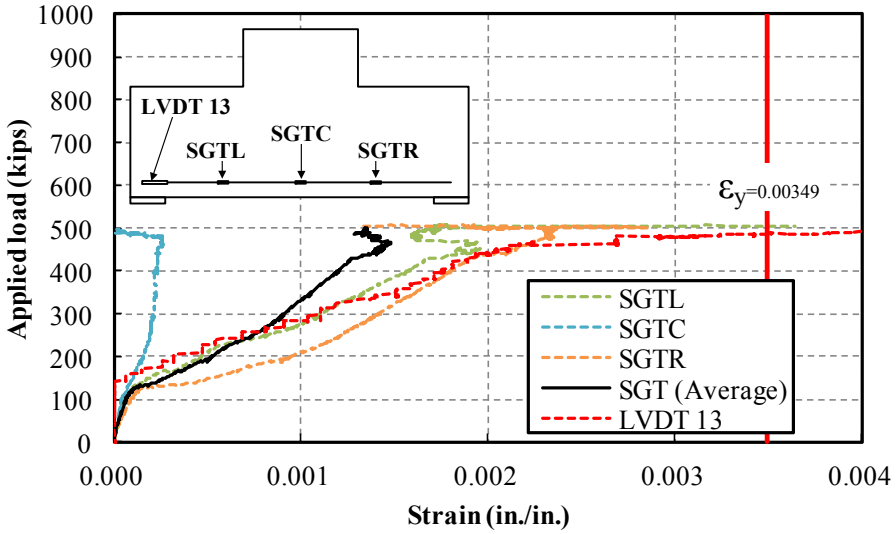

Figure D.9- Applied load vs. strain of longitudinal tension reinforcement for specimen CSR018-2

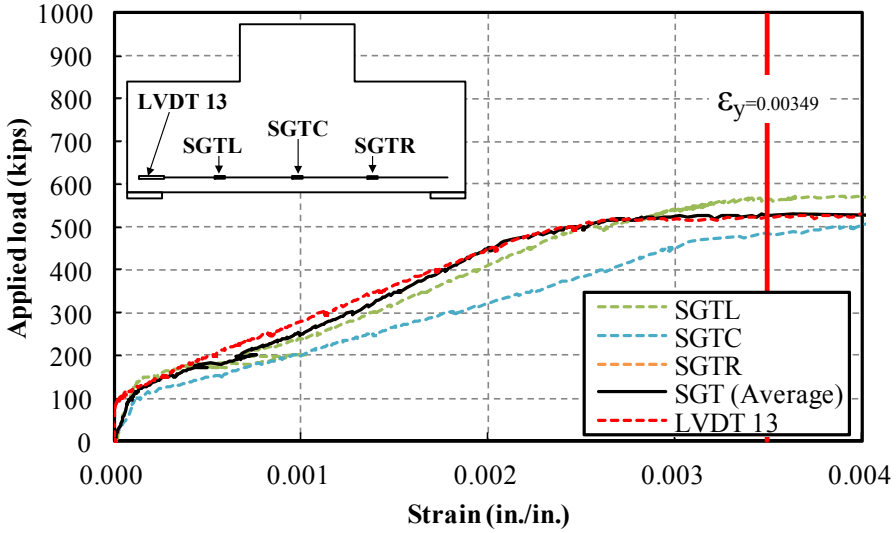

Figure D.10- Applied load vs. strain of longitudinal tension reinforcement for specimen CSR035

APPENDIX E

PLOTS FOR STRUT ANGLES

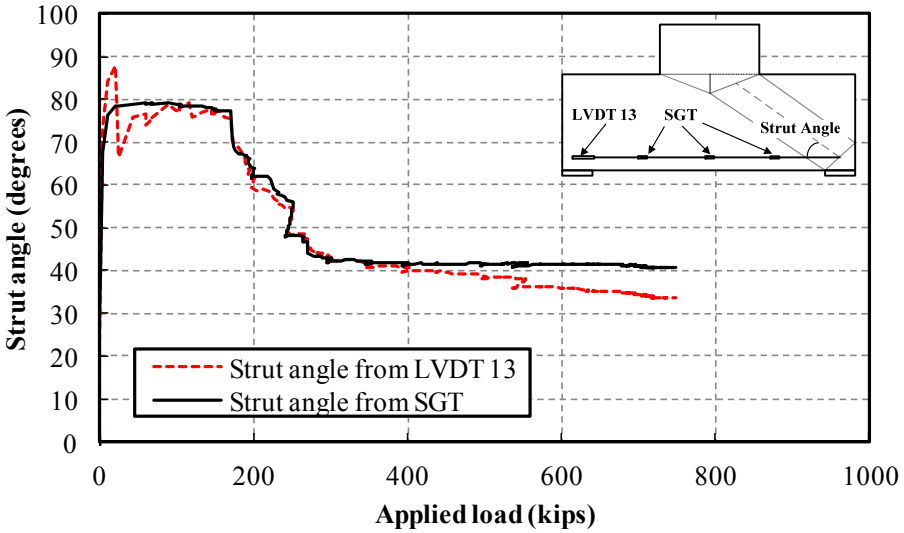

Figure E.1- Strut angle vs. applied load for AR014

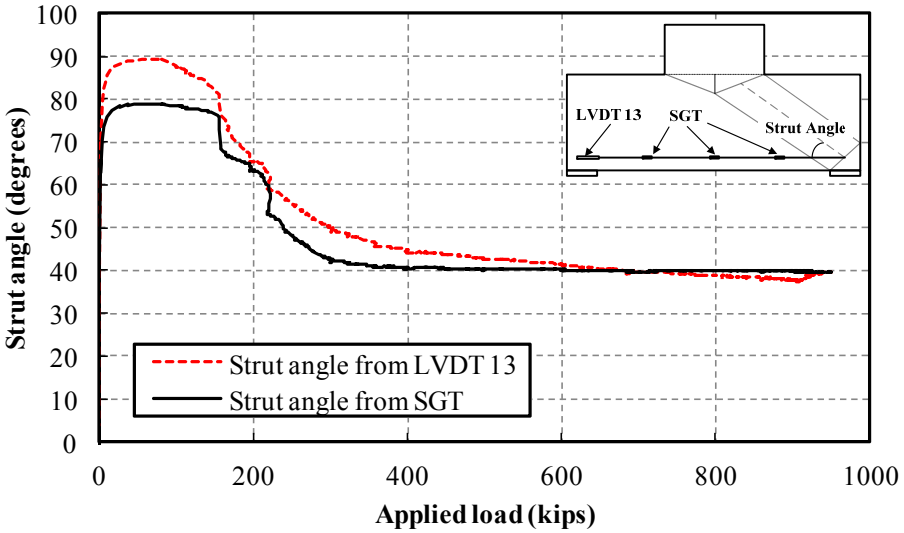

Figure E.2- Strut angle vs. applied load for AR035

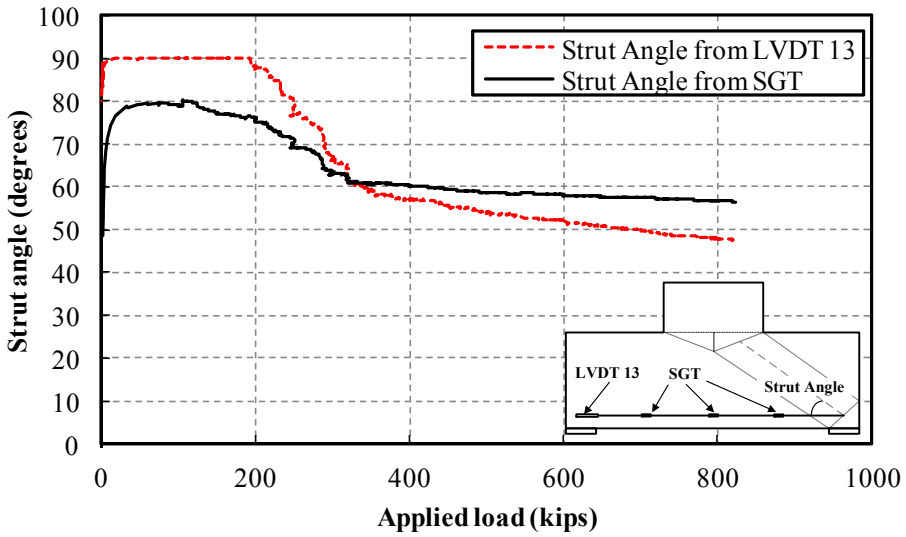

Figure E.3- Strut angle vs. applied load for BS00

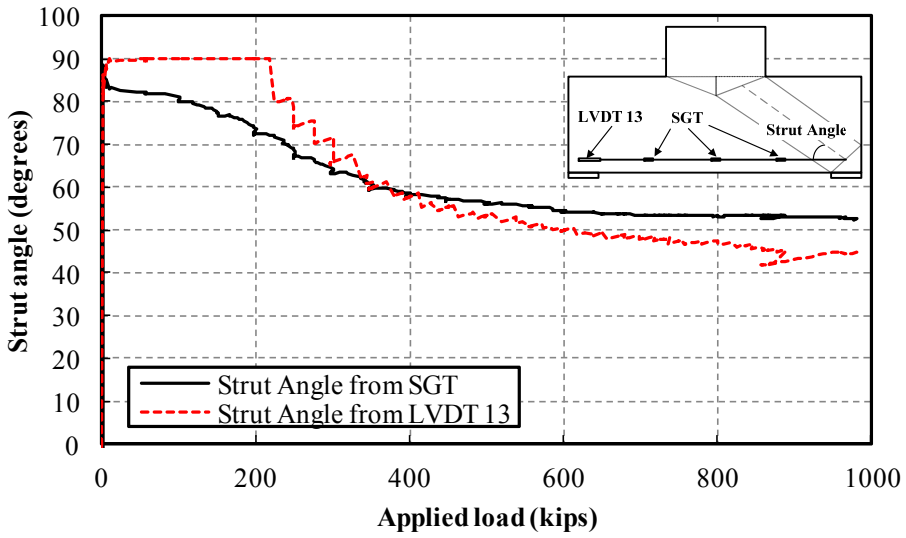

Figure E.4- Strut angle vs. applied load for BSR008

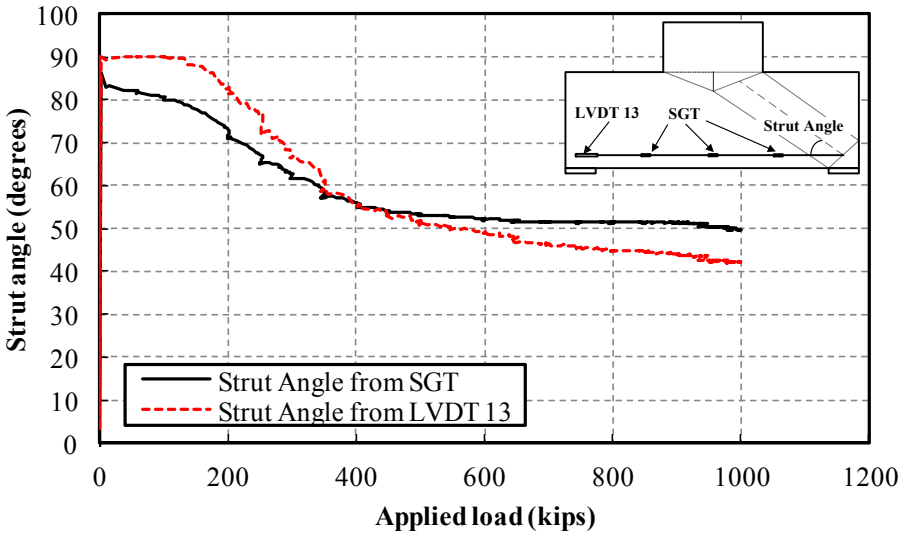

Figure E.5- Strut angle vs. applied load for BSR014

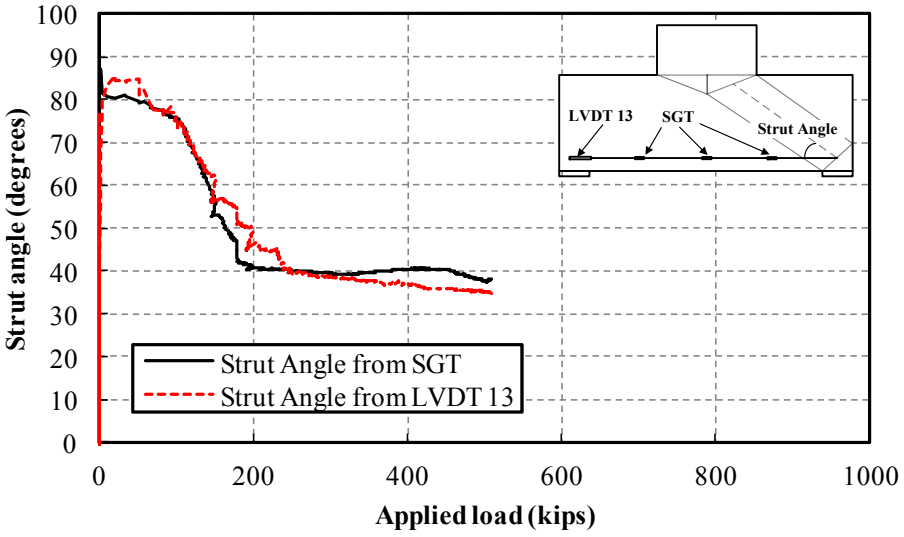

Figure E.6- Strut angle vs. applied load for CS00

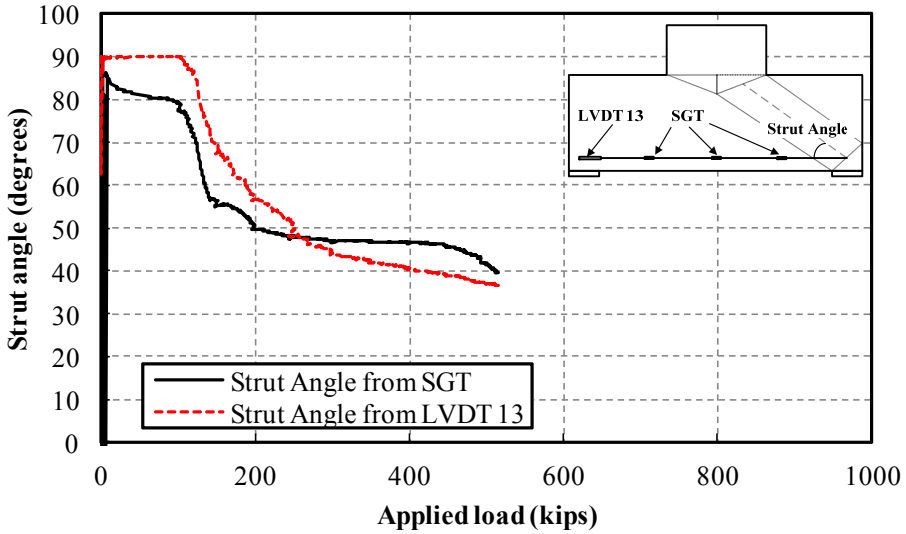

Figure E.7- Strut angle vs. applied load for CSR018-1

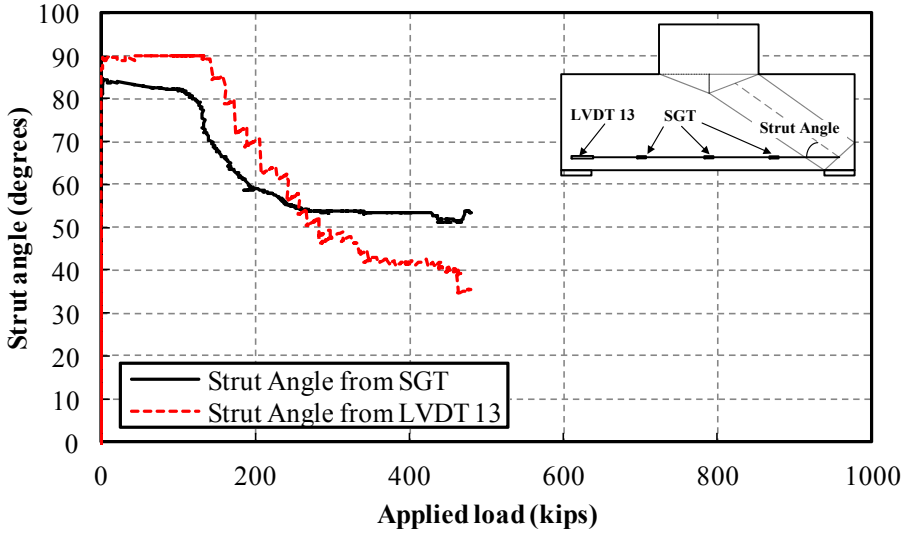

Figure E.8- Strut angle vs. applied load for CSR018-2

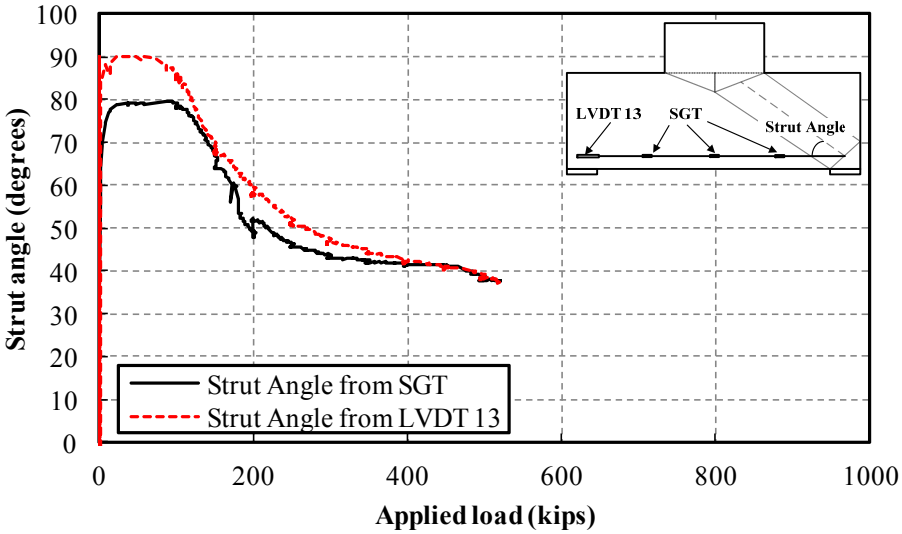

Figure E.9- Strut angle vs. applied load for CSR035

APPENDIX F

PLOTS FOR COMPRESSIVE STRAINS AT COMPRESSION ZONE

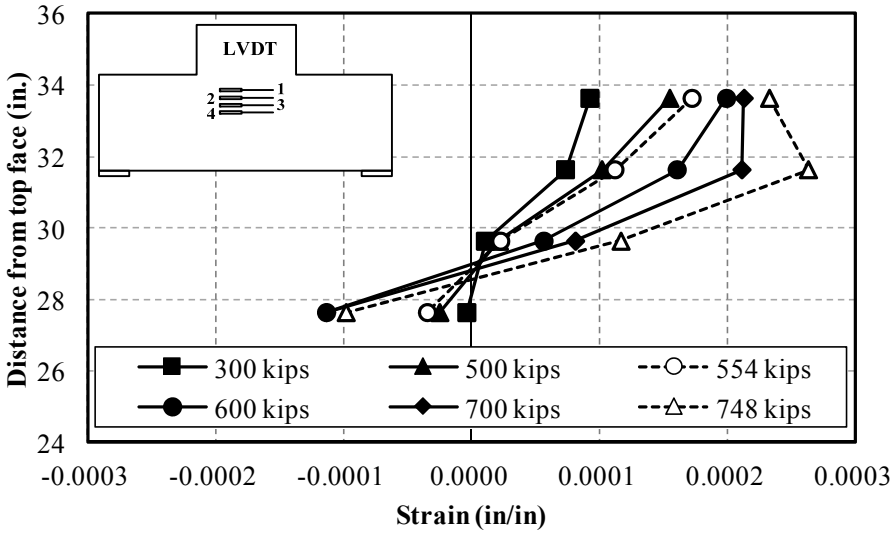

Figure F.1- Strain variations at the compression zone for AR014 specimen

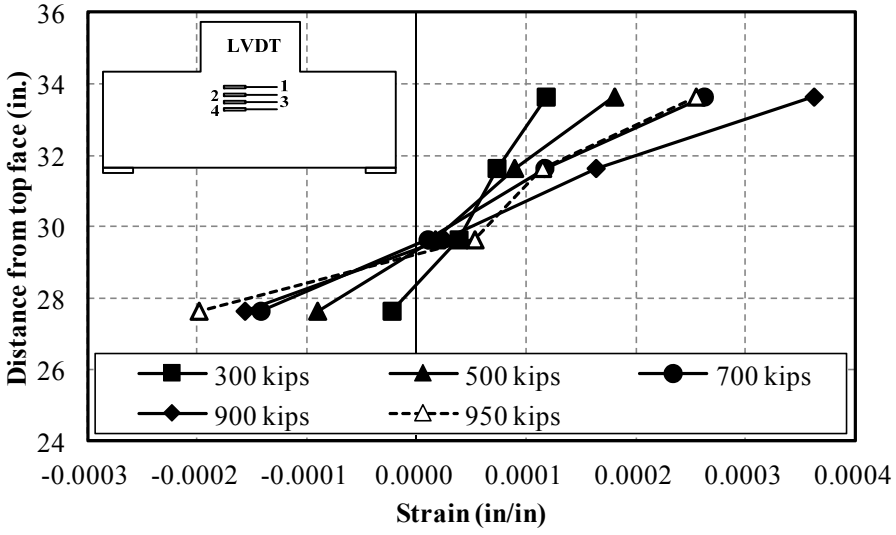

Figure F.2- Strain variations at the compression zone for AR035 specimen

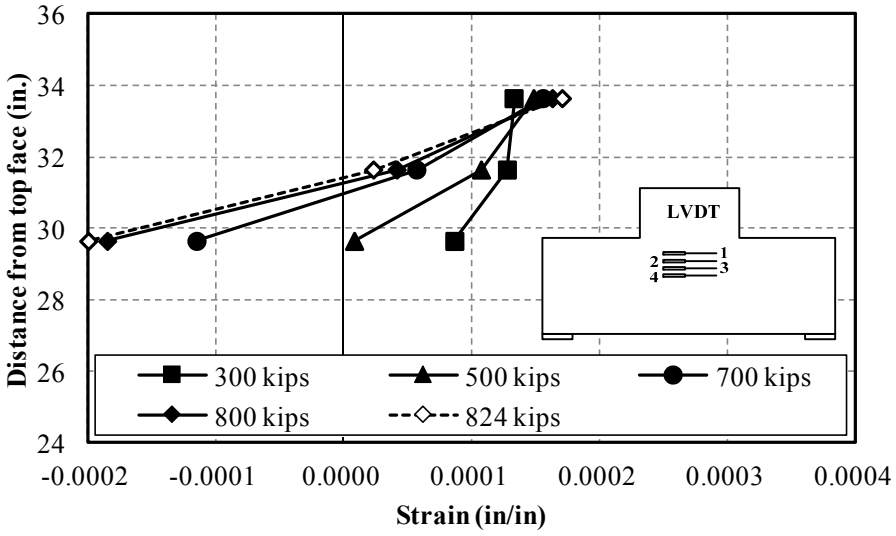

Figure F.3- Strain variations at the compression zone for BS00 specimen

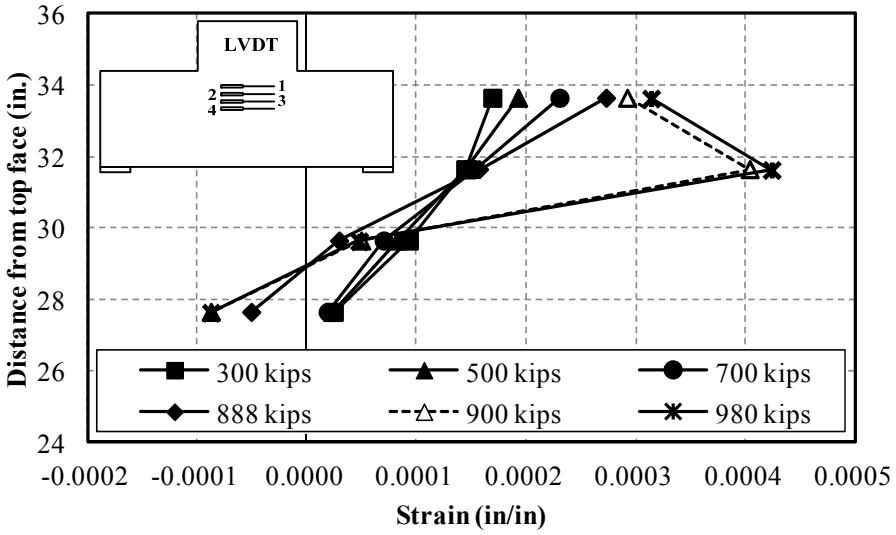

Figure F.4- Strain variations at the compression zone for BSR008 specimen

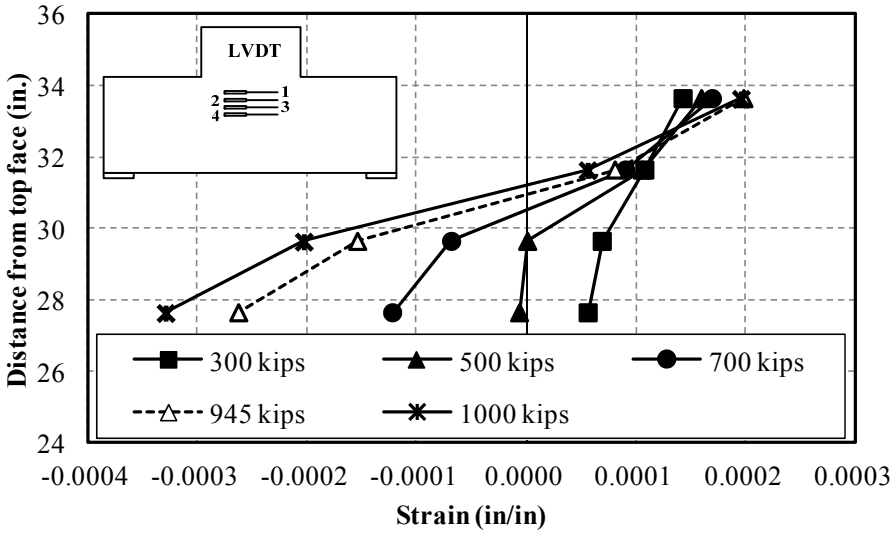

Figure F.5- Strain variations at the compression zone for BSR014 specimen

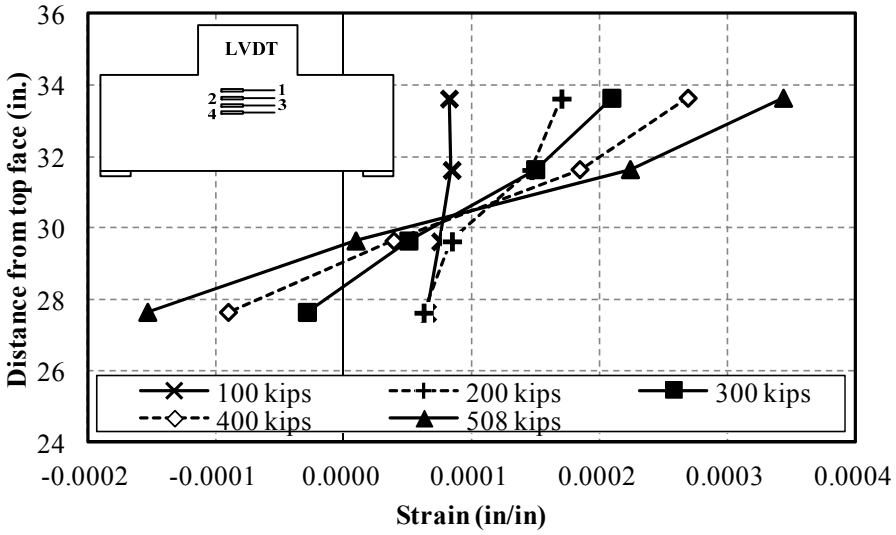

Figure F.6- Strain variations at the compression zone for CS00 specimen

APPENDIX G

REINFORCED CONCRETE DEEP BEAM DATABASE (294 SAMPLES)

Table G.1- Reinforced concrete deep beams database (294 samples)

Specimen ID	a (in.)	b	d_e (in.)	a/d	f_c' (psi)	f_y (ksi)	ρ (%)	ρ_v (%)
Clark (1954)								
C1-1	24.00	8.00	15.30	1.57	3720	47	2.075	
C1-2	24.00	8.00	15.30	1.57	3820	47	2.075	
C1-3	24.00	8.00	15.30	1.57	3475	47	2.075	
C1-4	24.00	8.00	15.30	1.57	4210	47	2.075	
C2-1	24.00	8.00	15.30	1.57	3430	47	2.075	
C2-2	24.00	8.00	15.30	1.57	3625	47	2.075	
C2-3	24.00	8.00	15.30	1.57	3500	47	2.075	
C2-4	24.00	8.00	15.30	1.57	3910	47	2.075	
C6-2	24.00	8.00	15.40	1.56	6560	47	3.093	
C6-3	24.00	8.00	15.40	1.56	6480	47	3.093	
C6-4	24.00	8.00	15.40	1.56	6900	47	3.093	
D1-1	18.00	8.00	15.50	1.16	3800	49	1.613	
D1-2	18.00	8.00	15.50	1.16	3790	49	1.613	
D1-3	18.00	8.00	15.50	1.16	3560	49	1.613	
D2-1	18.00	8.00	15.50	1.16	3480	49	1.613	
D2-2	18.00	8.00	15.50	1.16	3755	49	1.613	
D2-3	18.00	8.00	15.50	1.16	3595	49	1.613	
D2-4	18.00	8.00	15.50	1.16	3550	49	1.613	
D3-1	18.00	8.00	15.50	1.16	4090	49	2.419	
D4-1	18.00	8.00	15.50	1.16	3350	49	1.613	
C0-1	24.00	8.00	15.30	1.57	3580	54	0.980	
C0-2	24.00	8.00	15.30	1.57	3405	54	0.980	
C0-3	24.00	8.00	15.30	1.57	3420	54	0.980	
D0-1	18.00	8.00	15.30	1.18	3750	54	0.980	
D0-2	18.00	8.00	15.30	1.18	3800	54	0.980	
D0-3	18.00	8.00	15.30	1.18	3765	54	0.980	
B1-1	30.00	8.00	15.40	1.95	3388	47	3.093	
B1-2	30.00	8.00	15.40	1.95	3680	47	3.093	
B1-3	30.00	8.00	15.40	1.95	3435	47	3.093	
B1-4	30.00	8.00	15.40	1.95	3388	47	3.093	
B1-5	30.00	8.00	15.40	1.95	3570	47	3.093	
B2-1	30.00	8.00	15.40	1.95	3370	47	3.093	
B2-2	30.00	8.00	15.40	1.95	3820	47	3.093	
B2-3	30.00	8.00	15.40	1.95	3615	47	3.093	
B6-1	30.00	8.00	15.40	1.95	6110	47	3.093	
C3-1	24.00	8.00	15.30	1.57	2040	47	2.075	
C3-2	24.00	8.00	15.30	1.57	2000	47	2.075	
C3-3	24.00	8.00	15.30	1.57	2020	47	2.075	
C4-1	24.00	8.00	15.40	1.56	3550	47	3.093	
D1-6	18.00	6.00	12.40	1.45	4010	47	3.414	

D1-7	18.00	6.00	12.40	1.45	4060	47	3.414
D1-8	18.00	6.00	12.40	1.45	4030	47	3.414
B0-1	30.00	8.00	15.40	1.95	3420	54	0.974
B0-2	30.00	8.00	15.40	1.95	3468	54	0.974
B0-3	30.00	8.00	15.40	1.95	3410	54	0.974
Moody et al. (1954)							
III-24a	32.00	7.00	21.00	1.52	2580	46	2.721
III-24b	32.00	7.00	21.00	1.52	2990	46	2.721
III-25a	32.00	7.00	21.00	1.52	3530	45	3.456
III-25b	32.00	7.00	21.00	1.52	2500	45	3.456
III-26a	32.00	7.00	21.00	1.52	3140	44	4.245
III-26b	32.00	7.00	21.00	1.52	2990	44	4.245
III-27a	32.00	7.00	21.00	1.52	3100	46	2.721
III-27b	32.00	7.00	21.00	1.52	3320	46	2.721
III-28a	32.00	7.00	21.00	1.52	3380	45	3.456
III-28b	32.00	7.00	21.00	1.52	3250	45	3.456
III-29a	32.00	7.00	21.00	1.52	3150	44	4.245
III-29b	32.00	7.00	21.00	1.52	3620	44	4.245
III-30	32.00	7.00	21.00	1.52	3680	44	4.245
III-31	32.00	7.00	21.00	1.52	3250	44	4.245
Moody et al. (1954)							
II-a	32.00	7.00	20.75	1.54	3820	46	0.551
II-b	32.00	7.00	20.75	1.54	3720	44	0.854
II-c	32.00	7.00	20.75	1.54	4040	42	1.212
II-d	32.00	7.00	20.75	1.54	3440	42	1.652
II-17a	32.00	7.00	20.75	1.54	2650	47	2.176
II-17b	32.00	7.00	20.75	1.54	3000	47	2.176
II-18a	32.00	7.00	20.75	1.54	2170	46	2.754
II-18b	32.00	7.00	20.75	1.54	2700	46	2.754
II-19a	32.00	7.00	20.75	1.54	3030	45	3.497
II-19b	32.00	7.00	20.75	1.54	3240	45	3.497
II-20a	32.00	7.00	20.75	1.54	2890	44	4.296
II-20b	32.00	7.00	20.75	1.54	2960	44	4.296
Morrow and Viest (1956)							
B14-A6	17.50	12.00	14.50	1.21	6780	66	3.697
B21B2	24.50	12.00	14.44	1.70	2010	63	1.859
B21E2	24.50	12.00	14.75	1.66	1640	67	0.574
B21A4	24.50	12.00	14.50	1.69	4320	59	2.455
B21B4	24.50	12.00	14.50	1.69	3930	61	1.852
B21E4	24.50	12.00	14.38	1.70	3510	62	1.246
B21E4R	24.50	12.00	14.50	1.69	4630	60	1.236
B21F4	24.50	12.00	14.56	1.68	4560	66	1.118
B21A6	24.50	12.00	14.00	1.75	6570	65	3.829
B21B6	24.50	12.00	14.75	1.66	6600	63	1.820
Watstein and Mathey (1958)							
B-18-1	24.00	8.00	15.90	1.51	3680	39	2.995
B-18-2	24.00	8.00	15.90	1.51	3330	39	2.995
C-18-1	24.00	8.00	15.90	1.51	3710	71	1.863
C-18-2	24.00	8.00	15.90	1.51	3830	68	1.863
D-18-1	24.00	8.00	15.90	1.51	3720	105	1.163
D-18-2	24.00	8.00	15.90	1.51	3910	97	1.163
E-18-1	24.00	8.00	15.90	1.51	3250	100	0.731

E-18-2	24.00	8.00	15.90	1.51	3870	100	0.731
Rodriguez et al. (1959)							
E6N1	17.00	6.00	12.50	1.36	3213	43	2.637
E6N2	17.00	6.06	12.50	1.36	2627	45	2.611
E6N3	17.00	6.06	12.50	1.36	3277	45	2.611
C6N1	17.00	6.13	12.63	1.35	3640	47	2.555
C6N2	17.00	6.00	12.50	1.36	2963	46	2.637
C6N3	17.00	6.06	12.38	1.37	3153	46	2.637
Mathey and Watstein (1963)							
I-1	24.00	8.00	15.86	1.51	3680	39	3.045
I-2	24.00	8.00	15.86	1.51	3330	39	3.045
II-3	24.00	8.00	15.86	1.51	3170	68	1.884
II-4	24.00	8.00	15.86	1.51	3830	68	1.884
III-5	24.00	8.00	15.86	1.51	3730	71	1.854
III-6	24.00	8.00	15.86	1.51	3710	71	1.854
IV-7	24.00	8.00	15.86	1.51	3500	65	1.861
IV-8	24.00	8.00	15.86	1.51	3610	65	1.861
V-9	24.00	8.00	15.86	1.51	3350	101	1.163
V-10	24.00	8.00	15.86	1.51	3910	101	1.163
VI-11	24.00	8.00	15.86	1.51	3680	105	1.166
VI-12	24.00	8.00	15.86	1.51	3720	105	1.166
V-13	24.00	8.00	15.86	1.51	3250	103	0.752
V-14	24.00	8.00	15.86	1.51	3870	103	0.752
VI-15	24.00	8.00	15.86	1.51	3700	101	0.750
VI-16	24.00	8.00	15.86	1.51	3310	101	0.750
Kani (1967)							
46	10.70	5.95	5.35	2.00	3700	57	2.764
53	5.34	5.95	5.20	1.03	3870	57	2.844
54	5.34	5.95	5.35	1.00	3870	57	2.764
88	10.68	6.01	10.47	1.02	4560	58	2.813
94	21.36	6.03	10.76	1.99	3670	51	2.774
67	21.36	6.19	20.80	1.03	4400	59	2.749
69	21.36	6.11	21.35	1.00	3970	54	2.668
72	42.80	6.00	21.62	1.98	3600	56	2.706
3041	86.40	6.00	43.20	2.00	3900	55	2.724
Manuel (1974)							
11	17.00	4.00	16.00	1.06	4680	54	1.875
Smith and Vantsiotis (1982)							
0B0-49	14.50	4.00	12.00	1.21	3145	61	1.938
1B1-01	14.50	4.00	12.00	1.21	3200	63	1.938
1B3-29	14.50	4.00	12.00	1.21	2915	63	1.938
1B3-30	14.50	4.00	12.00	1.21	3020	63	1.938
1B6-31	14.50	4.00	12.00	1.21	2830	63	1.938
2B1-05	14.50	4.00	12.00	1.21	2780	63	1.938
2B3-06	14.50	4.00	12.00	1.21	2755	63	1.938
2B4-07	14.50	4.00	12.00	1.21	2535	63	1.938
2B4-52	14.50	4.00	12.00	1.21	3160	63	1.938
2B6-32	14.50	4.00	12.00	1.21	2865	63	1.938
3B1-08	14.50	4.00	12.00	1.21	2355	63	1.938
3B1-36	14.50	4.00	12.00	1.21	2960	63	1.938
3B3-33	14.50	4.00	12.00	1.21	2755	63	1.938
3B4-34	14.50	4.00	12.00	1.21	2790	63	1.938

3B6-35	14.50	4.00	12.00	1.21	2995	63	1.938
4B1-09	14.50	4.00	12.00	1.21	2480	63	1.938
0C0-50	18.00	4.00	12.00	1.50	3000	61	1.938
1C1-14	18.00	4.00	12.00	1.50	2790	63	1.938
1C3-02	18.00	4.00	12.00	1.50	3175	63	1.938
1C4-15	18.00	4.00	12.00	1.50	3290	63	1.938
1C6-16	18.00	4.00	12.00	1.50	3160	63	1.938
2C1-17	18.00	4.00	12.00	1.50	2880	63	1.938
2C3-03	18.00	4.00	12.00	1.50	2790	63	1.938
2C3-27	18.00	4.00	12.00	1.50	2800	63	1.938
2C4-18	18.00	4.00	12.00	1.50	2965	63	1.938
2C6-19	18.00	4.00	12.00	1.50	3010	63	1.938
3C1-20	18.00	4.00	12.00	1.50	3050	63	1.938
3C3-21	18.00	4.00	12.00	1.50	2400	63	1.938
3C4-22	18.00	4.00	12.00	1.50	2650	63	1.938
3C6-23	18.00	4.00	12.00	1.50	2755	63	1.938
4C1-24	18.00	4.00	12.00	1.50	2840	63	1.938
4C3-04	18.00	4.00	12.00	1.50	2690	63	1.938
4C3-28	18.00	4.00	12.00	1.50	2790	63	1.938
4C4-25	18.00	4.00	12.00	1.50	2685	63	1.938
4C6-26	18.00	4.00	12.00	1.50	3080	63	1.938
Rogowsky et al. (1986)							
BM1/1.5N T1	36.42	7.87	21.06	1.73	6150	66	1.121
BM1/1.5S T2	36.42	7.87	21.06	1.73	6150	66	1.121
BM2/1.5N T1	36.42	7.87	21.06	1.73	6150	66	1.121
BM2/1.5S T2	36.42	7.87	21.06	1.73	6150	66	1.121
BM3/1.5 T1	35.43	7.87	21.06	1.68	2103	66	1.121
BM3/1.5 T2	35.43	7.87	21.06	1.68	2103	66	1.121
BM4/1.5 T1	35.43	7.87	21.06	1.68	4714	66	1.121
BM4/1.5 T2	35.43	7.87	21.06	1.68	4714	66	1.121
BM5/1.5 T1	35.43	7.87	21.06	1.68	5743	66	1.121
BM5/1.5 T2	35.43	7.87	21.06	1.68	5743	66	1.121
BM6/1.5 T1	35.43	7.87	21.06	1.68	6527	66	1.121
BM6/1.5 T2	35.43	7.87	21.06	1.68	6527	66	1.121
BM7/1.5 T1	35.43	7.87	21.06	1.68	4409	66	1.121
BM7/1.5 T2	35.43	7.87	21.06	1.68	4409	66	1.121
BM8/1.5 T1	35.43	7.87	21.06	1.68	5395	66	1.121
BM8/1.5 T2	35.43	7.87	21.06	1.68	5395	66	1.121
BM3/2.0 T1	35.43	7.87	17.91	1.98	6164	67	1.098
BM3/2.0 T2	35.43	7.87	17.91	1.98	6164	67	1.098
BM4/2.0 T1	35.43	7.87	17.91	1.98	5555	66	1.098
BM4/2.0 T2	35.43	7.87	17.91	1.98	5555	66	1.098
BM5/2.0 T1	35.43	7.87	17.91	1.98	5961	67	1.098
BM5/2.0 T2	35.43	7.87	17.91	1.98	5961	67	1.098
BM6/2.0 T1	35.43	7.87	17.91	1.98	5424	66	1.098
BM6/2.0 T2	35.43	7.87	17.91	1.98	5424	66	1.098
BM7/2.0 T1	35.43	7.87	17.91	1.98	6788	67	1.098
BM7/2.0 T2	35.43	7.87	17.91	1.98	6788	67	1.098
Subedi et al. (1986)							
1B2	27.17	3.94	17.22	1.58	5366	72	0.921
1D2	50.79	3.94	32.79	1.55	6019	48	1.179
2D2	50.79	3.94	32.79	1.55	5714	44	1.179
Mansur et al. (1987)							

A1	15.51	5.91	7.76	2.00	3510	67	1.362
Tan and Mansur (1992)							
S14	27.56	5.91	13.78	2.00	5555	215	0.332
Kim and Park (1994)							
A1.5-1	15.95	6.69	10.63	1.50	7789	69	1.874
A1.5-2	15.95	6.69	10.63	1.50	7789	69	1.874
Xie et al.(1994)							
NNN-1	8.50	5.00	8.50	1.00	6470	61	2.071
NNN-2	17.00	5.00	8.50	2.00	5700	61	2.071
NNW-1	8.50	5.00	8.00	1.06	5470	61	3.200
Tan and Lu (1994)							
1-500/1.00	19.69	5.51	17.48	1.13	5424	75	2.591
2-1000/1.00	39.37	5.51	34.80	1.13	4467	75	2.602
3-1400/1.00	55.91	5.51	49.25	1.14	5120	75	2.601
4-1750/1.00	69.29	5.51	61.38	1.13	6498	75	2.596
Pandyala and Mendis (2000)							
∞(30)(2)	11.02	3.15	5.51	2.00	4931	59	2.016
140(30)(2)	11.02	3.15	5.51	2.00	4786	59	2.016
210(30)(2)	11.02	3.15	5.51	2.00	4641	59	2.016
2_140(30)(2)	11.02	3.15	5.51	2.00	5221	59	2.016
Anguilar (2002)							
STM-H	36.00	12.00	31.50	1.14	4130	61	1.254
STM-M	36.00	12.00	31.50	1.14	4130	61	1.254
Yang et al. (2003)							
L10-40	15.75	6.30	13.98	1.13	4554	117	1.011
L10-40R	15.75	6.30	13.98	1.13	4554	117	1.011
L10-60	23.62	6.30	21.85	1.08	4554	117	0.970
L10-75	29.53	6.30	26.97	1.09	4554	117	1.047
L10-75R	29.53	6.30	26.97	1.09	4554	117	1.047
L10-100	39.37	6.30	36.81	1.07	4554	88	0.901
Tanimura and Sato (2005)							
9	23.62	11.81	15.75	1.50	3321	66	2.202
10	23.62	11.81	15.75	1.50	3263	66	2.202
11	23.62	11.81	15.75	1.50	3336	66	2.202
12	23.62	11.81	15.75	1.50	3408	66	2.202
22	23.62	11.81	15.75	1.50	3800	66	2.202
23	23.62	11.81	15.75	1.50	3814	66	2.202
31	31.50	11.81	15.75	2.00	3858	66	2.202
32	31.50	11.81	15.75	2.00	3974	66	2.202
Brown et al (2006)							
I-CL-8.5-0	30.00	6.00	27.00	1.11	2580	68	1.951
I-CL-0-0	30.00	6.00	27.00	1.11	2370	68	1.951
II-N-E-5.8-8	27.00	18.00	16.00	1.69	2850	68	2.194
II-N-F-5.8-8	27.00	18.00	16.00	1.69	2850	68	2.194
II-N-F-5.8-3	27.00	18.00	16.00	1.69	2880	68	2.194
II-N-C-4.6-8	27.00	18.00	16.00	1.69	2880	68	2.194
II-N-E-4.6-8	27.00	18.00	16.00	1.69	2880	68	2.194
II-N-F-4.6-8	27.00	18.00	16.00	1.69	3130	68	2.194
III-2	24.00	8.00	16.00	1.50	3880	68	3.086
Guadagnini et al. (2006)							
SB42	9.84	5.91	8.82	1.12	7643	73	1.344

Zhang and Tan (2007)							
1DB35bw	13.56	3.15	12.32	1.10	3757	68	1.255
1DB50bw	19.66	4.53	17.87	1.10	3974	74	1.279
1DB70bw	27.80	6.30	25.28	1.10	4105	76	1.224
1DB100bw	39.15	9.06	35.59	1.10	4163	77	1.203
2DB35	13.60	3.15	12.36	1.10	3974	68	1.251
2DB50	19.88	3.15	18.07	1.10	4699	72	1.152
2DB70	28.15	3.15	25.59	1.10	3597	74	1.284
2DB100	40.10	3.15	36.46	1.10	4438	74	1.259
3DB35b	13.60	3.15	12.36	1.10	3974	68	1.251
3DB50b	19.66	4.53	17.87	1.10	4105	74	1.279
3DB70b	27.80	6.30	25.28	1.10	4163	76	1.224
3DB100b	39.15	9.06	35.59	1.10	4250	77	1.203
Alcocer and Uribe (2008)							
MT	55.12	13.78	43.31	1.27	5134	65	1.059
MR	55.12	13.78	43.31	1.27	5076	65	1.059
Birrcher et al. (2009)							
I-03-2	71.00	21.00	38.50	1.84	5240	73	2.286
I-03-4	71.00	21.00	38.50	1.84	5330	73	2.286
I-02-2	71.00	21.00	38.50	1.84	3950	73	2.286
I-02-4	71.00	21.00	38.50	1.84	4160	73	2.286
II-03-CCC2021	71.00	21.00	38.60	1.84	3290	64	2.309
II-03-CCC1007	71.00	21.00	38.60	1.84	3480	64	2.309
II-03-CCT1021	71.00	21.00	38.60	1.84	4410	66	2.309
II-03-CCT0507	71.00	21.00	38.60	1.84	4210	66	2.309
II-02-CCT0507	71.00	21.00	38.60	1.84	3120	69	2.309
II-02-CCC1007	71.00	21.00	38.60	1.84	3140	69	2.309
II-02-CCC1021	71.00	21.00	38.60	1.84	4620	69	2.309
II-02-CCT0521	71.00	21.00	38.60	1.84	4740	69	2.309
III-1.85-02	71.00	21.00	38.60	1.84	4100	66	2.309
III-1.85-025	71.00	21.00	38.60	1.84	4100	66	2.309
III-1.85-03	71.00	21.00	38.60	1.84	4990	69	2.309
III-1.85-01	71.00	21.00	38.60	1.84	5010	69	2.309
III-1.85-03b	71.00	21.00	38.60	1.84	3300	69	2.309
III-1.85-02b	71.00	21.00	38.60	1.84	3300	69	2.309
III-1.2-02	46.32	21.00	38.60	1.20	4100	66	2.309
III-1.2-03	46.32	21.00	38.60	1.20	4220	66	2.309
IV-2175-1.85-02	127.47	21.00	68.90	1.85	4930	68	2.372
IV-2175-1.85-03	127.47	21.00	68.90	1.85	4930	68	2.372
IV-2175-1.2-03	82.68	21.00	68.90	1.20	5010	68	2.372
IV-2123-1.85-03	36.08	21.00	19.50	1.85	4160	66	2.315
IV-2123-1.85-02	36.08	21.00	19.50	1.85	4220	66	2.315
IV-2123-1.2-02	23.40	21.00	19.50	1.20	4630	65	2.315
M-03-4-CCC2436	74.00	36.00	40.00	1.85	4100	67	2.925
M-09-4-CCC2436	74.00	36.00	40.00	1.85	4100	67	2.925
M-02-4-CCC2436	74.00	36.00	40.00	1.85	2800	65	2.925
M-03-4-CCC0812	74.00	36.00	40.00	1.85	3000	65	2.925
M-03-2CCC2436	74.00	36.00	40.00	1.85	4900	68	2.925
Roy and Breña (2008)							

DB1.0-1.00	24.00	6.00	22.90	1.05	4830	71	0.451
DB1.0-0.75	24.00	6.00	22.90	1.05	4600	71	0.451
DB1.0-0.50	24.00	6.00	22.90	1.05	4440	71	0.451
DB1.0-0.32	24.00	6.00	22.90	1.05	3915	71	0.451
DB1.0-0.75L	24.00	6.00	22.90	1.05	4340	68	0.640
DB1.0-0.28L	24.00	6.00	22.90	1.05	4265	68	0.640
DB1.5-0.75	24.00	6.00	15.90	1.51	4745	71	0.650
DB1.5-0.50	24.00	6.00	15.90	1.51	4945	71	0.650
DB1.5-0.38	24.00	6.00	15.90	1.51	4900	71	0.650
Bechtel (2011)							
AL1	39.00	18.00	32.80	1.19	3473	65	0.645
BL1	39.00	18.00	32.80	1.19	3352	80	0.645
AL2	39.00	18.00	32.12	1.21	3651	65	1.318
BL2	39.00	18.00	32.12	1.21	3353	80	1.318
BL3	39.00	18.00	32.12	1.21	3966	80	1.318
BL4	39.00	18.00	32.12	1.21	3874	80	1.318
BL5	39.00	18.00	32.12	1.21	3998	80	1.318
AS1	19.50	9.00	16.40	1.19	4123	79	0.630
AS2	19.50	9.00	16.40	1.19	4226	79	0.630
AS3	19.50	9.00	16.06	1.21	4036	76	1.384
AS4	19.50	9.00	16.06	1.21	4650	85	1.384
O'Malley (2011)							
1-S	41.00	12.00	32.25	1.27	3430	73	1.021
2-NS	41.00	12.00	32.25	1.27	3180	73	1.021
6-NS	41.00	12.00	32.25	1.27	3460	73	1.021

REFERENCES

[1] AASHTO. (2010). *LRFD Design Specifications 5th Edition,* Washington, D.C.

[2] ACI Committee 318. (2008). *Building Code Requirements for Structural Concrete and Commentary,* Farmington Hills, MI.

[3] Aguilar, G., Matamoros, A. B., Parra-Montesinos, G. J., Ramírez, J. A., Wight, J. K. (2002). "Experimental Evaluation of Design Procedures for Shear Strength of Deep Reinforced Concrete Beams." *ACI Structural Journal*. 99(4), 539-548.

[4] Alcocer, S. M., and Uribe, C. M. (2008). "Monolithic and Cyclic Behavior of Deep Beams Designed Using Strut-and-Tie Models." *ACI Structural Journal*. 105(3), 327-337.

[5] ASTM E-8. (2001). *Standard Test Methods for Tension Testing of Metallic Materials*, Conshohocken PA.

[6] ASTM C39/C39M. (2010). *Standard Test Method for Compressive Strength of Cylindrical Concrete Specimens,* Conshohocken PA.

[7] ASTM C469/C469M. (2010). *Standard Test Method for Static Modulus of Elasticity and Poisson's Ratio of Concrete in Compression*, Conshohocken PA.

[8] Bechtel, A. J. (2011). "External Strengthening of Reinforced Concrete Pier Caps." Ph. D. thesis, Georgia Institute of Technology, Atlanta, GA.

[9] Belarbi, A., Bae, S., Ayoub, A., Kuchma, D., Mirmiran, A., Okeil, A. (2011). *NCHRP 678: Design of FRP Systems for Strengthening Concrete Girders in Shear*. Washington D.C.

[10] Birrcher, D. B. (2009). "Design of Reinforced Concrete Deep Beams for Strength and Serviceability." Ph. D. thesis, The University of Texas, Austin, TX.

[11] Bousselham, A. and, Chaallal, O. (2006). "Behavior of Reinforced Concrete T-Beams Strengthened in Shear with CFRP- An Experimental Study." *ACI Structural Journal.* 103(3), 339-347.

[12] Brown, M. D., Sankovich, C. L., Bayrak, O., Jirsa, J. O., Breen, J. E., Wood, S. L. (2006). "Design for Shear in Reinforced Concrete Using Strut-and-Tie Models." Technical Report No. FHWA/TX-06/0-4371-2.

[13] Chaallal, O., Nollet, M. J., Saleh, K. (1998). "Use of CFRP Strips for Flexure and Shear Strengthening of RC Members." *2nd Conference on Composites in Infrastructure.* Tucson, AZ.

[14] Clark, A. (1951). "Diagonal Tension in Reinforced Concrete Beams." *Journal of the American Concrete Institute*. 48(11), 145-156.

[15] Collins, M. P., and Mitchell, D. (*1991*). *Prestressed Concrete Structures,* Prentice Hall, New Jersey.

[16] Deniaud, C., and Cheng, R. (2001). "Shear Behavior of Reinforced Concrete T-Beams with Externally Bonded Fiber-Reinforced Polymer Sheets." *ACI Structural Journal*. 98(3), 386-394.

[17] Fanning, P., and Kelly, O. (1999). "Shear Strengthening of Reinforced Concrete Beams: An Experimental Study using CFRP Plates." *8th International Conference on Structural Faults and Repair.* London.

[18] FIP Recommendations. (*1999*). *Practical Design of Structural Concrete*, SETO, London.

[19] Foster, S. J., and Gilbert, R. I. (1996). "The Design of Nonflexural Members with Normal and High Strength Concretes." *ACI Structural Journal*. 93(1), 3-10.

[20] Guadagnini, M., Pilakoutas, K., and Waldron, P. (2006). "Shear Resistance of FRP RC Beams: Experimental Study." *Journal of Composites for Construction.* 10(6), 464-473.

[21] ICRI No. 03732. (2002). *Selecting and Specifying Concrete Surface Preparation for Sealers, Coatings, and Polymer Overlays*, Des Plaines, IL.

[22] Islam M. R., Mansur, M. A., and Maalej, M. (2005). "Shear Strengthening of RC deep beams using externally bonded FRP Systems." *Cement and Concrete Composites*. 27(3), 413-420.

[23] Kim, J., and Park, Y. (1994). “Shear Strength of Reinforced High Strength Concrete Beams without Web Reinforcement.” *Magazine of Concrete Research*. 46(166), 7-16.

[24] Kani, G. (1964). “The Riddle of Shear Failure and Its Solution.” *Journal of the American Concrete Institute.* 61(4), 441-467.

[25] Mansur, M. A., Ong, C. G., and Paramasivam, P. (1987). “Shear Strength of Fibrous Concrete Beams without Stirrups.” *Journal of Strutctural Engineering.* 112(9), 2066-2079.

[26] Manuel, R. F. (1974). “Failure of Deep Beams.” *ACI Special Publication 42*. 425-440.

[27] Mathey, R. G., and Watstein, D. (1963). “Shear strength of beams without web reinforcement containing deformed bars of different yield strengths.” *Journal of the American Concrete Institute*. 60(2), 183-207.

[28] Moody, K. G., Viest, I. M., Elstner, R. C., Hognestad, E. (1954). “Shear Strength of Reinforced Concrete Beams Part 1-Tests of Simple Beams.” *Journal of the American Concrete Institute*. 51(15), 317-392.

[29] Moody, K. G., Viest, I. M., Elstner, R. C., Hognestad, E. (1954). “Shear Strength of Reinforced Concrete Beams Part 2-Tests of Restrained Beams Without Web Reinforcement.” *Journal of the American Concrete Institute*. 51(21), 417-434.

[30] Morrow, J., and Viest, I. M. (1957). “Shear Strength of Reinforced Concrete Frame Members without Web Reinforcement.” *ACI Journal*, 53(9), 833-869.

[31] O’Malley, C. J. (2011). “Experimental Testing, Analysis, and Strengthening of Reinforced Concrete Pier Caps by Exterior Post Tensioning.” Ph. D. thesis, Georgia Institute of Technology, Atlanta, GA.

[32] Pendyala, R. S., and Mendis, P. (2000). “Experimental Study on Shear Strength of High-Strength Concrete Beams.” *ACI Structural Journal*. 97(4), 564-571.

[33] Park, S., and Aboutaha, R. (2009). “Strut-and Tie Method for CFRP Strengthened Deep RC Members.” *Journal of Strutctural Engineering.* 135(6), 632-643.

[34] Rodriguez, J. J., Bianchini, A. C., Viest, I. M., and Kesler, C. E. (1959). “Shear Strength of Two-Span Continuous Reinforced Concrete Beams.” *Journal of the American Concrete Institute*. 30(10), 1089-1130.

[35] Rogowsky, D. M., MacGregor, J. G., Ong, S. Y. (1986). “Tests of Reinforced Concrete Deep Beams.” *ACI Journal*. 83(55), 614-623.

[36] Roy, N. C., and Breña, S. F. (2008). “Behavior of Deep Beams with Short Longitudinal Bar Anchorages.” *ACI Structural Journal*. 105(4), 460-470.

[37] Schlaich, J., Schäfer, K., Jennewein, M. (1987) “Toward a Consistent Design of Structural Concrete.” *PCI Journal.* 74-151.

[38] Schlaich, J., and Schäfer, K. (1991) “Design and Detailing of Structural Concrete Using Strut-and-Tie Models.” *The Structural Engineer.* 69(6), 113-125.

[39] Smith, K. N., and Vantsiotis, A. S. (1982). “Shear strength of deep beams.” *ACI Journal*. 79(3), 201-213.

[40] Subedi, N. K., Vardy, A. E., and Kubota, N. (1986). “Reinforced Concrete Deep Beams- Some Test Results,” *Magazine of Concrete Research*. 38(137), 206-219.

[41] Tan, K. H., and Mansur, M. A. (1992). “Partial Prestressing in Concrete Corbels and Deep Beams.” *ACI Structural Journal*. 89(3), 251-262.

[42] Tan, K. H., and Lu, H. Y. (1994). “Shear Behavior of Large Reinforced Concrete Deep Beams and Code Comparisons.” *ACI Structural Journal*. 96(5), 836-845.

[43] Tanimura, Y., and Sato, T. (2005). “Evaluation of Shear Strength of Deep Beams with Stirrups.” Quarterly Report of Railway Technical Research Institute. 46(1), 53-58.

[44] Vecchio, F. Collins, M. (1986). “The Modified Compression-Field Theory for Reinforced Concrete Elements Subjected to Shear.” *Journal of the American Concrete Institute.* 83(2), 219-235.

[45] Watstein, D., and Mathey, R. G. (1958). “Strains in Beams Having Diagonal Cracks,” *ACI Journal*, 55(12), 717-728.

[46] Xie, Y., Ahmad, S. H., Yu, T., Hino, S., Chung, W. (1994). “Shear Ductility of Reinforced Concrete Beams of Normal and High-Strength Concrete.” *ACI Structural Journal*. 91(2), 140-149.

[47] Yang, K., Chung, H., Lee, E., Eun, H. (2003). “Shear characteristics of high-strength concrete deep beams without shear reinforcements.” *Engineering Structures*. 25(10), 1343-1352.

[48] Zararis, P. (1988), “Failure Mechanisms in R/C Plates Carrying in Plane Forces.” *Journal of Structural Engineering.* 114(3), 553-574.

[49] Zararis, P. (2003). “Shear Compression Failure in Reinforced Concrete Deep Beams.” *Journal of Structural Engineering.* 129(4), 544-553.

[50] Zhang Z., Hsu, T., Moren, J. (2004). “Shear Strengthening of Reinforced Concrete Deep Beams Using Carbon Fiber Reinforced Polymer Laminates.” *Journal of Composites for Construction.* 8(5), 403-414.

[51] Zhang, N., and Tan, K. (2007). “Size effect in RC deep beams: Experimental investigation and STM verification.” *Engineering Structures*. 29(12), 3241-3254.

[52] Zureick, A., Ellingwood, B., Nowak, A., Mertz, D., Triantafillou, T. (2010). *NCHRP 655: Guide Specifications for the Design of Bonded FRP Systems for Repair and Strengthening of Concrete Bridge Elements.* Washington D.C.

[53] Zureick, A., Ellingwood, B., Bechtel, A., Kim, S., Krapf, C., O’Malley, C., Shah, F. (2013). *Georgia DOT Research Project 0805: Bridge Repair and Strengthening Study Part 1,* Atlanta, GA.

[54] Zureick, A., Ellingwood, B. R., and Kim, S. (2014). *Georgia DOT Research Project RP 11-09: Bridge Repair and Strengthening Study Part 2,* Atlanta, GA.